UCLA
UCLA Electronic Theses and Dissertations

Title
Invasive neurophysiological correlates of human visual and motor systems

Permalink
https://escholarship.org/uc/item/9654r8x2

Author
Niketeghad, Soroush

Publication Date
2021

Peer reviewed|Thesis/dissertation

eScholarship.org Powered by the California Digital Library
University of California

UNIVERSITY OF CALIFORNIA

Los Angeles

Invasive neurophysiological correlates of human visual and motor systems

A dissertation submitted in partial satisfaction of the requirements for the degree Doctor of Philosophy in Bioengineering

by

Soroush Niketeghad

2021

©Copyright by

Soroush Niketeghad

2021

ABSTRACT OF THE DISSERTATION

Invasive neurophysiological correlates of

human visual and motor systems

by

Soroush Niketeghad

Doctor of Philosophy in Biomedical Engineering

University of California, Los Angeles, 2021

Professor Wentai Liu, Chair

Functional brain mapping correlates the brain anatomy and physiology to our perceptions and behaviors and allows for development of neurotherapeutic technologies. Therapeutic direct stimulation of the cortex and subcortical areas, despite its high invasiveness, remains a crucial technique for studying the neurophysiological correlates of brain networks. For example stimulation of visual cortex for restoring vision and deep brain stimulation for treatment of movement disorders provide unique opportunities to study the neural correlates of visual perception and motor behaviors. While these techniques have been around for several decades, the functional role of targeted areas and their interaction with electrical stimulation is yet to be fully understood. This work takes advantage of invasive neurosurgical techniques to refine the

functional mapping of visual and motor systems. Through the application of a cortical visual prosthesis we created subject-specific retinotopic maps of the visual cortex. The functional efficacy of these maps were tested in blind subjects and was shown to restore some degree of vision allowing them to localize a static object and identify the direction of a moving target. Moreover we used intra-operative recordings from ventrolateral thalamus and sensorimotor cortex of patients with essential tremor to investigate the functional role of thalamo-cortical network in voluntary movement. By analyzing different measures of oscillatory power and connectivity, we depicted a casual mechanism in which thalamic low frequency oscillations modulate the movement-related cortical broad-band gamma activity. This understanding of visual and motor maps can advance the efficacy of visual prosthesis and deep brain stimulation therapy by highlighting the functional organization of the visual cortex and oscillatory mechanisms of thalamo-cortical interactions.

The dissertation of Soroush Niketeghad is approved.

Nader Pouratian

Nanthia Suthana

Martin M. Monti

Wentai Liu, Committee Chair

University of California, Los Angeles

2021

TABLE OF CONTENTS

©Copyright by i

Soroush Niketeghad i

2021 i

1 Introduction 1

1.1 The importance of invasive neurophysiological studies 1

1.2 Functional mapping of primary visual cortex via application of cortical visual prosthesis 2

1.3 Functional mapping of motor system based on movement-related dynamics of thalamo-cortical oscillations 4

2 An overview of cortical visual prostheses 7

2.1 Different approaches of creating artificial vision 8

2.1.1 Retinal stimulation 8

2.1.2 Stimulation of optic nerve and thalamus 9

2.1.3 Stimulation of visual cortex 10

2.2 History of cortical visual prostheses 10

2.3 Current State of cortical visual prostheses 12

2.3.1 The ICVP Project 14

2.3.2 CORTIVIS 15

2.3.3 Gennaris 16

2.3.4 Orion 18

2.4 Challenges and potential solutions 19

2.4.1 Subject selection 19

2.4.2 Electrode array design 20

2.4.3 Psychophysical testing 22

2.4.4 Machine learning 24

2.5 Discussion 25

3 Assessing safety and feasibility of subdural cortical visual stimulation 26

3.1 Methods 26

3.1.1 Subject selection 26
3.1.2 System overview and Surgical Procedure 27
3.1.3 Data acquisition and experimental design 28
3.2 Results 29
3.2.1 Impedances 30
3.2.2 Phosphene mapping 31
3.2.3 Phosphene thresholds 32
3.2.4 Consistency of the thresholds 36
3.2.5 Phosphene intensities 37
3.2.6 Adverse events 38
3.3 Discussion 39
4 Functional mapping of the primary visual cortex 44
4.1 Subjects and Device information 45
4.2 Data Acquisition 46
4.2.1 Anatomical Template Mapping Data 46
4.2.2 Absolute experimental Mapping Data 47
4.2.3 Relative experimental Mapping Data 47
4.3 Mapping Methods 48
4.3.1 Anatomical Template Mapping Procedure 48
4.3.2 Experimental Absolute Mapping Technique 50
4.3.3 Experimental Relative Mapping Technique 51
4.4 Mapping Evaluation 52
4.4.1 Evaluation using relative mapping experiment 52
4.4.2 Functional vision evaluation using simulation of direction of motion 53
4.4.3 Functional vision tests using camera 54
4.5 Results 55
4.5.1 Anatomical Template Mapping Results 55
4.5.2 Experimental Absolute Mapping Results 56
4.5.3 Mapping Evaluation Results using Relative Mapping Experiment 62
4.5.4 Functional Mapping Evaluation Results using Simulation of Direction of Motion 62
4.5.5 Visual Function Tests using the Orion Camera 65

4.6 Discussion 66
5 Functional mapping of motor system based on movement-related dynamics of thalamo-cortical oscillations 69
5.1 Subjects 70
5.2 Surgical procedures 71
5.3 Data acquisition 72
5.4 Experimental Protocol 73
5.5 Data processing 73
5.5.1 Electrode localization 73
5.5.2 Structural connectivity 73
5.5.3 Signal pre-processing 75
5.5.4 Power spectral density 76
5.5.5 Phase synchronization and directional connectivity 76
5.5.6 Phase amplitude coupling (PAC) 76
5.5.7 Partial Phase amplitude coupling 77
5.6 Statistical analysis 79
5.6.1 Power spectral density 79
5.6.2 Phase synchronization 79
5.6.3 Phase amplitude coupling 80
5.6.4 Band related statistics 80
5.7 Results 81
5.7.1 Clinically-defined VL is structurally connected to the pre-central gyrus 81
5.7.2 Movement is associated with redistribution of power 81
5.7.3 Phase coupling between VL and CS is dampened during movement 83
5.7.4 Alpha/low-beta to broadband-gamma PAC is suppressed during the movement 84
5.7.5 Validating the partial PAC method using a simulated dataset 87
5.7.6 Cortical PAC has confounding bias on the observed thalamocortical PAC 90
5.8 Discussion 90
6 Conclusion & future work 95
7 References 99

LIST OF FIGURES

Figure 2-1 Components of a cortical visual prosthesis (with permission from SecondSight Inc.) 14

Figure 2-2 WFMA structure including an ASIC (chip), microelectrodes (shorter pins), and wireless coil located on top of the ASIC providing transcutaneous inductive coupling (with permission from Laboratory of neural prosthetic research at IIT)..... 15

Figure 2-3 Overview of the implantation site of the electrode array on the surface of the lateral occipital cortex (Fernández & Normann, 2017) (with permission from the author)..... 16

Figure 2-4 Electrode placement and implantation site for Orion (with permission from SecondSight Inc.)..... 18

Figure 3-1 Phosphene mapping generated based on integration of subject's drawings and descriptions. Red shaded areas correspond to phosphene mapping experiment performed at month 8 of the study (3 trials per channel) and blue shaded areas correspond to the month 19 of the study (one trial per channel). Phosphene drawings are mapped to the polar space and connected to their corresponding electrode shown on the MRI slice of the right medial occipital lobe. Orange line represents the calcarine sulcus. 30

Figure 3-2 Impedances measured at the beginning of each session during the 81 week study. A) Box plot of the impedance values representing the median, first and third quartiles as well outliers as dots. B) Percent change of the impedance for each contact compared to the first measurement (week 1) over time. Red shaded area indicates ±20% change (chosen arbitrarily for scale). Numbers on the right axis represent the percent change of the last measurement (week 81) relative to initial measurement. 31

Figure 3-3 Current amplitude thresholds for different pulse width values for contacts A1(A) and B2(B). C and D represent the same data in the form of charge per trial (i.e., total charge over the 250 ms burst duration). Curves in A and B as well as lines in C and D were fitted to the data for better understanding of the relationship between stimulation parameters. 33

Figure 3-4 Current amplitude thresholds for different frequency values for contacts A3 (A) and B2 (B). C and D represent the same data in the form of charge per trial (i.e., total charge over the 250 ms burst duration). Curves in A and B as well as lines in C and D were fitted to the data for better understanding of the relationship between stimulation parameters. E and F represent the threshold testing experiment results for different frequencies and burst durations. Controlling the burst duration allows for delivering different number of pulses for each pulse frequency. Surface areas of the circles are proportional to the level of current thresholds. 35

Figure 3-5 Percent change of the threshold levels for current amplitude (A) and charge per trial (B) thresholds. Dashed lines correspond to the measurement during pulse interval threshold testing and straight lines indicates to the measurements during frequency threshold testing at months 1, 7 and 18 of the study. The ±20% change interval is highlighted by the red shaded bars for each contact. 37

Figure 3-6 Subjective intensities of the perception based on the amount of charge delivered. Increasing the delivered charge was achieved by increasing the current amplitude (amplitude modulation) or frequency (frequency modulation). 38

Figure 4-1 Visual field mapping procedure based on creating a subject specific anatomical map of the visual cortical surface and electrode array localization. 49

Figure 4-2 Cortical surface eccentricity (A) and polarity (B) maps for each subject. Visual field phosphene maps created based on the subject specific anatomical template (C). Phosphene map

for each subject. Columns of electrodes on the electrode array (right) are color-coded and plotted in the visual field (left) to demonstrate the nonlinear characteristic of these maps..... 56

Figure 4-3 The absolute experimental map of the visual field for each subjects. To avoided crowded maps each map is color-coded and illustrated in multiple figures corresponding to the electrode columns on the array (top). He center of each ellipse represents the average location of a phosphene produced by each electrode and the borders of the ellipse represent the standard deviation of location on x and y axes..... 57

Figure 4-4 (A) Variability of subject responses to stimulation of each electrode in terms of angular area of the standard deviation. (B) Normalized overlap between the standard deviation areas for each pair of phosphenes in terms of the percentage ratio of the overlapped area compared to the standard deviation area of each phosphene on the y axis. 58

Figure 4-5 the anatomical template and experimental absolute and relative phosphene maps for each subject illustrated in two figures to avoid crowded representation. Each map is color-coded based on the rows of electrodes on the array (top right)..... 61

Figure 4-6 Mean errors for the anatomical template map (anat tmp) and experimental absolute (abs exp) and relative (rel exp) maps based on phosphene connection experiment results. All statistical significance of differences are based on paired-sample t-test with $p<0.05$)..... 62

Figure 4-7 (A) Total error calculated by evaluating subjects' responses to a simulated moving object based on anatomical template map and experimental absolute and relative maps. (B) The distribution of error over different directions of motion for each map and subject..... 64

Figure 4-8 Results of visual function tests using experimental absolute map on months 6, 12, and 24 of the study. Mean errors were compared between device OFF and ON states using 2-tailed t test ($p<0.05$)..... 65

Figure 5-1 A) Our hypothetical model of the thalamocortical oscillations. B) Placement of the ECoG strip in relation to Central Sulcus over the reconstructed brain surface. C) Three cortical bipolar contacts representing the Central Sulcus (CS) and precentral gyri (postCS and preCS). 70

Figure 5-2 Average whole brain binary structural connectivity map seeded from the VL (contacts 0-1). Red represents areas across the whole brain with strong structural connectivity (probabilistic tractography binerized at threshold value of 0.01) to VL (Red) and gr een is the result of application of a pre-central gyrus mask. 75

Figure 5-3 Each cortical amplitude A was assigned to a 2D phase bin of thalamic phase φi and cortical phase θk and $EA|\varphi i, \theta k$ was calculated by averaging the amplitudes assigned to each phase bin. The probability distribution of amplitudes for each thalamic phase bin $EA|\varphi i$ can be calculated by weighted averaging the $EA|\varphi i, \theta k$ values based on the probability distribution of cortical phase for each thalamic phase $P\theta k|\varphi i$. 78

Figure 5-4 Distribution of power in VL and sensorimotor cortex during rest and movement trials. A) Group average,Power spectral density normalized to the resting state in the frequency range of 5-300 Hz. highlighted areas indicate the frequencies with significant spectral power difference between rest (blue) and movement (red). B) Frequency band powers for alpha/low-beta, high-beta, and broadband-gamma during rest and movement. Significant differences are marked by the asterisk (*) indicating significance at P<0.05 level. 82

Figure 5-5 Measures of thalamocortical connectivity between VL and sensorimotor cortex during rest and movement trials. A) dwPLI calculated in the frequency range of 5-300 Hz. Highlighted regions indicate the frequencies with significant dwPLI difference between rest (blue) and movement (red). B) Frequency band dwPLI for alpha/low-beta, high-beta, and broadband-gamma

during rest and movement. C) Resting state granger causality z-scores from VL to cortical contacts and vice versa. 84

Figure 5-6 A) Cortical PAC between the phase of cortical contacts and the amplitude of the same signal during rest and movement. B) Average cortical PAC between the phase of alpha/low-beta and amplitude of broadband-gamma activities during rest and movement. C) Thalamocortical PAC between the phase of VL and the amplitude of the cortical signals during rest and movement. D) Average thalamocortical PAC between the phase of alpha/low-beta and amplitude of broadband-gamma activities during rest and movement. E) Resting state thalamocortical partial PAC between the phase of VL and the amplitude of the cortical signals when the confounding bias of cortical phase was removed. F) Average thalamocortical PAC and partial PAC between the phase of alpha/low-beta and amplitude of broadband-gamma activities during rest. 86

Figure 5-7 A) Zoomed in segments of the simulated datasets. Simulated thalamic signal (blue) is a 13Hz sine wave and simulated cortical signal (red) is the combination of a 13Hz and a 150Hz sine waves. For the illustration purpose the random white noise in both signals is not included in this figure. Seg#2 of dataset#1 contains thalamic and cortical signals with phase synchrony cortical and thalamocortical PAC simultaneously. For dataset#2, seg#1 contains thalamocortical PAC, seg #2 contains thalamocortical phase coupling and seg#3 contains cortical PAC. B) Z-scores for thalamocortical and cortical PAC as well as thalamocrtical partial PAC for the simulated datasets. 89

LIST OF TABLES

Table 1 Subjects participated in Orion clinical study. 46

Table 2 Patients demographics and clinical information 71

Acknowledgement

I would like to express my special appreciation to my advisor Dr. Nader Pouratian. All the unique opportunities to study the human brain were only possible due to his tremendous skills and devotion to scientific research. Moreover his encouragement and priceless mentorship taught me the way of scientific research and kept me on the right path as he always asks “What is the scientific question you are trying to ask?”. I would also like to thank my committee chair, Professor Wentai Liu and Professor Nanthia Suthana and Professor Martin M. Monti for serving as my committee members. Also I want to thank my lab mates Mahsa Malekmohammadi, William Speier, and Evie Tsolaki for their help and guidance and special thanks to all the Essential Tremor patients that allowed us to conduct this valuable research. Finally special thanks to Michelle Armenta, Joeseph Bell and all the SecondSight staff as well as the blind subjects that devoted themselves to improve the life of blind individuals.

VITA

EDUCATION

MSc Biomedical Engineering	University of California, Los Angeles	2018
MSc Computer Engineering	University of Denver	2015
BSc Electrical Engineering	Isfahan University of Technology	2013

PUBLICATIONS AND PATENTS

Niketeghad S, Malekmohammadi M, Speier W, Tsolaki E, Sparks H, AuYong N, Pouratian N. A novel method to assess the cross-site phase amplitude coupling (Manuscript under preparation).

Caspi A, Barry MP, Patel UK, Salas MA, Dorn JD, Roy A, Niketeghad S, Greenberg RJ, Pouratian N. Eye movements and the perceived location of phosphenes generated by intracranial primary visual cortex stimulation in the blind. Brain Stimulation. 2021 May 13.

Barry MP, Salas MA, Patel U, Wuyyuru V, Niketeghad S, Bosking WH, Yoshor D, Dorn JD, Pouratian N. Video-mode percepts are smaller than sums of single-electrode phosphenes with the Orion® visual cortical prosthesis. Investigative Ophthalmology & Visual Science. 2020 Jun 10;61(7):927-.

Beauchamp MS, Oswalt D, Sun P, Foster BL, Magnotti JF, Niketeghad S, Pouratian N, Bosking WH, Yoshor D. Dynamic stimulation of visual cortex produces form vision in sighted and blind humans. Cell. 2020 May 14;181(4):774-83.

Mahoor MH, Niketeghad S, Hebb AO, Hanrahan SJ, Nedrud J, Golshan HM, inventors; University of Denver, assignee. Motor task detection using electrophysiological signals. United States patent US 10,588,534. 2020 Mar 17.

Niketeghad S, Muralidharan A, Patel U, Dorn JD, Bonelli L, Greenberg RJ, Pouratian N. Phosphene perceptions and safety of chronic visual cortex stimulation in a blind subject. Journal of neurosurgery. 2019 May 31;132(6):2000-7.

Niketeghad S, Pouratian N. Brain machine interfaces for vision restoration: the current state of cortical visual prosthetics. Neurotherapeutics. 2019 Jan;16(1):134-43.

Niketeghad S, Hebb AO, Nedrud J, Hanrahan SJ, Mahoor MH. Motor task detection from human STN using interhemispheric connectivity. IEEE Transactions on Neural Systems and Rehabilitation Engineering. 2017 Sep 21;26(1):216-23.

Niketeghad S, Hebb AO, Nedrud J, Hanrahan SJ, Mahoor MH. Motor task event detection using subthalamic nucleus local field potentials. In2015 37th Annual International Conference of the IEEE Engineering in Medicine and Biology Society (EMBC) 2015 Aug 25 (pp. 5553-5556). IEEE.

Niketeghad S, Hebb AO, Nedrud J, Hanrahan SJ, Mahoor MH. Single trial behavioral task classification using subthalamic nucleus local field potential signals. In2014 36th Annual International Conference of the IEEE Engineering in Medicine and Biology Society 2014 Aug 26 (pp. 3793-3796). IEEE.

Zadeh MZ, Niketeghad S, Amirfattahi R. A PLL based adaptive power line interference filtering from ECG signals. InThe 16th CSI International Symposium on Artificial Intelligence and Signal Processing (AISP 2012) 2012 May 2 (pp. 490-496). IEEE.

1 Introduction

Functional brain mapping draws a picture of how brain systems and their interactions correlate with perception and behavior. This allows for correlation of abnormalities in various brain networks with a patient's symptoms to provide proper treatments such as surgical intervention or neuromodulation. Moreover a patient specific functional map of the brain is an essential step towards development of a neural prosthesis to compensate for patient's deficits. Since its birth in 19th century, functional brain mapping has been radically refined through novel brain mapping techniques and modernization of the brain imaging equipment. Direct stimulation of the cortex and subcortical areas, despite its high invasiveness, remains a crucial technique for studying the neurophysiological correlates of human perception and behavior. Stimulation of visual cortex to restore some degree of vision to blind individuals was introduced more than 50 years ago however little progress has been made with respect to safety and efficacy. Moreover deep brain stimulation has been an effective therapy for treatment of movement disorders over the last three decades and despite expanding application to treatment of epilepsy and psychiatric disorders, its fundamental mechanism is yet to be fully understood.

1.1 The importance of invasive neurophysiological studies

Invasive Neurophysiological studies provide unique opportunities to access the human brain that would have been impossible or extremely challenging via non-invasive approach. For instance, procedures such as electrode implantation for treatment of epilepsy present unique opportunities to directly access the human visual cortex and understand the mechanisms of visual perception(W. Bosking et al., 2018). Invasive therapies can reach even further than the cortical tissue and access the deep brain nuclei. For example deep brain stimulation (DBS) therapy for movement disorders such as essential tremor (ET) allows for recording local field potentials (LFP) from the thalamus

and provides enough temporal resolution to study the oscillatory mechanism of thalamo-cortical network(Malekmohammadi et al., 2015).

The invasive nature of these studies not only furthers our reach to the human brain but also improves spatial and temporal resolution of neurophysiological signals compared to non-invasive approaches. Due to greater distance between cortical sources and extra-cranial sensors, non-invasive techniques are less sensitive to high frequency activity and thus may not reveal the full spectrum of an event-related power augmentation(Nathan E. Crone et al., 2011a). Hence analysis of high frequency local activities such as cortical broadband-gamma (60-200Hz) requires invasive recording of LFP signals(Petroff et al., 2016). However the down side of the invasive approach is that it is limited to the specific circumstances of the invasive therapy. For instance DBS electrode implantation surgery provides a short window of time to record from DBS electrodes as well as temporary placed ECoG strips for research purposes. During this time, patient is awake and able to perform behavioral tasks in the operating room however his/her movement and attention are extremely limited. Also, the number of deep brain electrodes and their location is limited to the requirements of the DBS surgical procedure.

1.2 Functional mapping of primary visual cortex via application of cortical visual prosthesis

When the light is projected on the retina, optical information is converted to neural spiking activity via photoreceptor cells, transmitted via retinal ganglion cells to the lateral geniculate nucleus of the thalamus, and conveyed to the primary visual cortex via thalamic synapses. Retinotopy of the visual cortex maps the visual input from the retina to the neurons of the V1 area. The first retinotopic map of the human primary visual cortex was created by Dr. Gordon Holmes when analyzing the disturbances of vision reported by World War I soldiers suffering from gunshot

injuries to the visual areas(Holmes, 1918). Holmes map depicted an orderly, topographic representation of the striate cortex where the representation of horizontal meridian runs along the base of the calcarine sulcus. The functional organization of this retinotopic map was confirmed by Brindley and Levin in 1968 based on localizing the visual perceptions (phosphenes) elicited by electrical stimulation of the primary visual cortex(Brindley & Lewin, 1968). Brindley and Levin's work was the first systematic efforts to restore some vision using stimulation of the visual cortex and it was continued by Dobelle and his colleagues(W. H. Dobelle & Mladejovsky, 1974b). They implanted cortical surface electrodes over the right medial occipital pole of previously sighted blind subjects. Stimulation of most of the electrodes elicited phosphenes located in a retinotopic order in different areas of the visual field. In Dobelle's earlier experiments, simple identifiable patterns (square or letter "L") were produced by stimulating multiple electrodes(W. H. Dobelle et al., 1974). This approach was followed by implementation of a "Cortical braille" capable of spelling the letters in a full sentence faster and more accurately than traditional tactile braille(Wm H. Dobelle et al., 1976). These studies demonstrated the feasibility of visual cortical prostheses in conveying potentially useful information. However, cases of seizure and device malfunction have been reported necessitating further study of safety and long term effectiveness of this approach(Naumann, 2012). Moreover, while previous studies described charge density thresholds for eliciting phosphenes and that phosphene perception changes with modification of stimulus parameters (amplitude, frequency, pulse-width and burst duration)(W. H. Dobelle & Mladejovsky, 1974b; Schmidt et al., 1996a), the effects of each parameter on the threshold and phosphene qualities were not completely characterized. Dobelle began to commercialize the device outside the United States in 2002 and 16 patients were implanted with a partially externalized device. The results of this project however were not published and study was terminated after Dr. Dobelle

passed away in 2004.Chapter 2 provides a brief description of different approaches toward visual prostheses followed by an extensive overview on the history, current state and challenges of developing cortical visual prostheses.

Through the application of cortical visual prosthesis we aim to refine the functional mapping of the primary visual cortex. We started with a pilot study reproduce previous results under current clinical safety standards and to progress the field. Chapter 3 describes the results of our two-year case study on a blind subject where we assessed the safety and feasibility of an off-the-shelf neurostimulator in eliciting visual perception. Followed by our efforts to assess safety and feasibility of subdural cortical visual stimulation we received the FDA approval for the first clinical trial of Orion, a subdural neurostimulator designed and built by SecondSight Inc. as a cortical visual prosthesis. Four blind subjects were implanted with Orion at UCLA and we started the clinical testing of the device while monitoring for adverse events. One of our main challenges was to map the visual field onto the electrode array located on the surface of the visual cortex to be able convert the image of the visual field to a sequence of electrical pulses delivered via a 60-electrode subdural array. Chapter 4 presents multiple mapping techniques inspired by the previous studies and improved by our current understanding of the visual cortex. Furthermore in the absence of a ground truth for the exact location of phosphenes, we propose evaluation paradigms to estimate the accuracy of phospehene localization for each mapping technique.

1.3 Functional mapping of motor system based on movement-related dynamics of thalamo-cortical oscillations

Oscillations form a ubiquitous feature of the functional brain mapping particularly in motor network where different phases of movement planning and execution is associated with

synchronization/desynchronization of specific oscillatory frequencies(Brittain & Brown, 2014). Movement initiation is associated with desynchronization of alpha (8-12Hz) and beta (12-35Hz) oscillations in sensorimotor cortices (N E Crone et al., 1998; Kilavik et al., 2013; Kondylis et al., 2016; Malekmohammadi, AuYong, Ricks-Oddie, et al., 2018) and basal ganglia (Cassidy et al., 2002; Foffani et al., 2005; Malekmohammadi, AuYong, Ricks-Oddie, et al., 2018; Singh & Bötzel, 2013; Tsang et al., 2012; Tsiokos et al., 2013, 2017) and increases in gamma oscillatory activity (60-200Hz) in motor cortical areas (N E Crone et al., 1998; Nathan E. Crone et al., 2006; Dalal et al., 2008; Ohara, 2000; Pfurtscheller et al., 2003). While oscillatory changes in distinct nodes of human brain motor network have been described, our understanding of how these nodes interact is not well developed, particularly with respect to the causal relationship across nodes in the brain. Oscillatory activity in the thalamus may theoretically serve to directly modulate or gate cortical gamma band activity. Alternatively, thalamic oscillations may serve to modulate similar low frequency oscillatory activity in structurally-connected cortical regions which in turn influence local gamma band activity. The distinction lies in whether the thalamus directly or indirectly (via phase-based coupling) modulates cortical function. While thalamo-cortical relationships were analyzed in a recent publication by Opri and colleagues (Opri et al., 2019), the question of relative contributions and influence of thalamic and cortical phase encoding frequencies on high frequency cortical activity remains undefined.

One model that has been proposed for interaction both within and across nodes is via cross frequency coupling, including phase-based coherence and phase-amplitude coupling (PAC), the latter of which can serve as a mechanism to link information conveyed by slower oscillatory activity that occur across large-scale brain networks to fast, local cortical processing(Canolty & Knight, 2010). Patients with Parkinson disease (PD) and essential tremor (ET) have exaggerated

resting state sensorimotor PAC (De Hemptinne et al., 2013; Kondylis et al., 2016). Moreover, therapeutic deep brain stimulation (DBS) of subthalamic nucleus (STN) and globus pallidus internus (GPi) suppresses cortical PAC in PD patients(De Hemptinne et al., 2015a; López-Azcárate et al., 2010; Malekmohammadi, AuYong, Ricks-Oddie, et al., 2018) highlighting the potential involvement of subcortical nuclei in regulating and perhaps even driving cortical PAC. We have previously shown a temporally causal role between thalamo-cortical coherence and cortical PAC across structurally-defined thalamo-cortical networks(Malekmohammadi et al., 2015) and others have shown similar results in other systems, such as the visual pathways(Saalmann et al., 2012). While prior work has demonstrated causal flow of low frequency oscillations from subcortical to cortical structures and an intimate relationship between phase-coupling and PAC, no analyses to date have been able to disentangle the relative contributions of thalamic and cortical low frequency oscillations to PAC.

In chapter 5 we use the intra-operative LFP recordings from the thalamus and sensorimotor cortex of ET patients to confirm the previous findings on movement-related cortical oscillations(N E Crone et al., 1998; Kondylis et al., 2016; Malekmohammadi et al., 2015; Opri et al., 2019) and draw a path of thalamo-cortical interactions using different measures of oscillatory coupling. Furthermore we apply a novel technique of "partial phase amplitude coupling" to clarify the casual role of this network.

2 An overview of cortical visual prostheses

The number of blind individuals has been increasing around the world and the United States. Globally, 32.4 million people were blind in 2010 which has increased by 600,00 since 1990 (Stevens et al., 2013). In 2015, a total of 1.02 million people were blind in the United States and it is projected to double to approximately 2.01 million people by 2050 (Varma et al., 2016). The negative impacts of this condition on individual physical and mental health include a higher risk of chronic health conditions (Crews & Campbell, 2004), unintentional injuries (Ivers et al., 2000), social withdrawal (Jones et al., 2009), depression (Jones et al., 2009; Zhang et al., 2013), and mortality (Freeman et al., 2005; Zheng et al., 2014). From a socioeconomic standpoint, blindness has a negative effect on educational and occupational opportunities as well as medical expenditure. In the United States, the excess medical expenditure (compared to individuals without visual impairments) was $2.5 billion in 2004 which was primarily attributed to homecare (Frick et al., 2007). Therefore, any effort leading to improvement in day to day life of these individuals not only improves their quality of life but also relieves a significant economic cost.

Common causes of blindness include cataracts , glaucoma, macular degeneration, infections, vitamin A deficiency, diabetes, and trauma (Congdon et al., 2003). Although in some of these conditions, blindness can be prevented in earlier stages (Javitt et al., 1996; Oliver et al., 2002; Resnikoff & Pararajasegaram, 2001; West & Sommer, 2001), many cases lead to irreversible loss of vision. Sensory substitution is an extensively explored approach to channel some degree of information via non-visual senses such as tactile (Bach-y-Rita & W. Kercel, 2003; Deroy & Auvray, 2012) or audible signals (Capelle et al., 1998; Hanneton et al., 2010). Although sensory substitution is non-invasive and easily available for majority of blind individuals, the quantity and

quality of information perception is extremely limited (Lenay et al., 2003). Hence a more direct approach may be helpful to generate a visual perception of the surrounding environment.

Visual neural prostheses represent an approach of generating visual perception via direct stimulation of visual pathway. The basic principle of visual prostheses is that any segment of the visual pathway can potentially interface with a prosthetic that captures the image of the visual field via a camera, properly maps it into temporally and spatially specific signals and stimulates the visual pathway accordingly. Stimulation in its simplest form induces perception of a spot of light called a phosphene and it could be used as a building block to construct a representation of the visual scene which conveys helpful information for communication and mobility. The site of stimulation is dependent of the pathology of the blindness and is chosen in a way that bypasses the damages segment of the visual pathway. Current visual prosthesis approaches include stimulation of the retina, optic nerve, lateral geniculate nucleus of the thalamus, optic radiations and visual cortices. In this chapter we briefly describe the different approaches of visual prostheses and extensively review the history and current state of visual cortical prostheses.

2.1 Different approaches of creating artificial vision

2.1.1 Retinal stimulation

Retinal prostheses aim to stimulate the surviving population of inner retina, retinal ganglion cells and/or bipolar cells in individuals with retinitis pigmentosa or age-related macular degeneration (Eyal Margalit et al., 2002). In theory, such an approach is the most advantageous as stimulation occurs at the earliest stage of visual perception, prior to any integration or “post-processing” of visual signals in the brain, including the lateral geniculate nucleus. Argus II (Second Sight Medical Products) is the first commercially approved retinal prosthesis using the epiretinal approach, in which the microelectrode array is implanted on the retinal surface near the nerve fiber directly

stimulating the ganglion cells (Luo & da Cruz, 2016). Argus II improved subjects performance in spatial-motor tasks (Ahuja et al., 2011a; Luo et al., 2015), detection of motion (Dorn et al., 2013), reading (Da Cruz et al., 2013; Sahel et al., 2011), and face recognition (Stanga et al., 2013). Subretinal implants are another approach for retinal prosthesis in which the electrode array sits on the outer surface of the retina relying on normal processing of inner and middle retinal layers (Weiland et al., 2005); Alpha-IMS is a subretinal implant that has been approved for commercial use in Europe (Edwards et al., 2018) and is shown to restore some level of light perception, motion detection, visual acuity and reading ability (K Stingl et al., 2012; Katarina Stingl et al., 2013; Zrenner et al., 2011). Retinal implants are currently the only visual prostheses that have approval for commercial use however potential candidates for such devices are a small portion of the blind population (Ammann et al., 1965; Bundey & Crews, 1984; Bunker et al., 1984; Gröndahl, 1986; Haim, 2002; Hu, 1987).

2.1.2 Stimulation of optic nerve and thalamus

Stimulation of the optic nerve has also been shown to elicit phosphenes (Veraart et al., 1998). Veraart et al. utilized a spiral cuff electrode with four contacts. Subject were able to discriminate the orientation of lines without error and recognize simple patterns with a recognition score of 63% (Veraart et al., 2003). This approach however requires an intact optic nerve and may not be applied to a large population of blind individuals. Deep brain stimulation of thalamus in proximity to the lateral geniculate nucleus (LGN) and optic radiations results in visual sensations (Marg & Dierssen, 1965). Microstimulation of LGN has been investigated in animal models based on visual saccades (Panetsos et al., 2011). Since the LGN is physically adjacent to the targets of deep brain stimulation for movement disorders, surgical access would require minor modifications to the common implant techniques(Pezaris & Reid, 2007). However, given the relatively small size of

LGN (6-7mm on a side with a volume of 250±50 mm^3)(Andrews et al., 1997), a dense electrode array is required to elicit perceptions spanning the visual field and therefore phosphene perception in human trials is yet to be explored.

2.1.3 Stimulation of visual cortex

Stimulation of early areas of the visual cortex (V1, V2, and V3) elicits perception of phosphenes and is used to develop cortical visual prosthetics. In this chapter we extensively address this cortical stimulation approach and provide an insight on the current state as well as current challenges of visual cortical prostheses.

2.2 History of cortical visual prostheses

Eliciting visual perception via electrical stimulation of the visual cortices was first reported in a case study by Löwenstein and Borchardt in 1918 where a wounded soldiers were able to see flickering light perceptions on the opposite half of their visual field after stimulation of occipital lobe (Löwenstein & Borchardt, 1918). This was then followed by the work of Förster and Krause who were able to expose the human occipital lobe under local anesthesia and reliably induce perception of phosphenes (Foerster, 1929; Krause, 1924). These studies set the groundwork for the first systematic effort to develop a visual cortical prosthetic by Brindley and Lewin (Brindley & Lewin, 1968). They implanted a blind subject with an intracranial array of 80 electrodes molded it to fit the calcarine sulcus and neighboring cortex of the right hemisphere. They were able to successfully elicit phosphenes in different areas of the visual field which provided a proof of feasibility for visual cortical prosthetics. This array was physically connected to an extracranial array of radio receivers that allowed for selective activation of intracranial electrodes.

Dobelle reported similar observations on a group of 15 sighted patients who were undergoing surgery for other clinical reasons and gathered a useful body of data on the proper electrode placement as well as the effects of electrode size and stimulation parameters on the quality of perceptions (W. H. Dobelle & Mladejovsky, 1974b). Subsequently, he implanted two blind individuals with a 64-electrode array and were able to elicit simultaneous phosphenes representing simple patterns including a square and a reverse letter "L" (W. H. Dobelle et al., 1974). In another experiment, they were able create English letters using 6 electrodes with phosphenes scattered in the visual field (Wm H. Dobelle et al., 1976). Using a combination of sequential and simultaneous stimulation of these 6 electrodes they developed a "cortical braille" that was able to present randomized alphabets and synthetize sentences. One of the subjects performed with up to 85% accuracy on recognizing the alphabets and was able to read short sentences with missing or misreading a few words. Moreover, they developed a portable version of the device that was capable of receiving input from a video camera (Wm H. Dobelle, 2000). They reported that the subject were able to read a 6 inch square "tumbling E" at five feet, as well as Snellen letters, HOTV test, Landolt rings, and Lea figures of similar size.

While Dobelle was making progress on improving the functionality of prosthetics with subdural electrode arrays, the NIH formed the neural prosthesis program that took another approach to decrease the current threshold required for eliciting phosphenes (Bak et al., 1990). Based on a previous study on non-human primates (Bartlett & Doty, 1980), they proposed that intracortical stimulation of striate cortex can generate more stable phosphenes with lower current thresholds. They inserted penetrating electrodes into the occipital lobe of three sighted volunteers whom were undergoing occipital craniotomies under local anesthesia. All subjects reported perception of phosphenes elicited by currents (10-300 μA) significantly lower of the threshold amount for

subdural electrodes (600-2000 µA). Following their success in sighted individuals, they implanted penetrating microelectrodes into the occipital lobe of a blind individual (Schmidt et al., 1996b). The microelectrode leads were assembled into groups of 8 or 10 and connected to the cables that exited the scalp through 4 separate incisions. 34 out of 38 electrodes were able to elicit phosphenes with threshold currents of 2-77 µA at 200 pulses per second (twice the rate of stimulation used by Bak et al.). They characterized the effects of stimulation parameters on current thresholds and showed that an increase in pulse-width and duration of stimulation decreased the current thresholds. Unlike most cases reported by Brindley and Lewin, the phosphenes were not perceived as flickering; they determined the interval between the two consecutive pulses needs to be shorter than 25 ms in order to generate a persistent (non-flickering) perception. Increasing current amplitudes had different effects depending on the site of stimulation, resulting in larger phosphenes in some electrodes, smaller in others, and no change in others. They also reported that phosphenes could be perceived in different colors (blue, red, violet, yellow but never green), with suprathreshold stimulation tending to elicit white or yellow phosphenes. They explanted the device after four months and concluded that their experiments demonstrate the feasibility of intracortical visual prosthetics.

2.3 Current State of cortical visual prostheses

Today, several teams are working towards understanding perceptual effects of visual cortex stimulation and development of safe and reliable visual cortical prostheses. Epilepsy patients with electrodes implanted in the occipital lobe provide a valuable opportunity to study the stimulation effects of visual cortex (W. H. Bosking, Beauchamp, et al., 2017). Functional mapping of the visual cortex (Lee et al., 2000; Richard & Bosking, 2012; Winawer & Parvizi, 2016; Yoshor et al., 2007a, 2008) and understanding the psychophysical correlates of phosphene perception (W.

Bosking et al., 2018; W. H. Bosking, Sun, et al., 2017) in these patients have extended our understanding of artificial vision and is providing an extremely valuable insight for development of visual cortical prostheses.

Multiple sites across the world are currently developing and testing visual cortical prosthetics with a general design similar to the most recent design of Dobelle (Wm H. Dobelle, 2000). As depicted in Figure 2-1, the visual information is captured by a camera located on a glass or head band (Troyk, 2017). Pixel information is then fed to a Video Processing Unit (VPU) and converted to a continuous sequence of commands that activate a subset of electrodes and determine the stimulation parameters (amplitude and waveform) (Troyk, 2017). The commands are transferred to an implanted system that delivers patterned stimulation. While Dobelle and others achieved promising outcomes with their systems, one of the main disadvantages of their design was the risk of infection and device breakage due to chronically externalized connections (Rush & Troyk, 2012). Hence, current designs take advantage of the state of the art Application Specific Integrated Circuits (AISC) and coil fabrication techniques to create a wireless data and power link between internal and external units (Kim et al., 2006). Similar to previous works, both intracortical and surface stimulation approach are being investigated. Here, we provide a brief description of multiple projects that are currently in the device development or human experimentation phase.



Figure 2-1 Components of a cortical visual prosthesis (with permission from SecondSight Inc.)

2.3.1 The ICVP Project

The NIH neural prosthesis program ended in 1996 and reconstituted in 2000 as the Intracortical Visual Prosthesis Project (ICVP) at the Illinois University of Technology. While maintaining the intracortical stimulation approach, they developed a Wireless Floating Microelectrode Array (WFMA) to eliminate the use of wires and chronic incisions (Rush & Troyk, 2012). WFMA consists of 16 microelectrodes with different lengths located on a 2mm by 2mm ceramic substrate platform (Figure 2-2) (Troyk, 2017). An Application Specific Integrated Circuit (AISC) along with a micro-coil are embedded in the platform to facilitate wireless power and datalink between the electrodes and an extra-corporal telemetry controller (TC). The TC is able to communicate with multiple implanted WFMAs and control each electrode individually.

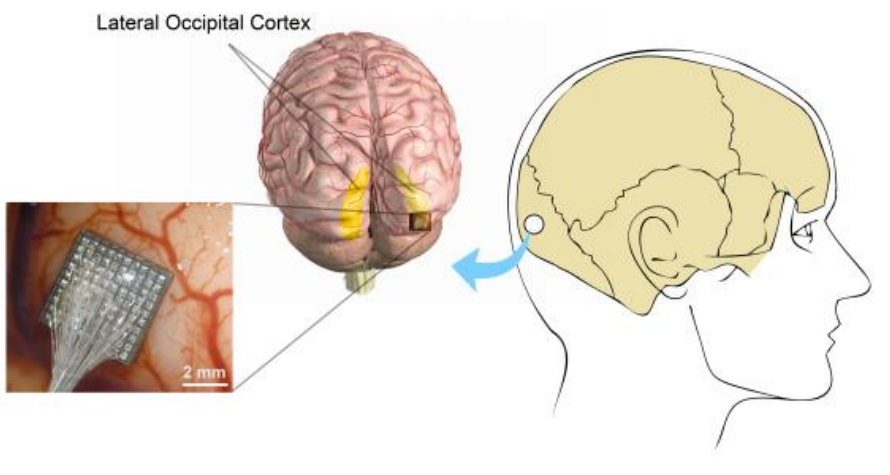


Figure 2-2 WFMA structure including an ASIC (chip), microelectrodes (shorter pins), and wireless coil located on top of the ASIC providing transcutaneous inductive coupling (with permission from Laboratory of neural prosthetic research at IIT)

Clinical testing of ICVP project has been planned but is not started yet (Troyk, 2017). The available anatomical areas are the occipito-dorso-lateral surface while placement of electrodes on the wall of medial occipital lobe will be avoided to minimize the surgical risks. This limits the exposed area for V1 and increases the chance of electrode placement over V2 and V3. For the early recipients of the device, the implantation of the WMFAs would be restricted to one hemisphere and about nine modules (144 electrodes). The anticipated components of experimental trials are phosphene threshold testing and intensity rating, phosphene mapping, and testing the ability to convey basic visual percepts such as simple geometric.

2.3.2 CORTIVIS

Cortical Visual Neuroprosthesis for the blind (CORTIVIS) is a multi-site project supported by the Commission of the European Communities aiming at developing an intracortical visual cortical prosthesis (Fernández & Normann, 2017). CORTIVIS takes advantage of the Utah Electrode Array (UEA) which has been FDA approved for long term human studies. UEA consists of 100 narrow silicon microelectrodes protruding 1.0–1.5 mm from a flat rectangular 4mm by 4mm base

that lays on the surface of the lateral occipital cortex (Figure 2-3) (Maynard et al., 1997). Similar to the ICVP project, an implanted AISC receives the stimulation parameters and power via wireless link from an external RF block connected to a pocket-size processor (Romero et al., 2006).

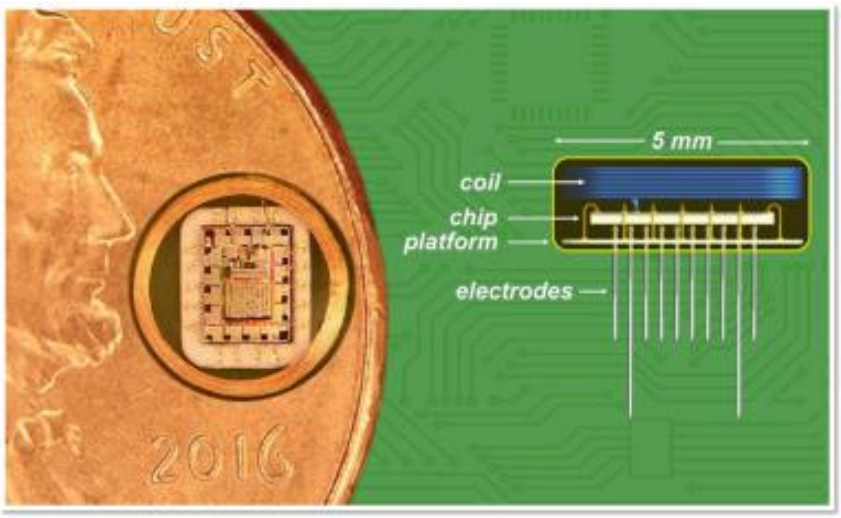


Figure 2-3 Overview of the implantation site of the electrode array on the surface of the lateral occipital cortex (Fernández & Normann, 2017) (with permission from the author)

Although clinical trials for the CORTIVIS project have not started, preliminary investigations have been conducted on epilepsy patients to establish the safety of the implantation procedure as well as phosphene assessment (Fernandez et al., 2015). All subjects perceived phosphenes and tolerated the procedure without complications. Stimulation of both early visual areas and extrastriate occipital cortex induced phosphenes with retinotopic representation. Phosphene were described as flashing, colored or uncolored lights and stars and their sizes ranged from a "pinpoint" to occupying almost the whole visual field depending on the location and stimulation parameters.

2.3.3 Gennaris

The Gennaris bionic vision system is an intracortical visual prosthesis developed by Monash Vision Group supported by the Australian Research Council. Similar to the ICVP project, Gennaris

uses a number of autonomous implant tiles to cover the visual cortex (Arthur James Lowery et al., 2017). Each ceramic tile holds 43 electrodes protruding from its base and contains a receiver coil and an ASIC. A custom-designed "Pocket Processor" extracts the useful features from the image captured by the camera and generates a pattern of electrode activation to create the most helpful information for the user depending on the task at hand (Arthur J. Lowery et al., 2015). They introduced the concept of Transformative Reality (TR) that instead of being restricted to the direct visual representation of a scene asks the following question: "What combination of sensors, processing and rendering gives the most usability?" (Li et al., 2013). This could be as a simple as an edge detection algorithm to present the boundaries of the objects or it can integrate additional data from the environment into the image and use more complicated image processing and machine learning algorithms. For example to help patients with navigating cluttered indoor areas, they developed a TR mode that renders the patches of empty ground as phosphenes. The algorithm detects the ground plane using RANSAC plane fitting and real-time accelerometer data by estimating the direction of gravity.

Although the clinical trials for Gennaris have not started yet, safety and efficacy of the system have been verified in multiple ways. Chronic implantations and stimulation of electrodes were performed in rat motor cortex and electrode impedances were measured along with the stimulation thresholds required to evoke motor output (C. Wang et al., 2013). Electrode impedances increased over the first four weeks of implantation and stabilized at weeks 5 and 6. Histology of the brain tissue collected after the implantation period demonstrated that healthy neurons were in close proximity to the neurons and there was minimal astrogliosis. Moreover, a sheep model was used to demonstrate the surgical implantation of Gennaris tiles. Preliminary data indicated the minimal damage to the cortex and wireless transmission of power and data between the external coil and

implanted tiles were achieved (Arthur James Lowery et al., 2017). Similar to the other intra-cortical electrode arrays, Gennaris tiles will niether be placed on the medial aspect of the hemispheres nor within the calcarine sulcus to prevent the damage to the adjacent cortex and ensure proper wireless communications. The initial plan is to insert up to 6 tiles (258 electrodes) above and below the calcarine sulcus. Psychophysics and patients training phase of the study will start with phosphene mapping and will followed by the integration of camera input.

2.3.4 Orion

Unlike other devices, the Orion device (Second Sight Medical Products) uses a surface grid for subdural stimulation of the visual cortex. Argus II is a retinal prosthetic device developed by the SecondSight that is commercialized and widely used specially in the United States. Orion inherits many features of Argus II including the external components (camera, VPU and transmitter coil) and frameware. The implantable components of Orion includes a receiver coil and internal circuit that sits on the skull (Figure 2-4) and controls the stimulation parameters delivered by the electrodes. The subdural electrode grid consists of 60 surface electrodes placed on the medial occipital lobe spanning a portion of calcarine sulcus.

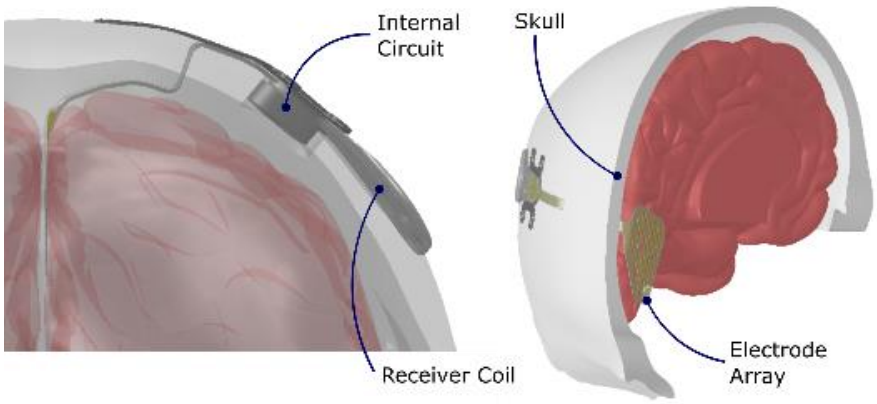


Figure 2-4 Electrode placement and implantation site for Orion (with permission from SecondSight Inc.)

Orion is the only visual cortical prosthesis that has started the clinical trials. A preliminary study was performed by our group on a blind individual using an off-the-shelf neurostimulator at the University of California Los Angeles. Two 4-contacts subdural electrode strips were implanted over the right medial occipital lobe spanning a portion of the calcarine sulcus. Electrode strips were connected to a Neuropace RNS stimulator (Neuropace RNS Inc., Mountain View, CA) placed within the cranium coplanar with the skull surface and was covered by the scalp. Phosphene mapping and threshold testing was performed for a period of 18 months and there were no clinical complication during and post implantation. Phosphenes were elicited by stimulation via all contacts and were scattered over the left side of the visual field. After confirming the safety and feasibility of cortical surface stimulation in generating phosphene perception, Orion received FDA approval for clinical trials. The device was implanted in six blind individuals at University of California Los Angeles and Baylor College of Medicine and all subjects reported perception of phosphenes. Chapter 4 provides further details on the clinical trial results and performance of the Orion.

2.4 Challenges and potential solutions

2.4.1 Subject selection

Although progress in development of visual cortical prosthesis is accelerating in the recent years, more work needs to be done to achieve a practical device. Hence, it is not ethical to expose patients with any potentially functional residual visual to invasive brain surgery as the potential risk of loss of residual vision can have severe functional impacts. Therefore performing visual function tests is an essential component for recruiting potential subjects as they estimate the subject's capability of performing real life tasks using his/her residual vision if any. Moreover, these tests can provide a quantified measurement of visual function which can be acquired at various time points during

the clinical trials and determine the device performance. For example square localization, direction of motion and grading visual acuity are visual function tests that have been used for potential recipients of retinal prosthetics as well as clinical trials for cortical prostheses (da Cruz et al., 2016). Given the advancement of commercially available retinal prostheses, subjects who are qualified for these implants may benefit from them and should be considered for that therapy rather than cortical implants (da Cruz et al., 2016; Merabet et al., 2007; Katarina Stingl et al., 2015).

2.4.2 Electrode array design

One major dilemma in designing cortical prosthetics is the choice between intracortical or surface electrodes. While both techniques have previously proven to be feasible, each has its own limitations.

2.4.2.1 Spatial specificity

Surface electrodes have relatively larger surface area and therefore require higher electrical currents to elicit phosphenes (Bak et al., 1990). In theory, when multiple electrodes are stimulated, these large currents can interact in a nonlinear fashion evoking phosphenes with spatial properties different from what each electrode evokes individually (Fernández & Normann, 2017). However Bosking et al. has shown that concurrent surface electrode stimulation of two sites separated by greater than 6-10mm reliably elicits two phosphenes that are spatially close to where stimulation of each single electrode would elicit (W. Bosking et al., 2018). Also configuration of three electrodes appeared to largely follow the same rules and they could stimulate up to 4-6 electrodes and achieve perception of up to 5 phosphenes. Although these results do not contradict with the problem of spatial distortion, their findings indicate that with certain considerations (such as the distance between stimulated electrodes) evoking concurrent phosphenes with predictable spatial pattern is possible using surface electrodes.

2.4.2.2 Long-term stability

While penetrating microelectrodes provide higher spatial resolution with lower current thresholds, the highly invasive nature of this approach may undermine their long-term reliability. The electrical, mechanical and biochemical mismatch between the electrodes and cortical tissue causes unwanted tissue responses including neuronal loss and glial encapsulation which can compromise stimulation capability of the device (Biran et al., 2005; Goss-Varley et al., 2017; Jorfi et al., 2015; X. Liu et al., 2006; Potter et al., 2012; Schwartz et al., 2006). Subdural electrodes on the other hand do not require penetration of the cortex and have greater long-term stability (Kipke et al., 2008; E. Margalit et al., 2003). This allows them to be a reliable candidate for many long-term applications including BCIs (Leuthardt et al., 2004; Thompson et al., 2017) and treatment of epilepsy (Nair et al., 2008; Wyler et al., 1984).

2.4.2.3 V1 accessibility

Retinotopic maps of visual cortex reveal that a large portion of early visual areas (V1, V2, and V3) is located in the medial surface of occipital cortex (Wandell et al., 2007). So far none of the microelectrode arrays has been or are planning to be implanted in the medial wall of the occipital lobe for two reasons: a) Risk of damage to the adjacent cortex, and b) difficulty in wireless transmission when the receiver and transmitter coils are orthogonal (Fernández & Normann, 2017; Arthur James Lowery et al., 2017; Troyk, 2017). Therefore, the occipito-dorso-lateral cortex is the preferred implantation site for microelectrode arrays and it might cover higher level visual areas (hMT+/V5 and LOC) where the likelihood of phosphene induction is relatively lower (Schaeffner & Welchman, 2017). Moreover this can potentially limits the eccentricity of the phosphenes as the ventro-medial areas of the occipital cortex is associated with the periphery of the visual field (N. C. Benson et al., 2014; W. H. Dobelle et al., 1979).

2.4.3 Psychophysical testing

Psychophysics experiments determine subject's ability to detect and identify an stimulus(Gescheider, 1997), thus psychophysical testing provide a benchmark for a preliminary evaluation of the device performance and allows for gathering essential data for creating complex percepts (Dagnelie, 2008). Obtaining threshold levels and phosphene locations for each electrode are the two major components of psychophysical testing and are required for proper integration of camera with the implant.

2.4.3.1 Threshold testing

Phosphene threshold is the minimum amount of current or charge required to elicit a phosphene. Thresholds may vary across the electrodes and depend on the stimulation parameters (frequency, pulse width and burst duration). For instance, Dobelle et al. reported current thresholds for surface electrodes in the range of 1-4mA for pulse-width of 0.25ms and frequency of 50 Hz (W. H. Dobelle et al., 1979). He also showed that increasing pulse-width and frequency tends to decrease the current thresholds while electrode size did not have a significant correlation with current thresholds (W. H. Dobelle & Mladejovsky, 1974b). Determining thresholds for each electrode allows of optimization of electrical stimulation delivery by minimizing the energy consumption and damage to the underlying tissue (Merrill et al., 2005a; Shannon, 1992). Moreover, small phosphenes are often more desirable as they allow for creating patterns with higher spatial resolution. Phosphene size has been shown to increase for higher current levels (W. H. Bosking, Sun, et al., 2017) therefore stimulation at the threshold levels can potentially generate smallest phosphenes for each specific electrode.

2.4.3.2 Phosphene mapping

The spatial representation of visual field is preserved and repeated multiple time across visual cortices, especially in the early visual areas (Wandell et al., 2007). Subject specific retinotopic mapping of early visual areas can be obtained using functional MRI and projected on the unfolded cortical surface (N. C. Benson et al., 2014). However this requires some degree of visual function hence it is not applicable to blind individuals. Therefore interactive phosphene mapping after implantation of visual cortical prosthesis is a necessary step to generate spatially relevant visual sensation. The most basic paradigm of phosphene mapping involves stimulation of each electrode and recording the location of the phosphene based on subjects feedback.

One of the challenges in collecting phosphene mapping data is the phosphene displacement in response to eye movement (W. H. Dobelle et al., 1974; Schmidt et al., 1996b; Veraart et al., 1998). When a phosphene appear in the periphery of the visual field, subjects tend to track the phosphenes with their eyes. This results in the perceived phosphene location following the direction of eye movement using optomotor feedback (Arathorn et al., 2013). To compensate for this effect subjects are asked to focus on the center of the field of view (FoV) using a tactile or an audio cue and maintain their gaze during stimulation. However this may not be applicable to the day-to-day usage of the device where tactile or audio feedbacks might not be available. On the other hand, tracking the eye positions in real-time and shifting the region of interest accordingly have been shown to improve the subjects' ability to locate a static object using retinal prosthesis (Argus II, SecondSight Inc.) and may be beneficial for cortical visual prosthesis(Caspi et al., 2018). This solution may not however be applicable to patients with enucleation or other traumatic causes of blindness which result in an absent globe.

2.4.4 Machine learning

Measuring threshold levels and phosphene mapping provide essential data for the integration of camera and the neurostimulator to form a brain computer interface (BCI). A visual prosthetic BCI in its simplest form maps the light intensities in the visual field to charge/amplitude levels deposited on the surface of the primary visual cortex. This however may be problematic given the limited number of electrode and nonuniform arrangement of their corresponding phosphenes in the visual field. Incorporation of machine learning into the BCI could potentially improve the device performance in different ways. The TR approach being developed by the Monash group is an example of using machine learning for image processing to produce visual perception optimized for the specific task in hand such as navigation or face detection.

There has been significant advances in decoding intracranial recording of the visual pathway to detect and discriminate the complex visual perceptions using machine learning (Ghuman et al., 2014; Kapeller et al., 2018; H. Liu et al., 2009). Moreover, stimulation of cortical areas further down the visual processing stream affects higher-level and complex visual perceptions (Aminoff et al., 2016; Blanke et al., 2000; Penfield & Rasmussen, 1950). For instance, stimulation of fusiform gyrus alters face perception (Parvizi et al., 2012; Rangarajan et al., 2014) and reading capabilities (Hirshorn et al., 2016; Mani et al., 2008). Although our understanding of this approach is too limited to produce relevant visual information, given the top-down and recurrent organization of the visual system (Kravitz et al., 2011, 2013), it could potentially serve as a supplement to earlier visual cortex stimulation to produce a rich and more natural visual experience.

2.5 Discussion

Development of cortical visual prosthetics has gained a great momentum in the recent years and based on current advances in electrode design and wireless communication, it is expected to restore some degree of vision in blind individuals. In this chapter we briefly reviewed the history and described the state of the art of theses prostheses aiming to provide a basic understanding of the approach and potential challenges.

3 Assessing safety and feasibility of subdural cortical visual stimulation

Electrical stimulation of human primary visual cortex is known to elicit topographically mapped sensations of light called phosphenes(Bak et al., 1990; Brindley & Lewin, 1968; W. H. Dobelle & Mladejovsky, 1974b; Schmidt et al., 1996a; Winawer & Parvizi, 2016; Yoshor et al., 2007b). As such, visual cortical prostheses hold the potential for restoring some useful artificial vision to previously sighted individuals who have completely lost their vision due to non-cortical etiologies. Such an approach may particularly be applicable to those who are not candidates for retinal prostheses as it bypasses the orbit, retina, optic nerves and tracts, and thalamic radiations. We took the advantage of a commercially available subcutaneously implanted neurostimulator to achieve three goals: 1) Assess the safety and feasibility of implanting and delivering chronic stimulation to the medial occipital lobe in a blind subject. 2) Assess current and charge thresholds required to elicit phosphenes and how stimulation parameters affect the quality of phosphenes. 3) Verify the reproducibility of the percepts and stability of thresholds during the 18-month follow-up.

3.1 Methods

3.1.1 Subject selection

A 30 year old woman with an 8 year history of bare light perception secondary to Vogt-Koyanagi-Harada disease provided informed written consent approved by Institutional Review Board (IRB) at the University of California Los Angeles. Although an Investigational Device Exemption (IDE) was sought, the Food and Drug Administration (FDA) indicated this was not required as this was an investigator-initiated study using an FDA-approved marketed product and the study's primary purpose was for scientific inquiry rather than therapeutic intent. While studies of stimulation thresholds could be conducted in animal models, evaluation in a human subject, particularly one

that is blind, was deemed necessary to demonstrate feasibility in the target population as well as to derive behavioral and experiential feedback that would inform future visual cortical prosthetic design. Note that additional studies were performed in this subject that are beyond the scope of the current report and will be reported in the future.

3.1.2 System overview and Surgical Procedure

A NeuroPace Responsive Neurostimulation System (RNS) system was used in this study. This device is FDA-approved for use in patients with epilepsy. It includes a cranially implantable programmable neurostimulator with the ability to both stimulate and record brain electrical activity. This was connected to two implanted cortical strips, each containing four non-penetrating subdural electrocorticographic (ECoG) electrodes measuring 3.18mm in diameter and spaced 10mm apart (center-to-center). The stimulation parameters were programmed using a laptop computer that runs proprietary NeuroPace Programmer Applications Software (RNS-300M) and utilizes a wand to communicate with an RNS Neurostimulator. The device was implanted under general anesthesia in a prone position via a posterior interhemispheric approach. Frameless neuronavgiation was used to define the site of the parasagittal 4 x 2 cm craniotomy (centered 8 cm above the torcula) as well as the trajectory of the two parallel 4 contact ECoG strips (which were sewn together before insertion). After anchoring the skull-mounted RNS generator in a position superior and lateral to the craniotomy, the dura was opened with a U-flap towards the sinus, the ECoG strips were inserted with navigation guidance, intraoperative fluoroscopy was obtained to confirm appropriate localization, and the dura was closed primarily before replacing the bone flap. Skin was closed in a standard layered fashion.

3.1.3 Data acquisition and experimental design

Experiments were performed with the subject seated and gazing straight forward with eyes open. A wand was held over the scalp using a cap to couple the neurostimulator to the programmer. Each stimulation burst was delivered after a verbal cue.

3.1.3.1 Impedance measurement

Electrode Impedances were captured at the beginning of every session. Impedances were evaluated using voltage measurements collected during delivery of single current-controlled monopolar (i.e. neurostimulator is used as the anode) charge-balanced biphasic square pulses with 3mA amplitude and 40us pulse-width.

3.1.3.2 Stimulation parameters

Rectangular current regulated pulses were delivered at different amplitudes (current), pulse-widths (PW), and frequencies with a constant burst duration of 250ms. Pulses were symmetric, biphasic (cathodic-first) with zero inter-phase gap and charge balanced. The stimulator can was used as the return node.

3.1.3.3 Phosphene mapping

A touch-screen display was placed in front of the subject with the center of the touch screen at the level of central gaze, 25 cm away from the eyes. Prior to delivery of stimulation in each trial, the subject was asked to put her right index finger on a small Velcro dot at the center of the touch screen and to maintain gaze on that target. After stimulation, the subject drew the outline of the percept using the left index finger and provided a description of the shape and size of the percept. Offline, the phosphene outline coordinates were imported into MATLAB and integrated with the subject descriptions to plot the phosphenes in a polar grid.

3.1.3.4 Threshold testing

Threshold testing was performed for a range of frequencies and pulse-widths to investigate the effects of these parameters on the minimum current required to elicit well-defined phosphenes. For each combination of stimulation parameters, amplitude was increased from 0.5 mA in steps of 0.5 mA (smallest step size allowed by the device) while holding other parameters constant. A well-defined phosphene was a perception easily identifiable and distinguished from the back ground.

3.1.3.5 Subjective intensity rating

Subjective ratings of phosphene intensity were obtained for different amounts of charge delivered per trial. Total charge was modulated by either adjusting the current amplitude (amplitude modulation) or frequency (frequency modulation). PW and burst duration were kept constant at 280 us and 250 ms respectively during these experiments. For amplitude modulation studies, current was initially delivered at 0.5 mA and ramped up to 7 mA with a constant frequency of 20 Hz. To study the frequency modulation frequency was ramped up from 5Hz to 200Hz with a constant current of 2mA. Immediately after each trial, the subject was asked to report the intensity of the percept using an eight-point scale, where 0 represents no perception, 1 represents minimal perception, 2 represents a well-defined perception (designated the threshold value), and 7 as the most intense perception possible.

3.2 Results

Experiments were initiated two weeks after implantation of the neurostimulator and were conducted for 81 weeks. In the first experimental session, all eight contacts (Figure 3-1) elicited phosphenes and no perception during sham stimulation.

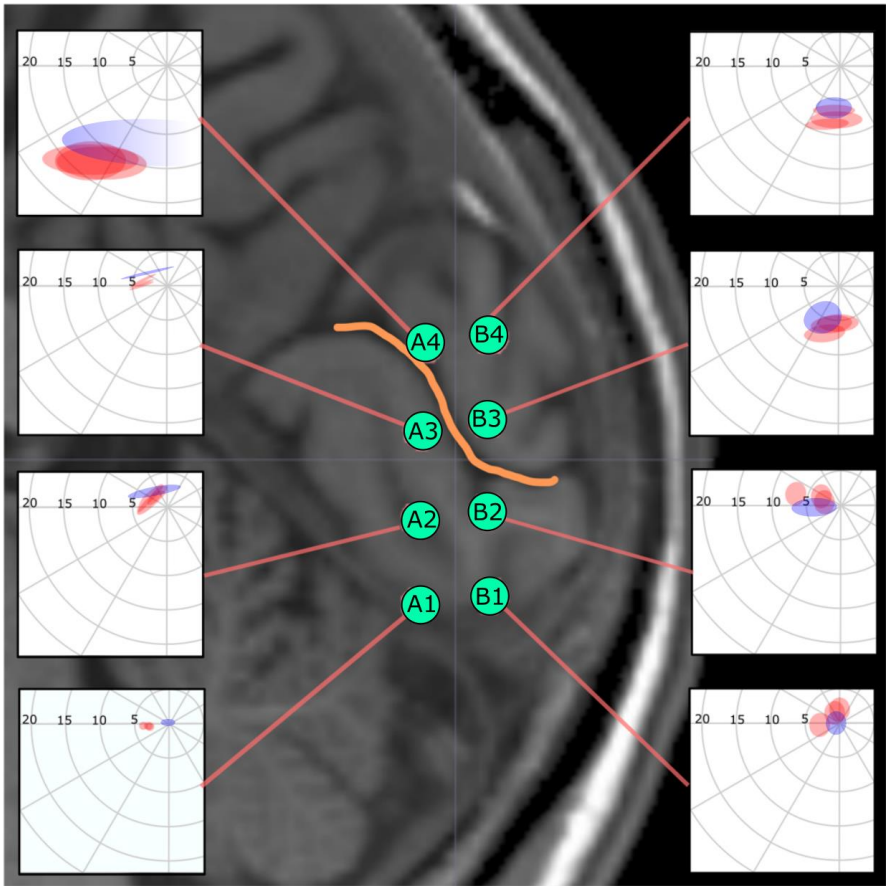


Figure 3-1 Phosphene mapping generated based on integration of subject's drawings and descriptions. Red shaded areas correspond to phosphene mapping experiment performed at month 8 of the study (3 trials per channel) and blue shaded areas correspond to the month 19 of the study (one trial per channel). Phosphene drawings are mapped to the polar space and connected to their corresponding electrode shown on the MRI slice of the right medial occipital lobe. Orange line represents the calcarine sulcus.

3.2.1 Impedances

Electrode impedances were measured at the beginning of 41 independent testing sessions during the study. Figure 3-2 illustrates the median and range of impedances as well as the temporal evolution of impedances over time for each contact. Out of the eight contacts, 50% of contacts demonstrated less than 20% variation over time.

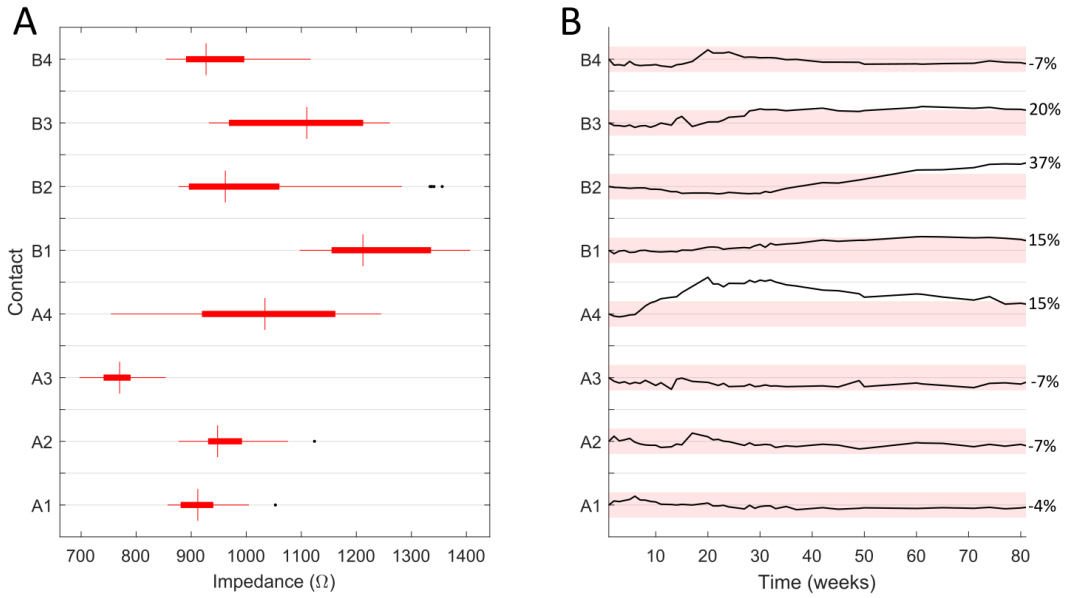


Figure 3-2 Impedances measured at the beginning of each session during the 81 week study. A) Box plot of the impedance values representing the median, first and third quartiles as well outliers as dots. B) Percent change of the impedance for each contact compared to the first measurement (week 1) over time. Red shaded area indicates ±20% change (chosen arbitrarily for scale). Numbers on the right axis represent the percent change of the last measurement (week 81) relative to initial measurement.

3.2.2 Phosphene mapping

For spatial mapping, stimulation amplitude, frequency and pulse width were chosen to be 2mA, 100Hz and 200us respectively. These parameters were based on initial threshold testing (described in greater detail below), allowing phosphenes for all contacts to be easily perceived and have pronounced boundaries. A total of 24 trials (3 for each contact) was performed in a randomized order. Phosphene drawings are shown in Figure 3-1 relative to the cortical location of each contact. Phosphenes were either completely (contacts A1, A2, A3, A4, and B2) or mostly (contacts B1, B3, and B4) in the left visual hemifield. As expected, stimulation of contacts superior to the calcarine sulcus (contacts A4, B3, and B4) were perceived in the superior hemifield and stimulation of contacts inferior to the calcarine sulcus (contacts A1, A2, A3, B1, and B2) were perceived at or below the horizontal visual meridian. The subject described the phosphene perceived during the

stimulation of contact A1 as a dot, contacts A2 and A3 as a line, contact A4 as an elliptical area filled with pinholes, contact B1 and B2 as circles, and contacts B3 and B4 filled ellipses.

The phosphene mapping experiment was performed twice, at months 8 and 19 of the study, to assess the consistency of the perceptions (Figure 3-1). The subject described the percepts elicited by contact A1 as a "small dot with the size of a pinhead", contact A2 as "a short thick line", contact A3 as "a short thin line", contact A4 as "an oval shape area full of pinwheels", contacts B1 and B2 as "circles in a size of quarter", and contacts B3 and B4 as "ovals". All phosphene shapes were consistent based on subject descriptions and did not change in size or location based on the drawings.

We investigated the relationship between phosphene size and its distance from the center of the visual field. Given limitations in the accuracy of the drawings, we categorized phosphenes into three sizes: small ($< 7\ deg^2$ described as dots, lines and small circles), medium ($> 7\ deg^2$ and$< 50\ deg^2$) and large ($> 20\ deg^2$ described as areas occupying a significant portion of field of view (FOV)). As illustrated in Figure 3-1, small phosphenes (elicited from contacts A1, A2, A3, B1, and B2) were located between 0 to 7 deg from the center of the visual field; Medium (elicited from contacts B3 and B4) and large phosphenes (contact A4) are located farther from the center of the visual field, 5 to 9 deg and 16 to 19 deg, respectively.

3.2.3 Phosphene thresholds

Detailed threshold testing was performed at contacts A1 and B2 in order to elucidate the effect of stimulation parameters on stimulation thresholds. To investigate the effects of pulse width, we evaluated current thresholds for eliciting a phosphene when stimulating with pulse widths of 40, 80, 120, 200, 280, 360, and 440 us with a fixed 20 Hz frequency and 250 ms burst duration (Figure

3-3-A and Figure 3-3-B). A $f(x) = \frac{a}{b+x}$ curve was fitted to the current threshold values to understand how PW modifies the current required to elicit a phosphene. Figure 3-3-C and Figure 3-3-D illustrate thresholds in the form of charge per trial and a line is fitted to the data with $R^2 = 0.98$ and $R^2 = 0.91$ for contacts A1 and B2 respectively.

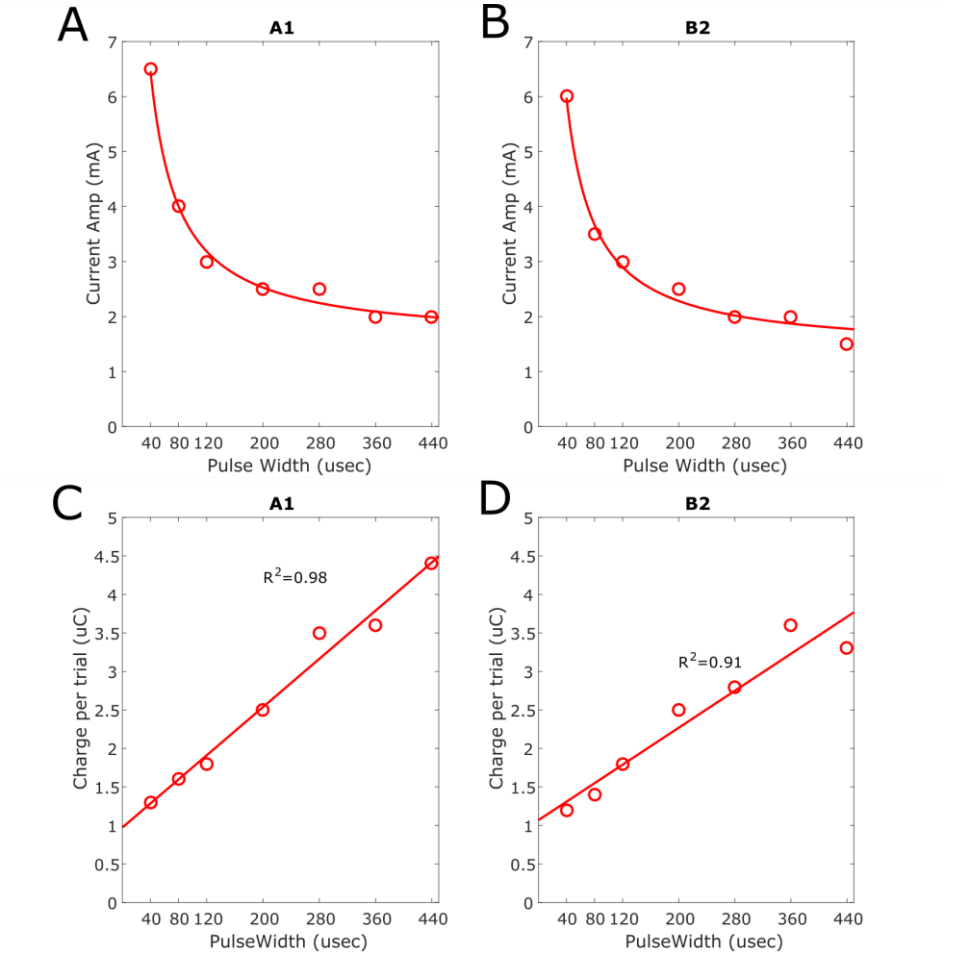


Figure 3-3 Current amplitude thresholds for different pulse width values for contacts A1 (A) and B2 (B). C and D represent the same data in the form of charge per trial (i.e., total charge over the 250 ms burst duration). Curves in A and B as well as lines in C and D were fitted to the data for better understanding of the relationship between stimulation parameters.

Threshold testing was also performed for frequencies of 10, 20, 40, 60, and 100 Hz on contacts A3 and B2 to study the effects of frequency on phosphene thresholds with fixed PW and burst duration of 280us and 250 ms respectively. Figure 3-4-A and Figure 3-4-B illustrates the current

thresholds and Figure 3-4-C and Figure 3-4-D represent the charge threshold for the frequency range of interest. As above, a nonlinear curve was fitted to the current amplitude and frequency threshold levels and a linear regression with $R^2 = 0.98$ and $R^2 = 0.97$ is fitted to the charge and frequency threshold levels for contacts A3 and B2 respectively.

To gain insight into the effect of number of pulses on thresholds, we adjusted frequency and burst duration to deliver a discrete number of pulses (Figure 3-4-E and Figure 3-4-F). At 20, 40 and 60Hz, increasing the number of pulses decreased the current threshold levels. At a stimulation frequency of 100 Hz, increasing the number of pulses did not impact the current required to elicit a phosphene. At 10 Hz stimulation, current thresholds increased from 2 to 3 pulses and 1 to 2 pulses for contacts A3 and B2 respectively.

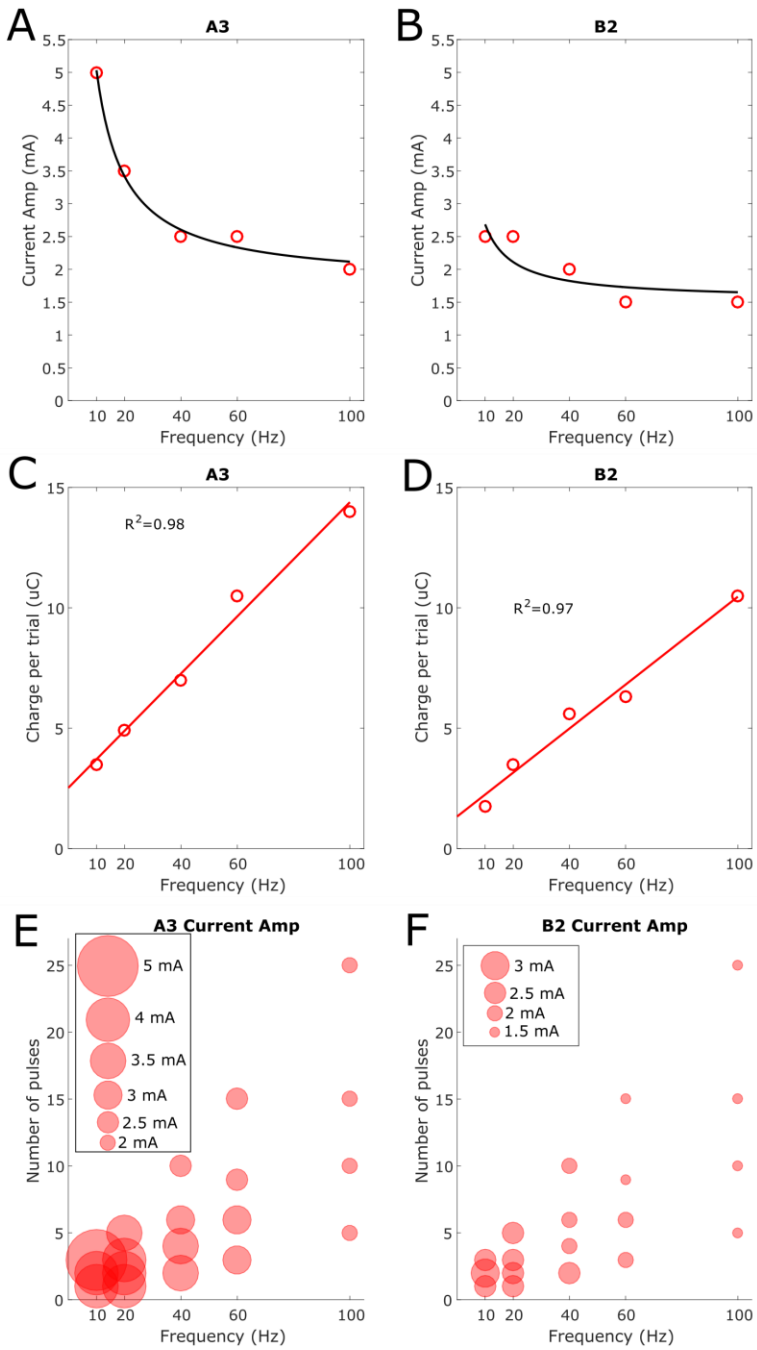


Figure 3-4 Current amplitude thresholds for different frequency values for contacts A3 (A) and B2 (B). C and D represent the same data in the form of charge per trial (i.e., total charge over the 250 ms burst duration). Curves in A and B as well as lines in C and D were fitted to the data for better understanding of the relationship between stimulation parameters. E and F represent the threshold testing experiment results for different frequencies and burst durations. Controlling the burst duration allows for delivering different number of pulses for each pulse frequency. Surface areas of the circles are proportional to the level of current thresholds.

3.2.4 Consistency of the thresholds

To evaluate the consistency of the thresholds over time, repeated testing was performed at months 1, 7 and 19 using pulse durations of 120, 280, and 440 us (constant frequency of 20Hz and burst duration of 250ms). Similarly threshold testing for frequencies of 10, 20, 40, 60, and 100 Hz (constant pulse duration of 280us and burst duration of 250ms) were performed at the same time points. Current threshold levels were either the same or changed by 0.5 mA (due to the limited resolution of RNS) between sequential tests (Figure 3-5, with the exception of contact A3 at 10Hz frequency). Current and charge thresholds decreased an average of 5% during pulse duration threshold testing and 8% and 12% respectively for frequency threshold testing.

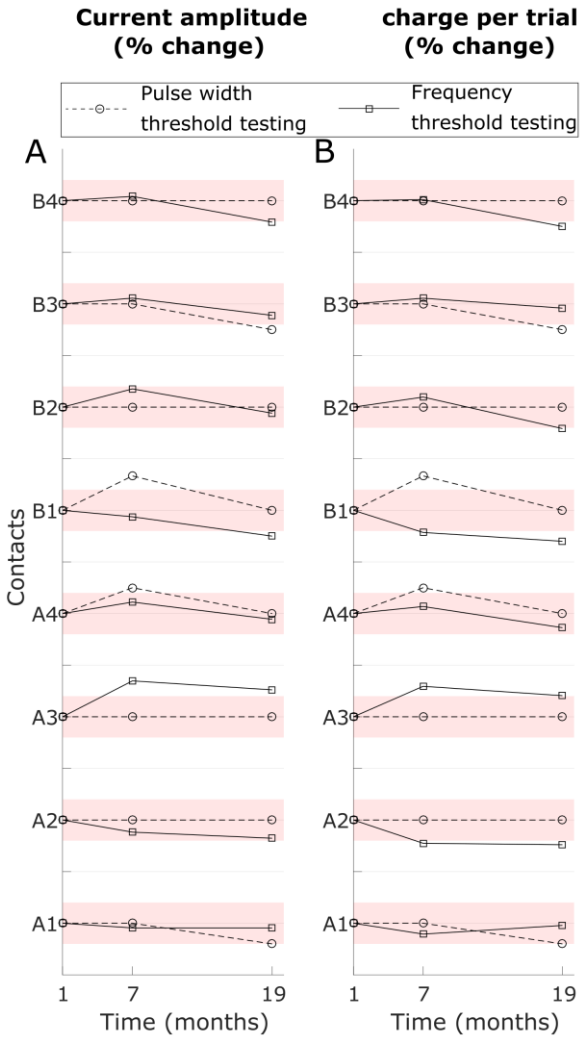


Figure 3-5 Percent change of the threshold levels for current amplitude (A) and charge per trial (B) thresholds. Dashed lines correspond to the measurement during pulse interval threshold testing and straight lines indicates to the measurements during frequency threshold testing at months 1, 7 and 18 of the study. The ±20% change interval is highlighted by the red shaded bars for each contact.

3.2.5 Phosphene intensities

Figure 3-6 illustrates the changes in subjective rating of phosphene intensity when delivered charge was modulated either by increasing the current amplitude (amplitude modulation) or frequency (frequency modulation). Increasing stimulation currents uniformly resulted in brighter phosphene

perception. Increasing frequency was also generally associated with brighter phosphene perception, although brightness did not scale in the same manner relative to charge per trial. Current modulation had a greater impact on perceived intensities compared to frequency modulation for the same amount of delivered charge.

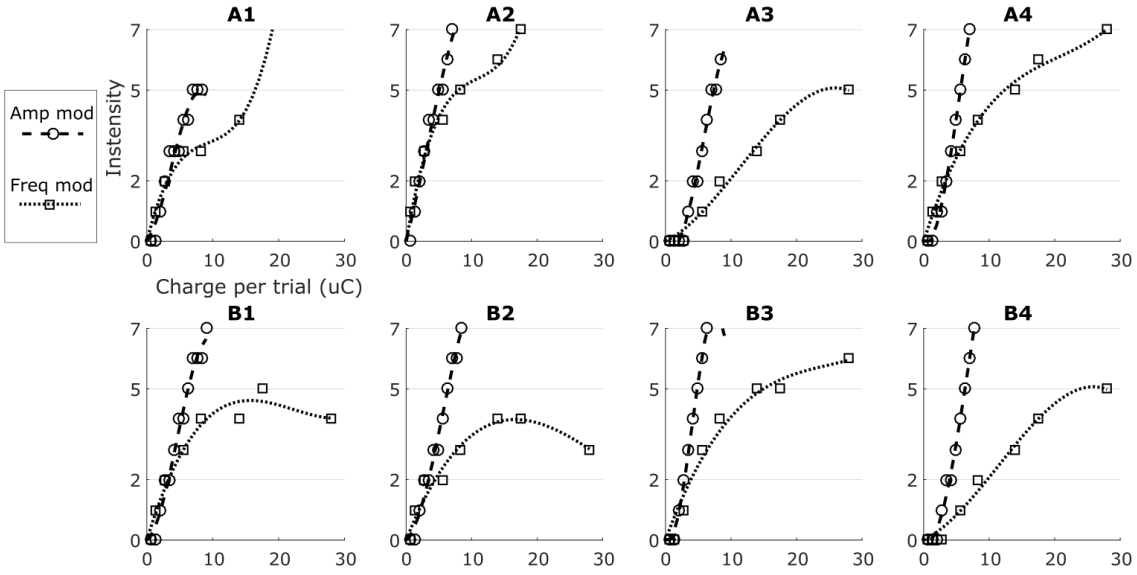


Figure 3-6 Subjective intensities of the perception based on the amount of charge delivered. Increasing the delivered charge was achieved by increasing the current amplitude (amplitude modulation) or frequency (frequency modulation).

3.2.6 Adverse events

The subject did not experience any serious adverse events. Out of 41 two-hour long study sessions, three non-serious adverse events were noted across three sessions. On session 12, stimulation at 3mA, 6Hz, 480 μs PW, and burst duration of 5.7 sec at contact B2 resulted in a subjective experience of sinus pressure and dizziness for a few minutes after the stimulation. Real time bipolar ECoG recordings from the implanted electrodes showed a ~1 Hz spiking activity for about 10 s after the stimulation burst was delivered, consistent with after-discharges. We did not have the opportunity to record the ECoG signal for further analysis. One week later, with the same

stimulation parameters the subject did not feel any pain or dizziness, however she reported feeling pressure in the sinus area. In general, however, we avoided using long duration (i.e., >5sec) fixed parameter stimulation subsequent to this event to minimize the risk of further after-discharges. Finally, during session/week 39, approximately one hour after testing began, the subject experienced a mild headache. Due to subject's discomfort, the session was terminated. All events were resolved within a few hours. None required treatment. None were associated with long term sequelae. At the conclusion of active testing, the subject remains implanted with the current RNS system under a continuation of the original IRB-approved study, providing her with the option to be explanted if she chooses.

3.3 Discussion

Visual cortical prostheses could potentially provide a restorative solution for the blind. However, challenges persist including an incomplete understanding of the consistency and safety of chronic visual cortex stimulation and how stimulation parameters affect perceptions. Recent studies on stimulation of visual areas in humans have been conducted in epilepsy patients undergoing invasive monitor for seizures for clinical purposes(W. Bosking et al., 2018; W. H. Bosking, Sun, et al., 2017; Winawer & Parvizi, 2016). Although these studies are valuable, evaluation in the target population (previously sighted individuals with bare or no light perception) is critical to gain insight into feasibility and to understand the quality of the conscious visual perception. Moreover, previous studies on blind subjects have been performed decades ago and may not satisfy current safety standards and regulations. Hence, use of an FDA approved and commercially available neurostimulator seem to provide a primary evaluation of safety and feasibility and establish a framework for future devices specifically designed for visual prosthesis. While the number of contacts used in this study are limited, we report the longest duration of thoroughly studied chronic

direct cortical stimulation for phosphene production in a blind subject. The procedure is safe with limited non-serious adverse events and phosphene production was consistent in threshold and shape over time. Moreover, we define parameters that affect thresholds for eliciting phosphenes and modify the perception of phosphenes.

Reproducibility and specificity of phosphene locations are necessary factors for generating more complex and coherent perceptions that have been reported in previous studies(Brindley & Lewin, 1968; W. H. Dobelle et al., 1979). By analyzing the size of the phosphenes and its relation to the distance from the center of the FoV, the current results suggest that phosphenes located in the periphery of the visual field tend to occupy a larger area of the FoV likely due to the pattern of cortical magnification in V1. In the portion of V1 corresponding to the periphery of the FoV, a small amount of tissue responds to a large area in the visual field while the same amount of tissue in a portion representing the center of visual field responds to a very small part of the FoV(Winawer & Parvizi, 2016). This indicates that visual cortical prosthetics with a uniform distribution of the electrodes on the V1 cortical surface tend to be most precise for the objects in the center of the FoV and this nonlinear mapping could be potentially compensated for by adjustment of the cortical area of activation.

Stability of impedances as one of the electrical properties of the electrode-tissue interface is critical to device performance. In particular, an electrode with a relatively high impedance may be incapable of delivering efficient stimulation to the tissue. Figure 3-2 shows that for 50% of electrodes (A4, B1, B2, and B3) impedances increase after 18 months however their thresholds decrease or remain unchanged during this period (Figure 3-5). Moreover, a long term study of impedances on the same neurostimulator indicates that although electrode impedances significantly change in short-term, long-term impedances are stable after one year(Sillay et al.,

2013). Determining phosphene thresholds is an important factor for designing visual cortical prosthetics as it can contribute to both efficient and safe stimulation. The strength-duration curves in Figure 3-3 indicates that a minimum threshold charge can be achieved by using the shortest pulse duration. This however might not be the case when the current amplitude exceeds the safety limit for such small pulse durations(Shannon, 1992). Similarly, phosphene perception can be achieved by delivering a single pulse although from a more practical stand point, a continuous burst of pulses may be required to create a steady perception for a longer duration. Finally, increasing both current amplitude and frequency increases phosphene intensity. However, the effects of amplitude seem to be consistently monotonic and require less charge per trial for a certain intensity level, suggesting amplitude modulation may be a more efficient means to modulate phosphene intensity.

Threshold curves can also shed light on mechanism of conscious visual perception. The curve derived from the pulse duration threshold testing seems to share the two qualitative characteristics of strength-duration curve for neuronal cell excitation(Geddes & Bourland, 1985; Merrill et al., 2005b). First, for longer charge durations, less current amplitude is required to trigger an action potential. Second, there exists a rheobase current that is required for initiating an action potential when the pulse duration is infinitely long. This similar behavior between phosphene perception and neuronal excitation thresholds indicates that these two are directly related. Therefore, current knowledge of optimizing stimulation for initiation of action potentials could be potentially used for generation of basic visual perceptions.

Phosphenes elicited by each contact were consistent both within and across trials during the 18 months of testing, with only slight differences in location and size (Figure 3-1). The variance over time in phosphene localization was approximately the same as that seen within trials. It is unlikely

lead migration led to changes in phosphene localization as head CT 6 month's post-implant demonstrated stable lead position. This slight deviation in phosphene perception could be the result of limitations in accuracy of the subject's drawing due to slight deviations in hand and eye position. On the other hand, the subject's verbal descriptions of phosphene qualities remained consistent. Threshold testing during month 1, 7 and 19 of the study revealed that phosphene thresholds did not change by more than 0.5 mA (with the exception of contact 13 at 10Hz). Given that 0.5 mA is the smallest step size for changing the current amplitude levels with the RNS device, thresholds were reliably consistent through time. This consistency of phosphene mapping and threshold levels are a crucial requirement for a visual prosthetic device. The results of this preliminary study provided foundation to begin clinical trials for Orion, a neurostimulation device specifically designed as a visual cortical prosthesis. Taking advantage of 60 surface electrodes each with a 2mm surface diameter, this device is theoretically capable of producing significantly greater number of smaller phosphenes across over the visual field. This capability should enable estimation of functional retinotopic maps of visual cortex and identify potential challenges such as electrode array displacement over time which was not possible in this study due to the limited number of electrodes, large phosphenes, and a single subject. Moreover, the device is designed to try and produce more complex and functionally useful perceptions by simultaneous and/or sequential stimulation of multiple contacts based on the visual input from a video camera and a video processing unit. While the purpose of the current investigation was to demonstrate stability of phosphenes over time (an important pre-requisite for a visual cortical prosthetic), transforming these simple phosphenes elicited by cortical stimulation into functionally useful vision will require extensive additional work to define temporal and spatial patterns of useful visual cortical stimulation. It is likely, at least with current technology, that visual cortical stimulation will never

recreate normal vision like that which sighted people appreciate. However, it is conceivable and probable that one could learn with visual rehabilitation to use the perceptions elicited by visual cortical stimulation to interpret the visual environment in meaningful ways.

4 Functional mapping of the primary visual cortex

The first schematic map of the visual field in the striate cortex was created by Dr. Gordon Holmes when analyzing the disturbances of vision reported by World War I soldiers suffering from gunshot injuries to the visual cortex(Holmes, 1918). While this observation provided fundamental insight on the functional structure of visual cortex, it had limited precision due to substantial individual variation in volumetric position(Amunts et al., 2000). On the other hand, if the visual field is mapped onto the curvatures of the cortical surface, one can observe a more consistent location across individuals(Hinds et al., 2008). Hence Benson et al. were able to predict the internal retinotopic function of striate cortex based on the surface topology of each individual brain(N. C. Benson et al., 2012). Using fMRI on 25 participants they measured polar angle and eccentricity corresponding to each individual voxel of their visual cortex(Sabuncu et al., 2010). Then a generic template of the retinotopic visual cortex map was generated by fitting these data to a deterministic algebraic model of visual-field representation(Schira et al., 2010).

As described in chapter 2, a functional map of the visual cortex can be created by eliciting phosphenes via electrical stimulation and recording subject's feedback. While this approach provides consistent phosphene locations in sighted individuals, it remains a challenge in blind subjects(Beauchamp et al., 2020) potentially due to lack of a visual reference and impaired visuo-motor coordination. Furthermore, lack of a visual reference may introduce another source of localization error due to inconsistent eye position throughout the phosphene mapping experiments(Caspi et al., 2018).

Brindley and Lewin used a "hemispheric bowl" to find the general location of phosphenes produced by stimulation of the striate cortex(Brindley & Lewin, 1968). The blind subject was asked to grasp a small knob projecting from the inner surface of a concaved gridded surface with

her right hand and fixate her eyes on the knob while pointing to the phosphene on the surface with her left hand. Similar technique has been used by Dobelle (W. H. Dobelle & Mladejovsky, 1974a) and Schmidt et al.(Schmidt et al., 1996a) to mark the absolute location of phosphenes elicited by stimulation of every single electrode.

In addition to using the "hemispheric bowl", Brindly and Lewin used sequential stimulation of two electrodes with adjacent phosphenes and asked the subjects to describe the relative location of the phosphenes(Brindley & Lewin, 1968). While they did not report any systematic approach for this analysis, it seems like that the relative location information served as a secondary mechanism to refine localization of the phosphenes and enhance the spatial resolution of the map. Absolute localization of phosphenes based on subject's drawings has a limited accuracy mainly due to the limited hand-eye coordination of the blind individuals and therefore a technique that can minimize this source of inaccuracy seems to be essential for a more accurate map.

While there is no ground truth for the exact location of the phosphenes perceived by blind patients, we designed an empirical based evaluation method to provide some measure of accuracy for the proposed mapping techniques. By carefully selecting the consistent and reliable responses from the empirical mapping paradigm, we tested the accuracy of each map in estimating the relative location of phosphenes. Furthermore we designed a simulated experiment to quantify the functional vision of the subjects when perceiving moving objects.

4.1 Subjects and Device information

This study was approved by the Institutional Review Board of University of California Los Angeles and all subjects provided written informed consent. Four blind subjects participated in this study as part of the clinical trial for Orion visual cortical prosthesis (SecondSight Inc). All

subjects had late onset blindness with zero light perception, except for subject 1 who has minimal bare light perception in one eye (Table 1).

Table 1 Subjects participated in Orion clinical study.

Subject Code	Age at time of implant	Gender	Cause of Blindness	Implant duration as of 4/1/21 (months)
Subject 1	56	M	Optic neuropathy	38
Subject 2	29	M	Traumatic Injury	36
Subject 3	64	F	Endophthalmitis	35
Subject 4	52	M	Congenital Glaucoma	34

All subjects underwent electrode implantation surgery with a 60-electrodes array of subdural electrodes (2mm diameter) over the medial surface of left occipital lobe. The electrode array is connected to the Orion internal circuit implanted subcutaneously over the skull. A camera implanted on the eye glasses sends the visual field information to a video processing unit to be converted into electrical pulse information and sent to the internal circuit via an external transmitter coil. For the purpose of this study, a programming laptop was connected to the VPU instead of the camera and electrical stimulation information were directly sent using the Orion clinician programming software developed by SecondSight.

4.2 Data Acquisition

4.2.1 Anatomical Template Mapping Data

All subjects underwent clinical pre-operative magnetic resonance imaging (MRI) included T1-weighted magnetization prepared rapid acquisition gradient echo (MPRAGE) image (slice thickness=1mm). After electrode array implantation, a post-operative full head computed tomography (CT) scan was obtained (slice thickness=0.6mm). The anatomical template of human

striate and extra-striate retinotopy was downloaded in the form of eccentricity and polarity values for each surface triangle of the FreeSurfer dual template (corresponding to the MNI305 space)(N. Benson, 2012).

4.2.2 Absolute experimental Mapping Data

Subjects were asked to wear the device and sit in front of a touch screen monitor while the device was connected to the programming laptop. A circular Velcro (1/2 inch diameter) marker was attached to the left side of the touchscreen frame and vertically centered. Subjects were positioned so that the marker aligns with their center of the visual field at 12 inches distance. For each trial subjects were asked to hold their left index finger on the marker and fixate their eyes on their finger. Then a burst of 2-5 biphasic stimulation pulses at 120Hz with 200us pulse width were delivered via a single electrode using the Orion direct stimulation software. After perception of a phosphene subjects used their right index finger to draw the phosphenes on the touchscreen while they are keeping their eyes fixated on the left index finger. This phosphene mapping paradigm was performed several times during the course of this study with variable number of trials for each electrode. In some trials subjects were asked to only point to the center of the phosphene on the touch screen while in some trials they were asked to draw the shape of the phosphene if it was larger than a point or consisted of multiple points.

4.2.3 Relative experimental Mapping Data

For each trial, two electrodes were sequentially stimulated with a burst of 2 pulses per electrode at 120Hz. For each possible pair of electrodes a vector connection the first electrode to the second was calculated based on both absolute experimental map and anatomical template map. The pairs with highest angular difference between the two mappings were chosen for sequential stimulation where the number of pairs depended on the amount of time we had available with each subject.

Similar to the absolute phosphene mapping method, subjects were asked to put their left index finger on the touchscreen marker and wait for the stimulation. They were instructed to keep their index finger on the marker for the whole period of stimulation and if the first stimuli attracted their eye gaze to bring the gaze back and fixate on the marker before the second stimulus. After both stimuli were delivered, subjects drew a line from the first perception to the second. The interval between the two stimuli was carefully chosen to be 2s which gives subjects enough time to fixate their eyes on the marker.

4.3 Mapping Methods

4.3.1 Anatomical Template Mapping Procedure

Cortical Reconstruction and Template Registration. A 3D reconstruction of cortical pial surface (Figure 4-1-E) was created based on subjects' MRI (Figure 4-1-A) using the recon_all tool in FreeSurfer toolbox(Dale et al., 1999b). The cortical surface of the FreeSurfer dual template (Figure 4-1-C, Figure 4-1-D) was resampled onto each subject's reconstructed pial surface to assign the anatomical template of the V1, V2, and V3 areas using mri_surf2surf tool (Figure 4-1-I, Figure 4-1-J).

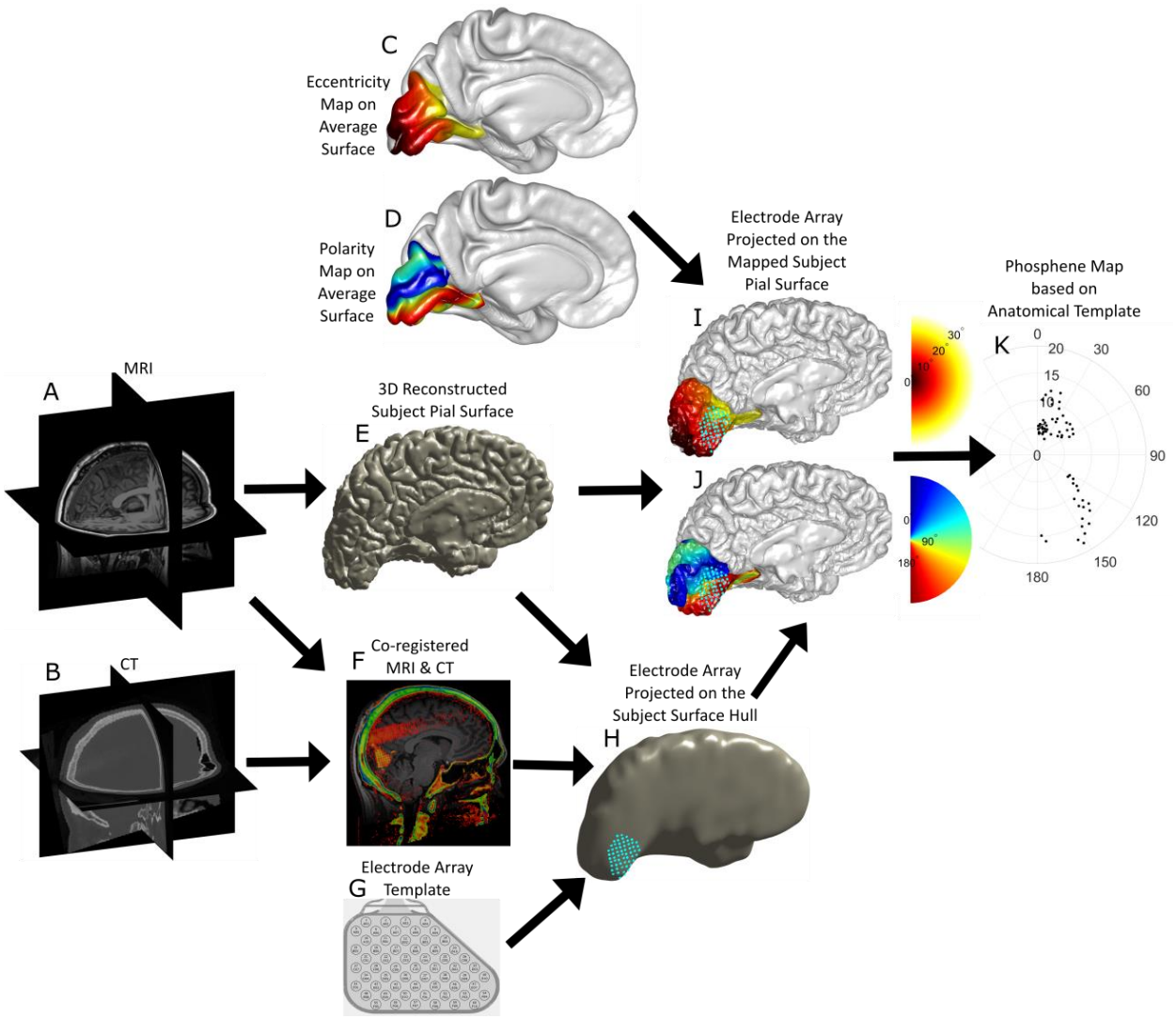


Figure 4-1 Visual field mapping procedure based on creating a subject specific anatomical map of the visual cortical surface and electrode array localization. A 3D pial surface (E) was reconstructed for each subject based on his/her MRI (A). The post-operative CT scan (B) for each subject was transformed into the MRI domain (F) and the location of the electrode array was estimated by fitting a template of the array (G) to the co-registered CT scan on top of the cortex hull (H). The eccentricity/polarity atlas on the average surface (C and D) was registered on each individual's reconstructed pial surface (I and J) and the phosphene location for each electrode was estimated based on the closest pial surface triangle (K).

MRI/CT co-registration. The CT image (Figure 4-1-B) was co-registered with the MRI image via an affine transformation with 9 degrees of freedom using FLIRT(FMRIB's Linear Image Registration Tool) in FSL toolbox(Jenkinson, 2002)(Figure 4-1-F). The volumetric location of

each electrode was manually assigned on the co-registered CT image (Figure 4-1-F) and the electrode array was localized by fitting a template of the Orion array (Figure 4-1-G) to the electrode assignment locations with 6 degrees of freedom (translation and rotation) using fieldtrip toolbox(Oostenveld et al., 2011).

A 3D hull of the pial surface (Figure 4-1-H) was created for each subject and the electrode array was realigned onto the medial surface of the hull(Dykstra et al., 2012). Given the volumetric location of the electrode array, the eccentricity and polarity values of the closest pial surface triangle was assigned to each electrode (Figure 4-1-K).

4.3.2 Experimental Absolute Mapping Technique

For the purpose of phosphene mapping, if the phosphene drawing of a trial includes more than one point, a single point representing the center of the mass of the drawing was assigned as the phosphene location for the trial. As illustrate in Figure 2-1, the Cartesian coordinates of each phosphene (x, y) were transformed into polar-cartesian coordinates $(\hat{x}, \hat{y})$on the horizontal plane,

$$\hat{x} = \tan^{-1}\left(\frac{x}{D}\right)$$

$$\hat{y} = \tan^{-1}\left(\frac{y}{D}\right)$$

where D is the distance between the touch screen marker and subject's eyes. Consequently the polar coordinates $(\hat{r}, \hat{\theta})$ for each phosphene were calculated as

$$\hat{r} = \sqrt{\hat{x}^2 + \hat{y}^2}$$

$$\hat{\theta} = \tan^{-1}\left(\frac{\hat{y}}{\hat{x}}\right)$$

where r is eccentricity, θ is polarity.

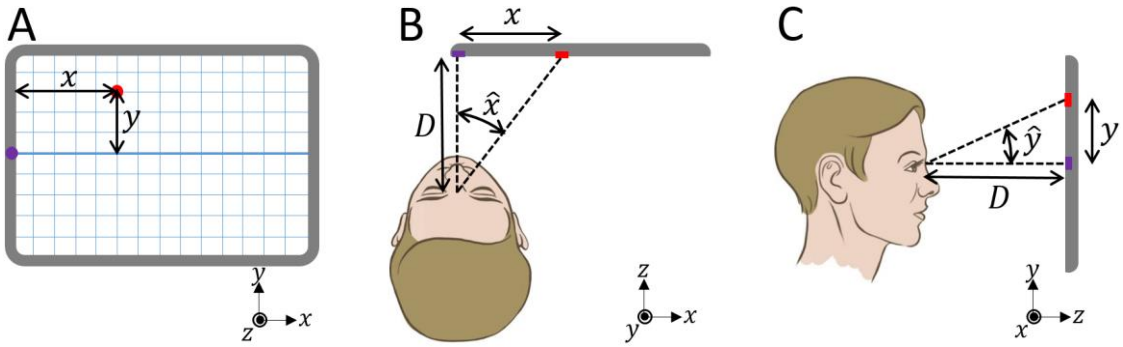


Figure 4-2 A) Cartesian coordinates of the phosphene (red dot) with reference to the marker (purple dot). B) The relationship between Cartesian coordinate, x, and polar cartesian coordinate, $\hat{x}$, with respect to the subject's distance from the touch screen, D, from the top angle. B) The relationship between Cartesian coordinate, y, and polar cartesian coordinate, $\hat{y}$, with respect to the subject's distance from the touch screen, D, from the side angle.

4.3.3 Experimental Relative Mapping Technique

A vector $\boldsymbol{d}_{ij}$ connecting the first and last point of the drawing was assigned to each trial where i and j are the first and second electrodes stimulated. For each trial $\boldsymbol{d}_{ij}$was transformed to polar coordinates $\left(\hat{d}_{ij}, \hat{\delta}_{ij}\right)$ based on the method described in previously subsection where $\hat{d}_{ij}$is the angular length and $\hat{\delta}_{ij}$ is the phase component of the vector. Since for each pair we performed the experiments in both orders we combined the trials by reversing the phase of the connection vectors for reverse trials so that $\left(\hat{d}_{ij}, \hat{\delta}_{ij} + \pi\right)$ were the polar coordinates for vector $\boldsymbol{d}_{ij}$. To remove the effects of outliers we calculated the medians $(\hat{d}^*_{ij}, \delta^*_{ij})$ among all the trials collected for each pair of electrodes. Our objective was to find a phosphene map that generates relative location vectors closest to the ones form phosphene connection experiments. Therefore we defined an optimization function

$$f_{rel} = \sum_{i,j}\left(\sqrt{\left(\hat{x}_i - \hat{x}_j\right)^2 + \left(\hat{y}_i - \hat{y}_j\right)^2} - \hat{d}^*_{ij}\right)^2 + \sum_{i,j}\left(\tan^{-1}\left(\frac{\hat{y}_i - \hat{y}_j}{\hat{x}_i - \hat{x}_j}\right) - \hat{\delta}^*_{ij}\right)^2$$

where the absolute locations of the phosphenes, $(\hat{x}_i, \hat{y}_i)$ and$\left(\hat{x}_j, \hat{y}_j\right)$, are the variables of the optimization.

Using only f_{rel} would allow the map to be in any location in the space as long as it satisfies the relative distance constraints therefore another factor must be added to our optimization function to account for the deviation of the phosphenes from their expected general absolute location

$$f_{abs} = \sum_{k} (\hat{x}_k - \hat{x}_k^*)^2 + (\hat{y}_k - \hat{y}_k^*)^2$$

Where $\hat{x}_k^*$ and $\hat{y}_k^*$ are the polar-Cartesian coordinates of phosphenes based on the experimental absolute mapping. The final optimization function is a combination of f_{rel} and f_{abs}

$$f_{opt} = k f_{rel} + (1 - k) f_{abs}$$

Where k and $(1 - k)$ are the weights of relative and absolute mapping optimization functions. We chose k to be 0.98 for all of our analysis as the goal of this analysis is to find the best relative map and f_{abs} is only to bias the optimization towards the expected location of the map in visual space.

When it comes to evaluating the mapping techniques unfortunately there is no ground truth to compare the phosphene maps against. However given the results of the phosphene connection experiments, phosphene pairs with consistent relative locations are reliable metrics for quantifying the phosphene maps. Moreover we must also consider how each map can affect the functional vision for the subjects when they use the device on a day to day basis.

4.4 Mapping Evaluation

4.4.1 Evaluation using relative mapping experiment

We used the data collected from phosphene connection experiments to evaluate the three anatomical template and absolute and relative experimental maps. We only chose the phosphene pairs for which we have performed the phosphene connection test for 5 or more trials. Also to quantify the reliability of the subject responses, for each pair the difference between the first and

third quartiles of connection vector phases, $\hat{\delta}_{ij}$, was calculated as a confidence interval and only pairs with 20 degrees or less confidence interval were chosen for evaluation. For each map, we calculated the mapping error

$$e_{map} = \frac{1}{M}\sum_{i,j}\left|\tan^{-1}\left(\frac{\hat{y}_i - \hat{y}_j}{\hat{x}_i - \hat{x}_j}\right) - \hat{\delta}^*_{ij}\right|$$

where M is the number of pairs used for evaluation, $(\hat{x}_i, \hat{y}_i)$ and $(\hat{x}_j, \hat{y}_j)$ are the polar-Cartesian coordinates of the absolute locations for electrodes i and j, and $\hat{\delta}^*_{ij}$ is the median phase of phosphene connection vectors.

To avoid training bias when evaluating the relative experimental map, we used a "leave-one-per-out" method for each subjects. We used $M - 1$ pairs for optimization and 1 pair for evaluation and repeated this process M times so that each pair was evaluated exactly once. Then the errors were averaged over the number of evaluation repeats M.

4.4.2 Functional vision evaluation using simulation of direction of motion

To evaluate the functional performance of the phosphene mappings, we designed a test in which subjects had to judge the direction in which a white circle in a blank background is moving. We simulated the animation of a white circle with 10 pixel diameter in 8 different directions on a 50×20 pixels black background. Each frame of this animation was mapped to electrode array based on each specific mapping technique. Although the animation was not shown to the subjects during the experiment, the simulation produced the exact sequence of stimulation as if the animation was captured by the video camera. The subjects were asked to draw a line on the touch screen corresponding to the direction they perceived from the moving object.

4.4.3 Functional vision tests using camera

To test the functionality of the Orion system a set of visual function tests (VFT) were performed throughout the study at months 6^{th}, 12^{th}, and 24^{th}. As these tests were designed prior to implantation of Orion to evaluate the overall performance of subjects through time only experimental absolute map were used. These tests are standard techniques that have been used by SecondSight to evaluate their visual prosthesis (Argus, SecondSight) and are required by FDA as a benchmark to confirm the functionality of visual prostheses. For all experiments a 19 inch (48.3 cm) touch screen display located 12 inches (30.5 cm) from subjects were used to display the visual stimuli and record subjects' responses. All tests were performed while device was ON and OFF to compare the performance of the subjects with and without the device. Mean errors were compared between device ON and OFF with 2-tailed t test assuming unequal variances and statistical significance of $p<0.05$.

4.4.3.1 Square Localization

Square localization test was designed to evaluate subjects' performance in spatial-motor task(Ahuja et al., 2011b). A white square (5.85 cm^2, 200 $pixel^2$) appeared in random location on a dark background followed by an audio cue for subjects to locate and touch the screen. Subjects' responses were followed by an automated verbal feedback indicating "correct" if anywhere on the square was touched or "close" if anywhere in the vicinity of 100 pixels (2.9 cm) from the square were touched. A corrective feedback was given if subjects' response was "close" or incorrect indicating to the relative location of square to the subjects' response. Subjects were instructed to move their head to find the square while keeping their eyes centered relative to their head position. Each experiment included 40 trials and the location of subject response were recorded by the touch screen for the off-line calculation of average error from the center of the square.

4.4.3.2 Identifying Direction of Motion

Direction of motion test was designed to evaluate subjects' ability to identify the direction of a moving object(Dorn et al., 2013). A 1.4 inch (3.6 cm) white bar moved across the touchscreen at a randomly chosen angle with a constant speed. Subjects were instructed to draw a straight line on the touchscreen in the direction of perceived motion. An automated verbal feedback was given after each response indicating "correct" if subjects' response was within 15 degrees of the stimulus angle in either direction; otherwise a corrective verbal feedback was given indicating to the direction in which the bar moved (For example "It moved down and left"). Each experiment consisted of 80 trials and subjects were instructed to keep their head still and eyes focused on the center of the touch screen during the task. For each trial the angular difference between the stimulus direction and subjects' response was calculated as error and averaged over the trials.

4.5 Results

4.5.1 Anatomical Template Mapping Results

A phosphene map of the visual field (Figure 4-3-C) was created based on cortical surface eccentricity (Figure 4-3-A) and polarity (Figure 4-3-B) maps for each subject. The phosphene map (Figure 4-3-C) for each subject is illustrated in two figures due to the high number of electrodes.

Each row of the electrode array has been color coded and connected on the phosphene map to show the nonlinear characteristic of these maps.

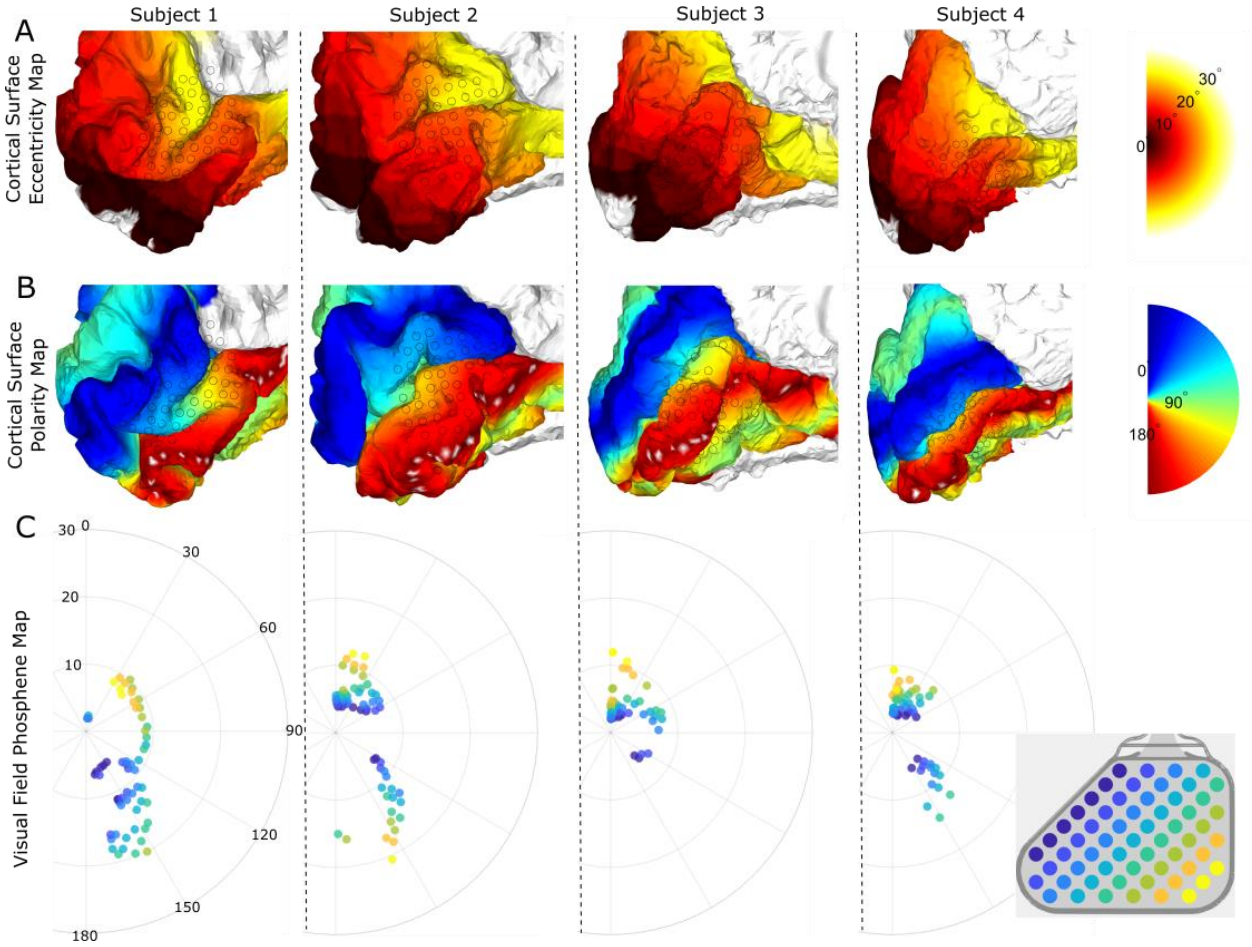


Figure 4-3 Cortical surface eccentricity (A) and polarity (B) maps for each subject. Visual field phosphene maps created based on the subject specific anatomical template (C). Phosphene map for each subject. Columns of electrodes on the electrode array (right) are color-coded and plotted in the visual field (left) to demonstrate the nonlinear characteristic of these maps.

4.5.2 Experimental Absolute Mapping Results

Figure 4-4 illustrates the experimental absolute mapping results for each subject. To avoid crowded representation the phosphene map for each subject is color-coded and illustrated in multiple figures each corresponding to a column of electrodes on the array. The center of each

ellipse reprents the average location of the phosphenes produced by stimulation of an electrode and the outline of the ellipse shows the standard deviation of phosphene locations in x and y axes.

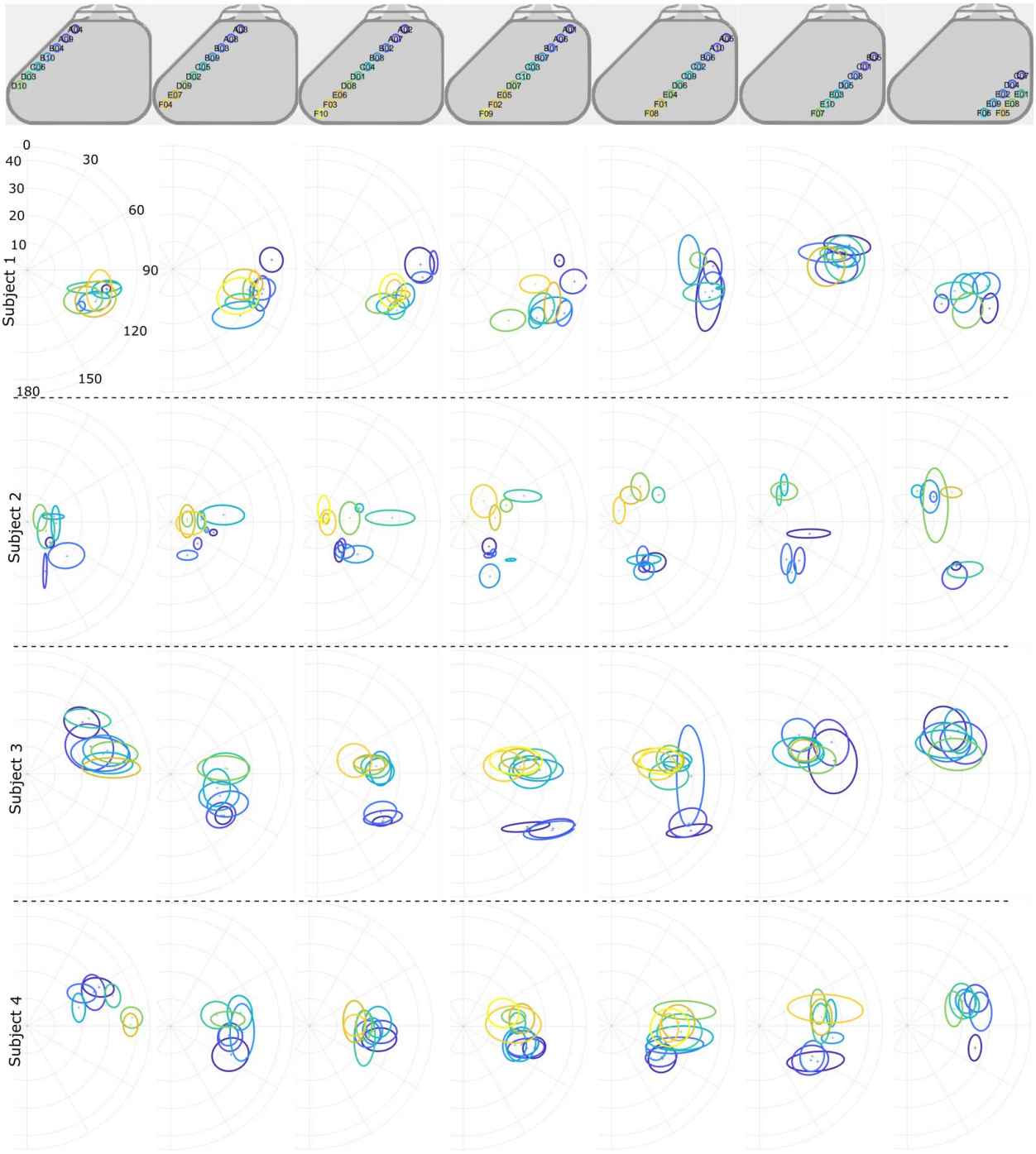


Figure 4-4 The absolute experimental map of the visual field for each subjects. To avoided crowded maps each map is color-coded and illustrated in multiple figures corresponding to the electrode columns on the array (top). He center of each ellipse represents

the average location of a phosphene produced by each electrode and the borders of the ellipse represent the standard deviation of location on x and y axes.

The variability of subjects' responses to stimulation of each electrode was quantified in terms of the angular area of the standard deviation shown in Figure 4-5-A. The average standard deviation areas were 106±69, 39±36, 148±81, and 103±55 squared degrees for subjects 1, 2, 3, and 4 respectively. The normalized overlap between the standard deviation areas of each pair of phosphenes was calculated by dividing the absolute overlap area by the standard deviation of area of each phosphene shown in Figure 4-5-B. The number of phosphenes with at least 50% overlap with another phosphene were 46, 41, 57, and 53 for subjects 1, 2, 3, and 4 respectively.

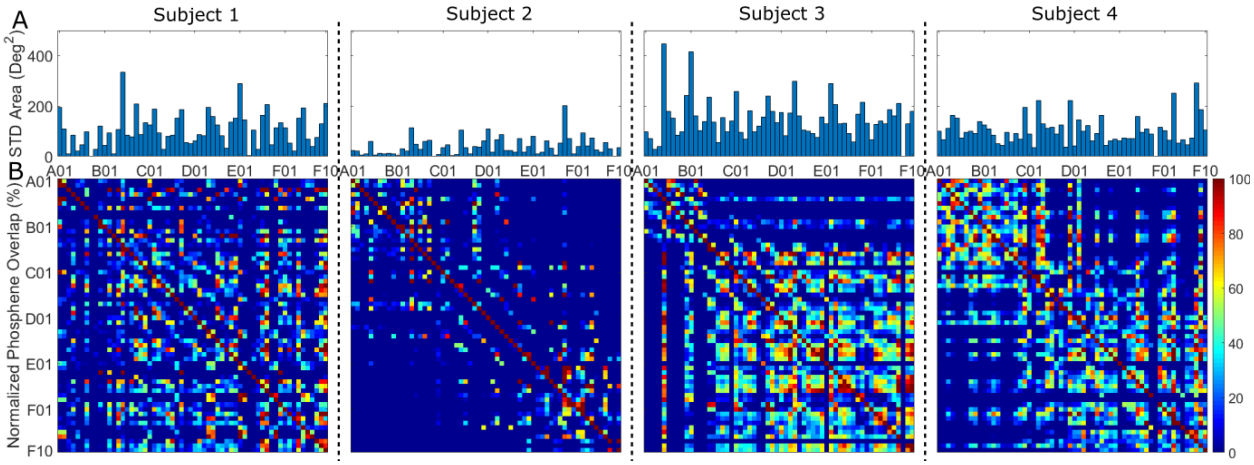


Figure 4-5 (A) Variability of subject responses to stimulation of each electrode in terms of angular area of the standard deviation. (B) Normalized overlap between the standard deviation areas for each pair of phosphenes in terms of the percentage ratio of the overlapped area compared to the standard deviation area of each phosphene on the y axis.

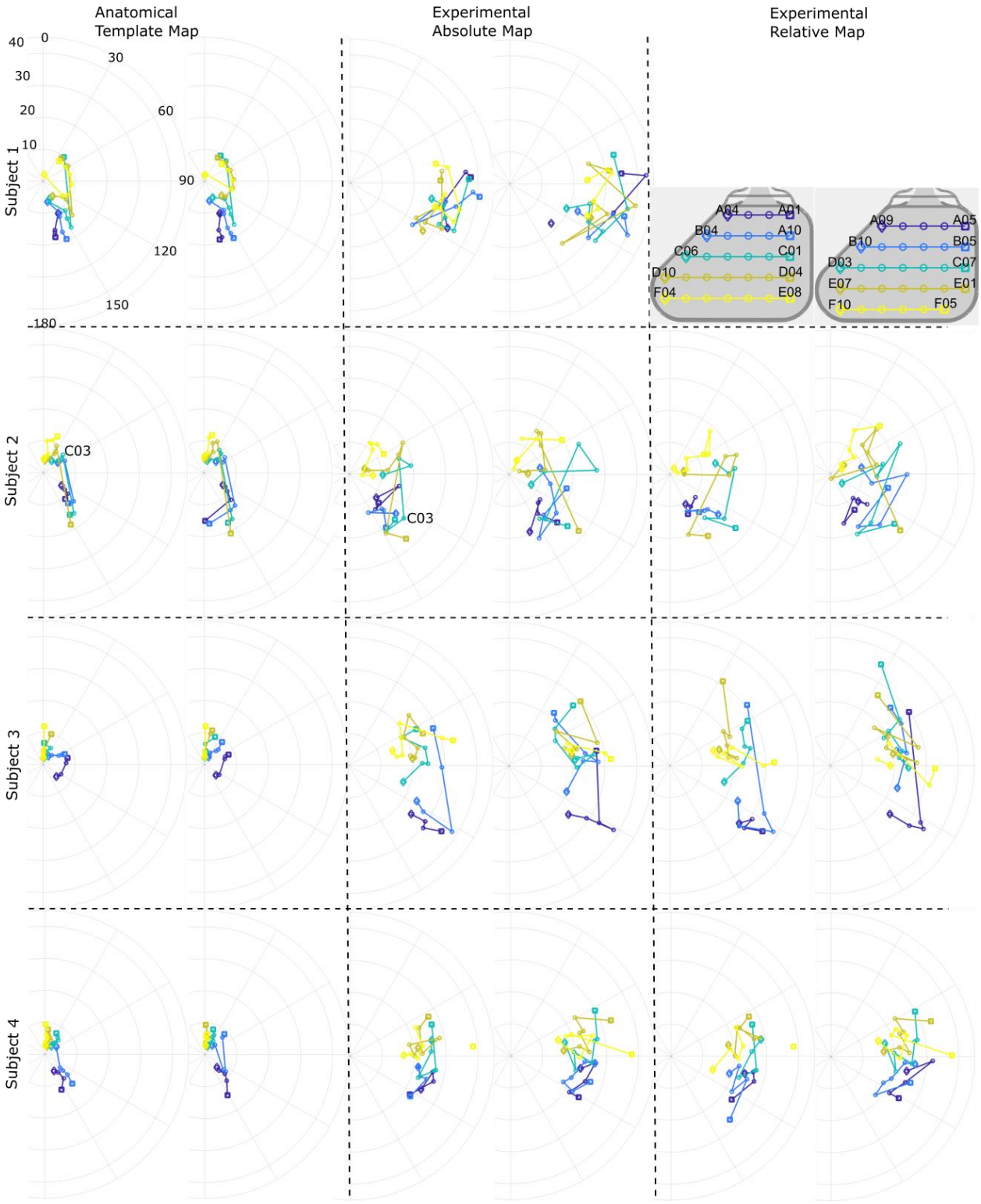


Figure 4-6 shows the experimental relative phosphene maps generated for each subject. To avoid

crowded representation each map is illustrated in two figures and color-coded based on the rows of electrodes on the array. We were not able to perform phosphene connection experiments for subject 1 as the subject did not participate in the phosphene connection experiments.

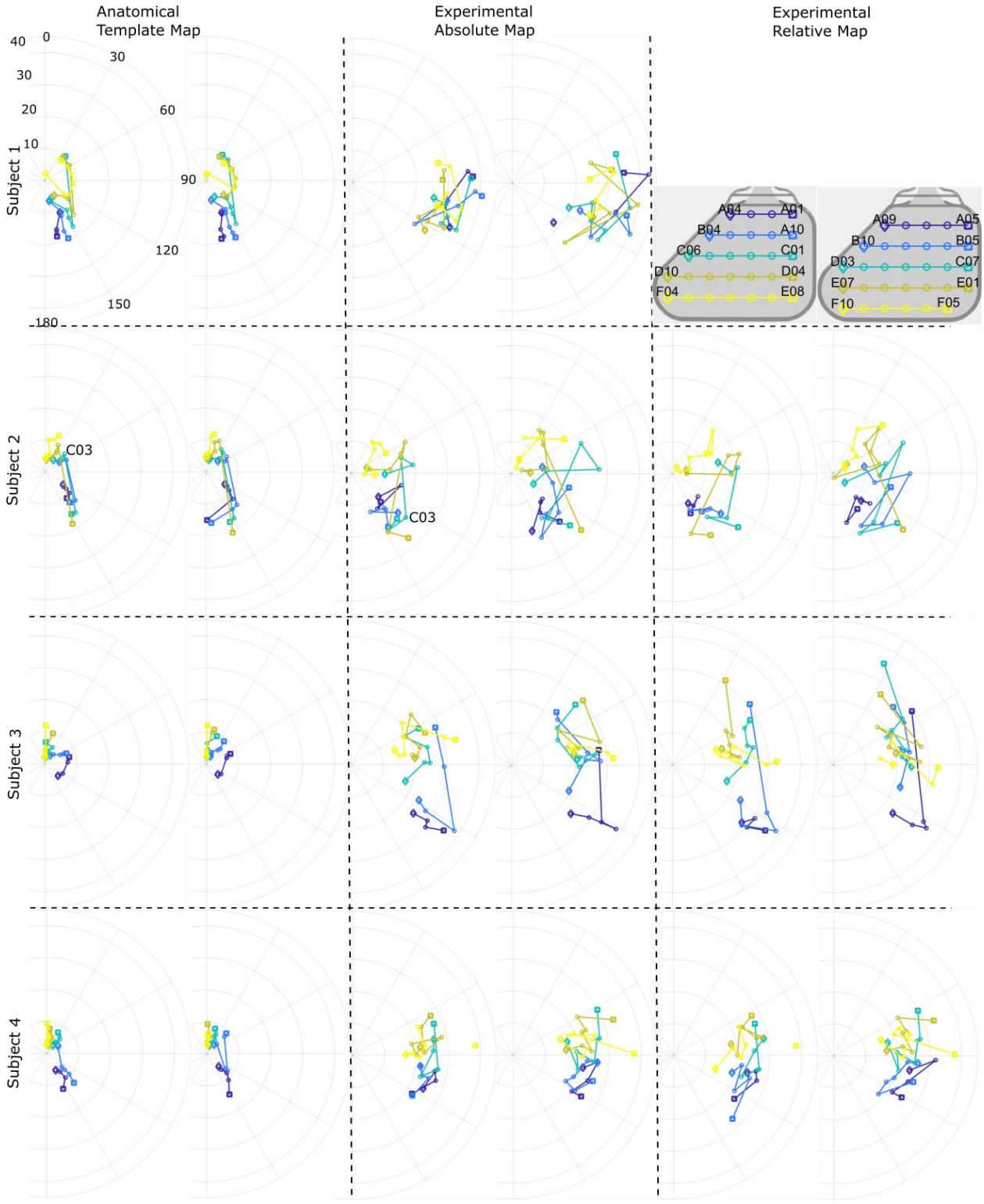


Figure 4-6 the anatomical template and experimental absolute and relative phosphene maps for each subject illustrated in two figures to avoid crowded representation. Each map is color-coded based on the rows of electrodes on the array (top right).

4.5.3 Mapping Evaluation Results using Relative Mapping Experiment

We evaluated the accuracy of the anatomical template map and experimental absolute and relative maps for each subject by finding the error between the relative location phosphenes in each map and the phosphene connection experiment results (Figure 4-7). The average mapping error was lowest for experimental relative map and highest for anatomical template map for all subjects. All differences in average error were statistically significant ($p<0.05$, two-sample t-test) except for the difference between anatomical and absolute map and also the difference between absolute and relative map in subject 4.

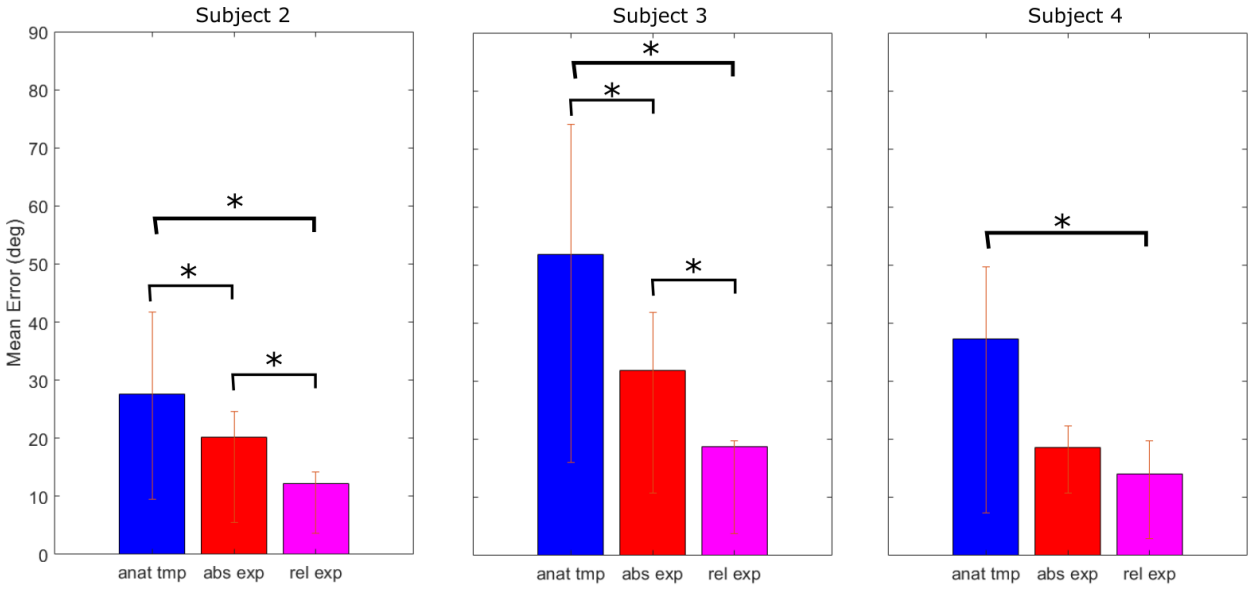


Figure 4-7 Mean errors for the anatomical template map (anat tmp) and experimental absolute (abs exp) and relative (rel exp) maps based on phosphene connection experiment results. Error bars indicate the first and third quartiles of the errors. The number of pairs used for subjects 2, 3, and 4 were 91, 67, and 20 respectively. All statistical significance of differences are based on independent sample t-test with $p<0.05$).

4.5.4 Functional Mapping Evaluation Results using Simulation of Direction of Motion

The accuracy of each mapping was evaluated based on subject's performance in detecting the direction of motion of a simulated moving circle. Figure 4-8-A shows the average response error

of each subject for all maps. The detailed distribution of error for each direction of motion is illustrated in Figure 4-8-B which represents the performance of each subject for detecting specific directions. For example subject 2 seems to have a relatively low performance in detecting diagonal movement from bottom left to top right and vice versa for all mappings while his performance in detecting horizontal direction is very high for anatomical map.

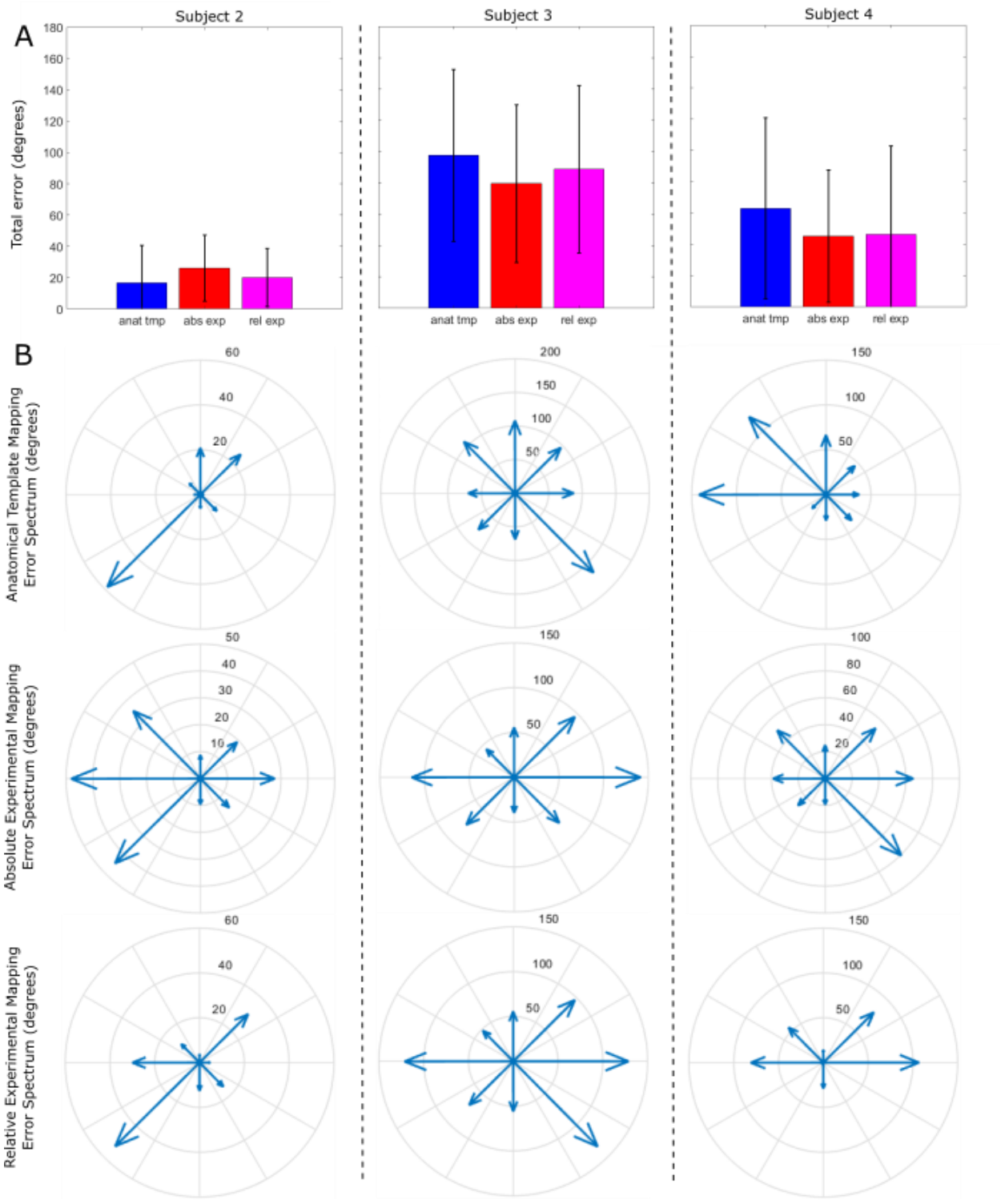


Figure 4-8 (A) Total error calculated by evaluating subjects' responses to a simulated moving object based on anatomical template map and experimental absolute and relative maps. (B) The distribution of error over different directions of motion for each map

and subject. Each subject performed 120 direction of motion trials (5 trials per mapping per direction). Error bars represent the standard deviation of the errors.

4.5.5 Visual Function Tests using the Orion Camera

Square localization and direction of motion tasks were performed 6, 12, and 24 months after implantation of Orion for each Subject. An experimental absolute map was used to program the VPU for all subjects. Figure 4-9 compares the results of square localization and direction of motion tests between device OFF and ON states ($p<0.05$). Subject 1 performed better for both tasks with device ON only at the 12-months test. Subject 2 had higher performance with device ON for both tasks at all time-points. Subject 3 performed better with device ON in square localization at 24-months' time-point while for direction of motion task he performed better at months 6 and 12. Subject 4 performed better with device ON at both tasks and all-times with the exception of month 6 for direction of motion task.

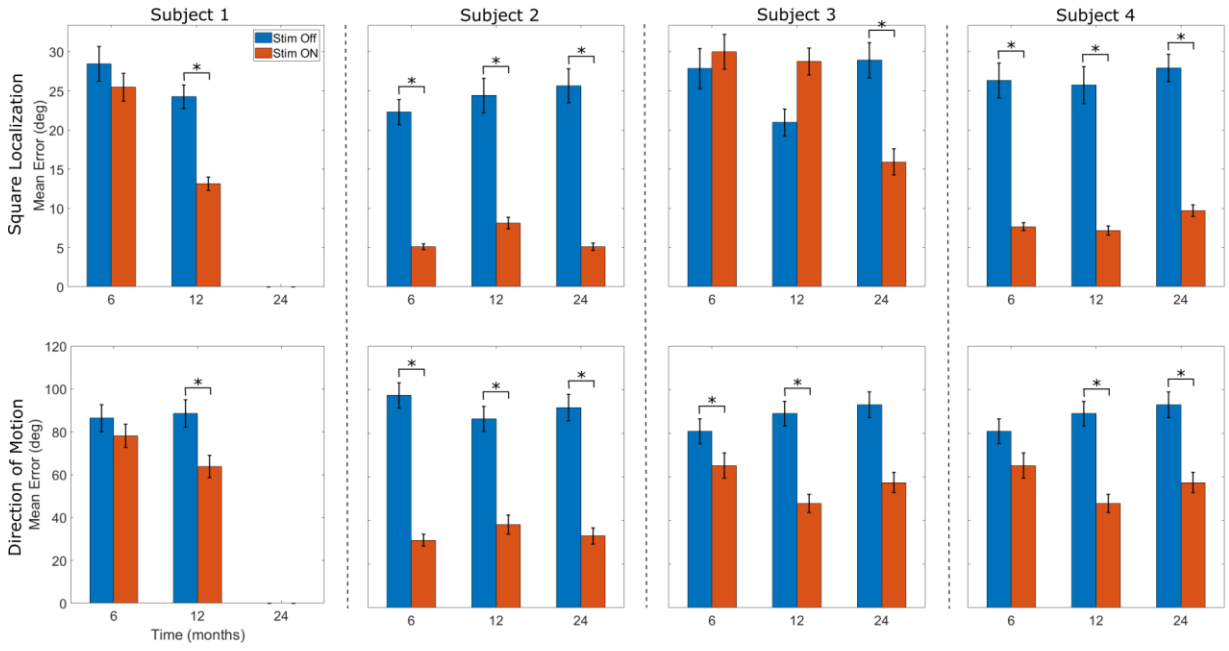


Figure 4-9 Results of visual function tests using experimental absolute map on months 6, 12, and 24 of the study. Mean errors were compared between device OFF and ON states using 2-tailed t test ($p<0.05$). For each session of square localization test, each subject

performed 40 trials with stimulation OFF and 40 trials with stimulation ON. For each session of direction of motion test, each subject performed 80 trials with stimulation OFF and 80 trials with stimulation ON. Error bars represent the standard deviation of the errors.

4.6 Discussion

We used three different methods to create a subject specific phosphene map. The anatomical template mapping method fits an average visual cortex retinotopic map to each individual brain and can be produce a phosphene map immediately after the device Implantation surgery. As reported by Benson et al. (N. C. Benson et al., 2012) the median prediction errors for eccentricity and polarity maps were 0.91 and 11.43 degrees respectively. In addition to this error, MRI/CT co-registration and electrode localization process could potentially introduce more error to the template mapping process. While we did not have a ground truth to quantify these errors, comparing the anatomical template map and experimental absolute maps can provide an evidence for such errors. For example the phosphene elicited by stimulation of electrode C03 in subject 2 was consistently drawn on the bottom of the visual field by the subject, however the anatomical template mapping predicted the location of this phosphene to be in the top hemi field with a polarity of 46 degrees. This mapping difference was observed in all subjects and was particularly significant for electrodes close the calcarine sulcus. Hence this error may be due to inaccurate localization of electrode array relative to the calcarine sulcus.

The experimental absolute map uses a reverse engineering method to predict the location of each phosphene based subjects' response to stimulation of each electrode. This approach is the most straightforward and common among visual prosthesis developers and allows to directly find the absolute location of each phosphene. The variation in location of phosphenes throughout the period of this study shown in Figure 4-4 and quantified in Figure 4-5-A, created significant overlaps

among the estimated location of phosphenes (Figure 4-5-B). While this method has been shown to produce accurate results in sighted patients with temporally implanted surface electrodes(Yoshor et al., 2007b), the lack of visuo-motor feedback in blind individuals is potentially one of the main factors in low accuracy of this mapping method.

The experimental relative mapping approach was to minimize the visuo-motor feedback error by providing a visual reference for the subjects. While the experimental absolute maps poorly localized phosphenes that are close to each other, sequential stimulation can clarify the relative locations of these phosphenes. Since Orion VPU requires an absolute map, we used an optimization function to find the absolute location of each phosphene that produces the closest relative locations to the phosphene connection trials.

In addition to the experimental relative map, phosphene connection experiments provided reliable information for evaluation of mapping techniques. By selecting the phosphene pairs with consistent response from subjects, we were able to evaluate how accurately each map predicts the results of phosphene connection experiments. This evaluation method showed that the experimental relative map is the most accurate for predicting the relative location of the phosphenes. Even though the experimental relative map utilized the phosphene connection results, the leave-one-pair-out method guaranteed that the pairs used for evaluation would not contribute to the mapping process.

The simulation of direction of motion experiment was designed to evaluate the "functional performance" of each map by simulating the stimulation sequence produced by a moving white ball in a black background. Simulation of the moving ball allowed us to use the direct stimulation mode on the Orion programmer without using external visual stimuli and the camera which would limit our capability of randomly shuffling the mappings and also would produce additional errors

due to subjects' eye and head movement. While we avoided some sources of error, there were still multiple factors that could have contributed to the inaccuracies in the subjects' responses. The non-uniform topology of the phosphene maps is one of the main obstacles in creating smooth and precise movement perception. Moreover difference in phosphene size and brightness could also be a misleading factor in perception of direction of motion.

The visual function tests were designed to evaluate the overall performance of the subjects using the whole Orion system including the camera and video processing unit. Given the limitations of evaluating mapping techniques using simulation of direction of motion, we determined that visual function test would inherit the same limitations with addition of potential subject head movement. We compared the subjects performance between device ON and OFF throughout the period of the study using only the experimental absolute map. Visual function test results clearly show that the device was beneficial for detecting static and moving objects especially after 24 months from implanting the device.

5 Functional mapping of motor system based on movement-related dynamics of thalamo-cortical oscillations

The ventrolateral (VL) nucleus of the thalamus is a well-documented target for DBS (Lozano, 2000; Vaillancourt et al., 2003) and thalamotomy (Narabayashi, 1989; Ohye et al., 1982) for the treatment of tremor. VL is structurally connected to motor cortices (Ge, Md, & Mr, 1989; Tsolaki, Downes, Speier, Elias, & Pouratian, 2018) and cerebellum (Gallay et al., 2008) forming a cerebello-thalamocortical (CTC) network. In ET patients, all nodes of the CTC network manifest oscillatory activity at tremor frequency and its first harmonic pointing to the pathological alteration of communication in this network (Schnitzler et al., 2009). Alpha oscillations in the motor cortex of ET patients decrease during high frequency stimulation of VL (Air et al., 2012) confirming functional connectivity between VL and motor cortex and, perhaps more importantly for the current discussion, thalamic influence on cortical activity. In a recent study thalamocortical PAC and coherence is shown to peak at the same frequency during rest and decrease with movement suggesting a gating role of the thalamus in movement execution(Opri et al., 2019). However, how these distinct frequency bands inter-relate across nodes remains unclear due to lack of causal analyses and more sophisticated analyses that can isolate the effects of each node on observed cross-frequency coupling relationships.

Intraoperative recording of cortical and subcortical local field potentials (LFP) in subjects undergoing DBS for movement disorders has provided valuable data (Malekmohammadi et al., 2015; D. D. Wang et al., 2018; Yu et al., 2012). In this chapter, we aim to confirm the movement-related spatiotemporal evolution of oscillatory changes in thalamus and motor cortex and to use these recordings to better understand the dynamic interactions between thalamic and cortical oscillatory activity in movement execution. Because of underlying coherence between the nodes,

distinctions between local and cross-site coupling are not clear, necessitating application of a novel method of "partial phase amplitude coupling", based on the same principle of partial coherences. As demonstrated in Figure 5-1-A we hypothesize the thalamus serves to regulate low frequency cortical activity which in turn modulates cortical gamma band activity as a cascade of events in the motor network.

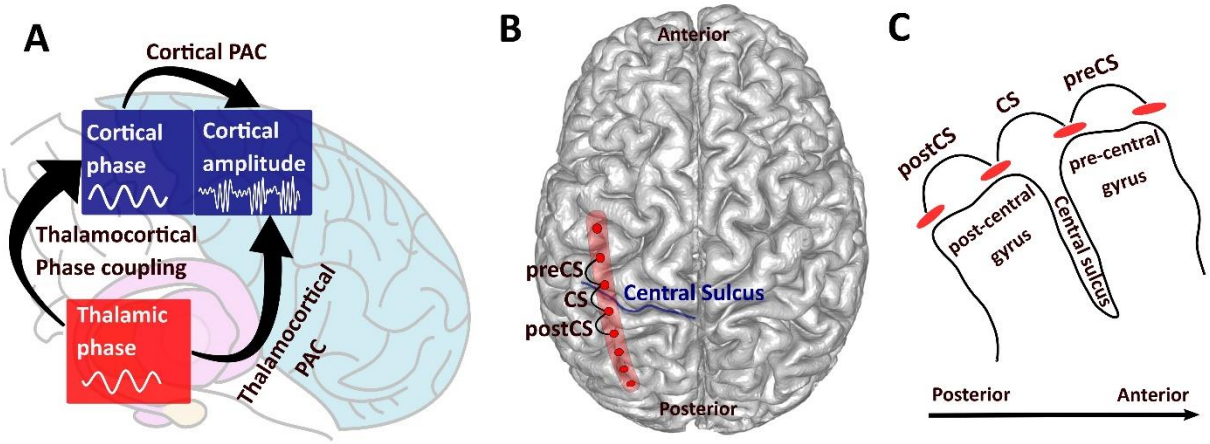


Figure 5-1 A) Our hypothetical model of the thalamo-cortical oscillations where the thalamus regulates low frequency cortical activity via phase synchrony and modulates the cortical broadband activity via PAC. B) Placement of the ECoG strip in relation to Central Sulcus over the reconstructed brain surface. C) Three cortical bipolar contacts representing the Central Sulcus (CS) and precentral gyri (postCS and preCS).

5.1 Subjects

Eleven patients (3 males and 8 females with 52±14 years of age) undergoing stereotactic implantation of DBS lead targeting VL participated in this study and were diagnosed with ET (Table 2). All patients provided written informed consent approved by the Institutional Review Board (IRB) at the University of California Los Angeles.

Table 2 Patients demographics and clinical information

Subject Code	Age	Gender	Handedness	Total tremor score	Recorded hemisphere
P1	76	M	R	50	R
P2	79	M	R	71	R
P3	59	F	R	75	R
P4	37	F	R	58	L
P5	67	F	R	45	L
P6	59	M	R	36	L
P7	66	F	R	41	L
P8	35	F	R	NA	L
P9	71	F	R	37	L
P10	75	F	R	NA	R
P11	63	F	L	57	R

5.2 Surgical procedures

DBS electrode implantation for all subjects targeted VL located ~5-6mm anterior to posterior commissure, 11mm lateral to the third ventricular wall, and at the depth of the anterior commissure-posterior commissure line. Intraoperative awake macrostimulation testing was performed to confirm the clinically valid placement of implanted DBS leads with tremor suppression. Before implantation of the DBS lead (left side for the unilateral left DBS cases and right side for unilateral right and bilateral DBS cases), an eight contact ECoG strip (platinum-iridium 4-mm contacts with 1-cm spacing; AdTech Medical, USA) was implanted subdurally

posteriorly towards the central sulcus through the frontal burr hole placed for DBS lead implantation (Figure 5-1-B). The burr hole was always located at or up to 1cm anterior to the coronal structure. Location of DBS electrodes and the ECoG strip was assessed using a single-view lateral fluoroscopy image captured after implantation of the DBS lead(s) and postoperative stereotactic thin slice CT (DBS lead only). The ECoG strip was removed after conducting the experiments, prior to anchoring the DBS lead.

5.3 Data acquisition

All patients underwent pre-operative MR and CT and post-operative CT imaging. Pre-operative MR was a T1-weighted magnetization prepared rapid acquisition gradient echo (MPRAGE) image (slice thickness = 1 mm, repetition time = 2100 ms, echo time, 2.98 ms, flip angle = 15º, 3T, Siemens Skyra) and a 64-direction diffusion tensor image (DTI) acquired using a spin echo single phase encoding direction sequence (TR=7000 ms, TE=72 ms, matrix 128 × 128, 2 mm isotropic voxels, flip angle= 90, slice thickness=3 mm, number of slices=52). One volume was acquired without use of a diffusion gradient (that is, b = 0 seconds/mm^2). Pre-operative CT scan was performed after a Leksell stereotactic head frame (Elekta Instruments) was applied to the skull using 1-mm slice thickness (Siemens Sensation 64). ECoGs and thalamic LFPs were recorded using g.USBamp 2.0 amplifiers (gTec, Austria) and BCI2000 v3 data acquisition software. The sampling frequency was 2400Hz and the data was band pass filtered (0.1Hz-1000Hz) online. The ground and reference electrodes were placed on the scalp for all subjects. Thalamic LFPs were recorded by a DBS lead with four ring macroelectrode contacts (numbers 0 to 3 ventral to dorsal, DBS Lead Model 3387, Medtronic Inc. MN, USA) in the final implant position.

5.4 Experimental Protocol

Patients performed 3 blocks of finger tapping hand movement initiated by a verbal cue, using the hand contralateral to the ECoG strip placement. Each movement block lasted 30 seconds and was preceded by a 30 second period of rest with eyes open. A kinematic glove (5DT Data Glove) was used to measure the flexure of each finger during the experiment. The five-channel kinematic data with original sampling rate of 75Hz was recorded using BCI2000 software oversampled at 2400Hz.

5.5 Data processing

5.5.1 Electrode localization

Thalamic recordings were always used from the most ventral contact on the DBS lead (contact 0) and therefore bipolar contact 0-1 was selected to represent thalamic activity. A method proposed and validated by Randazzo et al. was adopted to localize the ECoG contacts (Randazzo et al., 2016). Pre and post-op scans were co-registered to the MR image using Statistical Parameter Mapping (SPM) toolbox (SPM12, http://www.fil.ion.ucl.ac.uk/). The cortical surface was reconstructed from the pre-operative MR image using FreeSurfer (Dale et al., 1999a) and ECoG contacts were mapped to the reconstructed cortical surface (Figure 5-1-B). Bipolar contacts spanning the central sulcus (CS) and bipolar contacts located immediately anterior (preCS) and posterior (postCS) to CS were chosen for further analysis (Figure 5-1-C).

5.5.2 Structural connectivity

To ensure the structural and functional relevance of the thalamo-cortical analyses, probabilistic diffusion tractography was performed to define the structural connectivity between the bipolar

DBS contact 0-1 and the whole brain. Before proceeding with diffusion tensor imaging (DTI) analysis, for each patient, contacts were delineated in native T1 space based on the electrode location in CT image that was transferred to T1 using FSL linear transformation (FLIRT) (Jenkinson et al., 2002). The coordinates of the inter contact distance were used as a center point to create a 2 mm sphere mask. To register the contact mask to preoperative DTI space, linear and non-linear transformations (FLIRT-FNIRT) (Andersson et al., 2007; Jenkinson et al., 2002) were performed to register pre-operative T1 and DTI to MNI152 template (using mutual information as cost function, 6 degrees of freedom for DTI to T1 registration and 12 for registration to MNI152) and the derived transformation matrices were used for the transformation.

DTI data preprocessing included skull extraction and eddy current correction after which a multi-fiber diffusion model was fitted to the data (Behrens et al., 2007). This model uses Bayesian techniques to estimate a probability distribution function (PDF) on the principal fiber direction at each voxel, accounting for the possibility of crossing fibers within each voxel. Using these PDFs and PROBTRACKX, we could then determine the probability of connectivity between thalamic recording site and the whole brain. From each voxel in the seed, 5,000 streamlines were generated; a loop check termination was used and a 0.2 curvature threshold was chosen. Each patient's whole brain probabilistic tractography map was divided by the overall number of streamlines and then binarized at 0.01 threshold value. Each binary map was transformed into MNI-152 space before summing all maps and dividing by the total number of subjects in order to define the average connectivity map. The precentral gyrus region for each subject was identified using FreeSurfer v 5.3.0 for cortical surface reconstruction and automatic volumetric segmentation. For each subject, the precentral gyrus mask was transformed to MNI152 space using the matrices derived from the

registration of T1 to MNI152 space and the mean precentral gyrus binary mask across the subjects was derived (Figure 5-3, green mask).

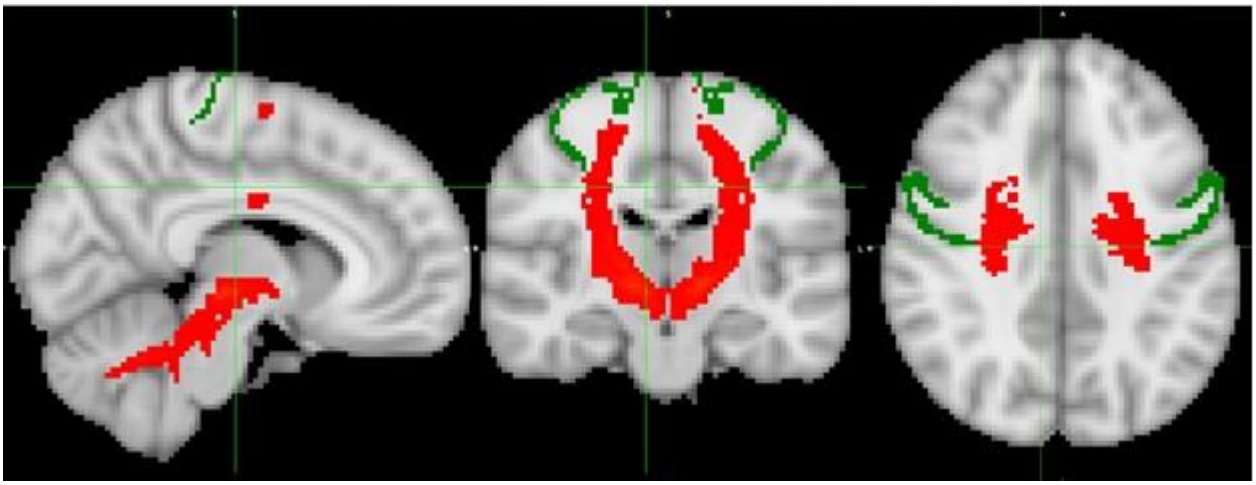


Figure 5-2 Average whole brain binary structural connectivity map seeded from the VL (contacts 0-1). Red represents areas across the whole brain with strong structural connectivity (probabilistic tractography binerized at threshold value of 0.01) to VL (Red) and green is the result of application of a pre-central gyrus mask.

5.5.3 Signal pre-processing

All LFP analyses were performed offline using Matlab (Mathworks Inc. NA. USA). All signals were bipolar re-referenced to enhance signal to noise ratio (SNR) and spatial specificity. An adaptive notch filter was used to remove power line noise (at 60 Hz) and its harmonics up to 270 Hz (Mewett et al., 2001) and signals were band pass filtered using a zero phase FIR filter (2-800 Hz, EEGLab (Delorme & Makeig, 2004)) to prevent any phase delay or distortion. Blocks of rest and movement were identified using the kinematic finger movement data and three pairs of consecutive rest and movement blocks were chosen for each subject.

5.5.4 Power spectral density

Fourier analysis was performed on 1 second consecutive non-overlapping windows for each block using Thomson's multi-taper method (frequency bandwidth = 2Hz, 3 tapers) implemented in Chronux toolbox (Bokil et al., 2010). To compensate for inter-subject/block variability in baseline power, each resting block was normalized to the total power (5-300 Hz) and each movement block was normalized to the total power of its preceding resting block. Power spectral density for each condition was then calculated by multiplying the normalized Fourier coefficients by their complex conjugate.

5.5.5 Phase synchronization and directional connectivity

The de-biased weighted phase lag index (dwPLI) method was used to measure the phase coupling between VL and cortical signals because it is a functional connectivity metric that is insensitive to volume conduction (Vinck et al., 2011). To estimate the direction of information routing between thalamus and cortex, the direct transfer function (DTF) implemented in the eConnectome MATLAB toolbox(He et al., 2011) was used to estimate the granger causality. DTF is a frequency-domain estimator of granger causality, based on multivariate autoregressive (MVAR) modeling (Kaminski & Blinowska, 1991). The DTF computation function utilized ARfit package (Schneider & Neumaier, 2001) to estimate the MVAR model $H(f)$ which represents how a current value of channels is dependent on the previous values of itself and other channels.

5.5.6 Phase amplitude coupling (PAC)

Modulation Index (MI) (Tort et al., 2010) was used to measure the PAC in the thalamo-cortical network. Hilbert transform along with a zero-phase FIR bandpass filter were used to obtain instantaneous phase (4-35 Hz) and amplitude (60-200 Hz) of the signals. Band width for

calculating the instantaneous phase was set to 2 Hz while for instantaneous amplitude bandwidth was adjusted as twice the phase of interest to fit the sidebands caused by the assumed modulating lower frequency band(Aru et al., 2015). Phases were divided into N=18 bins (bin width = 2pi/N), $\{\varphi_1, \varphi_2, \dots, \varphi_N\}$, and the mean amplitude $\langle A \rangle(\varphi_i)$ was calculated and normalized for each bin to form a probabilistic distribution function $P(i)$ where

$$P(i) = \frac{\langle A \rangle(\varphi_i)}{\sum_{k=1}^{N} \langle A \rangle(\varphi_k)}$$

Then MI is calculated by quantifying how P deviates from a uniform distribution (U) based on measuring Kullback-Leibler distance (D_{KL}):

$$MI = \frac{D_{KL}(P, U)}{\log(N)}$$

5.5.7 Partial Phase amplitude coupling

To estimate whether observed thalamo-cortical PAC is an epiphenomenon of thalamo-cortical phase coupling and cortical PAC, a method of "partial phase amplitude coupling" was used to show that thalamo-cortical PAC is partially dependent on the causal thalamo-cortical phase coupling led by VL. Partial PAC calculates phase amplitude coupling between the phase of thalamic signal and amplitude of cortical signal while assuming thalamic and cortical phase are *independently* coupled to the cortical amplitude. If the thalamo-cortical partial PAC is significantly smaller than thalamo-cortical PAC then we can safely conclude that thalamo-cortical PAC is at least partially dependent on cortical PAC.

Let $\Phi = \{\varphi_1, \varphi_2, \dots, \varphi_N\}$ be thalamic phase, $\Theta = \{\theta_1, \theta_2, \dots, \theta_N\}$ be the cortical phase, and A be the cortical amplitude. $P(i)$ in the previous subsection could also be written as $E[A|\varphi_i]$ where $E[\,]$

represents the expected value and can be estimated by averaging the cortical amplitudes that correspond to each thalamic phase. We can introduce Θ into this equation by adding another phase dimension for Θ (Figure 5-3) and write $E[A|\varphi_i]$ as:

$$E[A|\varphi_i] = \sum_{k=1}^{N} P(\theta_k|\varphi_i)E[A|\varphi_i, \theta_k]$$

Where $E[A|\varphi_i, \theta_k]$ is the expected value of the cortical amplitudes corresponding to φ_i and θ_k phases and $P(\theta_k|\varphi_i)$ is the probability distribution of each θ_k for eachφ_i. If the thalamocortical PAC is independent of causal phase coupling from θ_k toφ_i, then we can substitute the $P(\theta_k|\varphi_i)$ with $P(\theta_k)$:

$$E[A|\varphi_i] = \sum_{k=1}^{N} P(\theta_k)E[A|\varphi_i, \theta_k]$$

And calculate the modulation index and PAC which we call "partial modulation index" and "partial phase amplitude coupling".

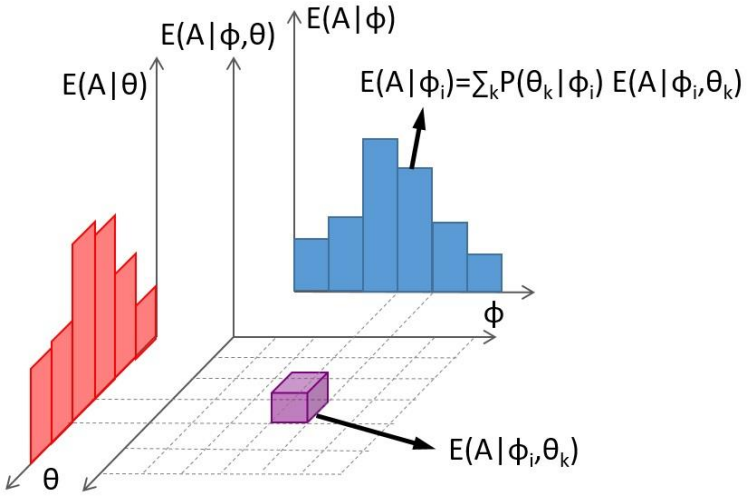


Figure 5-3 Each cortical amplitude A was assigned to a 2D phase bin of thalamic phase φ_i and cortical phase θ_k and $E[A|\varphi_i, \theta_k]$ was calculated by averaging the amplitudes assigned to each phase bin. The probability distribution of amplitudes for each thalamic

phase bin $E[A|\varphi_i]$ can be calculated by weighted averaging the $E[A|\varphi_i, \theta_k]$ values based on the probability distribution of cortical phase for each thalamic phase $P(\theta_k|\varphi_i)$.

5.6 Statistical analysis

5.6.1 Power spectral density

To determine the significance of movement related spectral power changes, we performed a two-group test of spectrum to test the null hypothesis that two conditions (rest and movement) have equal spectra over the range of 5-300 Hz. We calculated the group spectral mean and variance for each condition and obtained the Z statistics using asymptotic probability distribution (Bokil et al., 2007). We chose this method based on asymptotic probability distributions and jackknife correction of the difference z-scores as it corrects for the bias inherent to the spectral estimation process(Malekmohammadi, AuYong, Price, et al., 2018). To correct for multiple comparisons we only rejected the null hypothesis for the frequencies constituting bands whose width was larger than the double bandwidth of multi-taper method (4Hz)(Bokil et al., 2007; Malekmohammadi, AuYong, Ricks-Oddie, et al., 2018).

5.6.2 Phase synchronization

To determine the statistical significance of movement related changes in coupling measured by dwPLI method, a non-parametric permutation testing (N=1000) was used. We generated a pool of dwPLI values corresponding to both conditions. At each permutation, we randomly selected two equal subgroups from the pool and calculate the group difference for the null hypothesis. We used Fisher Z-transform to generate a normal distribution of the condition difference under the null hypothesis. The significance of the condition difference was determined for p=0.05 and corrected

for multiple comparisons using False Discovery Rate (FDR) method (Benjamini & Hochberg, 1995).

5.6.3 Phase amplitude coupling

A non-parametric permutation testing was used to determine the significance of PAC values during rest and movement blocks (N=1000). We generated surrogate data by randomly shifting the phase data while keeping the amplitude signal unchanged and calculated the z-scores. The significant PAC values were determined for p=0.05 and corrected for multiple comparison using FDR method.

5.6.4 Band related statistics

Total power of each frequency band was calculated by summing the spectral power density values over the frequency range of interest. Thalamo-cortical phase coupling over each frequency band was obtained by averaging dwPLI values over the frequency range of interest. For DTF analysis, surrogate data (N=1000) was generated by phase shifting the original time series and z-scores were calculated for each direction of connectivity. The z-scores were then averaged over the trials and the frequency range of interest. For cross-frequency coupling analysis, PAC between the phase of alpha/low-beta and amplitude of broad-band gamma (60-200 Hz) was obtained by averaging over two dimension of frequencies. To determine the significance of PAC between the frequency bands for each subject, a non-parametric permutation testing was performed using the surrogate data described in the previous subsection. After obtaining band related measures of power, phase coupling and PAC for each subject, significance of each movement related change was assessed. Due to the limited number of subjects, Shapiro-Wilk test was used to quantify the normality of the distribution. If the normality condition was satisfied, the paired sample t-test was used. Otherwise

Wilcoxon signed rank test was used to assess the significant difference. The resulting p-values were corrected using Bonferroni method.

5.7 Results

5.7.1 Clinically-defined VL is structurally connected to the pre-central gyrus

We evaluated whole brain probabilistic tractography seeded from the clinically-confirmed VL (contacts 0-1) (Figure 5-2). The average binary connectivity map reveals white matter projections from VL to peri-rolandic cortices, centered on pre-central gyrus along with projections to the cerebellum.

5.7.2 Movement is associated with redistribution of power

Thalamic and cortical resting state power spectra reveal a peak between the classically defined alpha and low-beta bands (Figure 5-4-A, 11.7±3.1Hz, 12.0±2.8Hz, 12.0±2.1Hz, and 11.1±1.9Hz for VL, postCS, CS and preCS contacts respectively). Movement significant decreases cortical power between 5.2-32.8 Hz for the post-CS, 5.2-35.1Hz for the CS, and 5.2-41Hz for pre-CS recordings. On the other hand, higher frequency cortical powers (39.2-209.2 Hz for post-CS, 42.8-246.7Hz CS and 43.3-210.4Hz for pre-CS) increase during movement. Thalamic LFP demonstrate movement-related suppression of 5.2-18.8 Hz, but no power increase in the broadband gamma range, as seen in the peri-rolandic cortices.

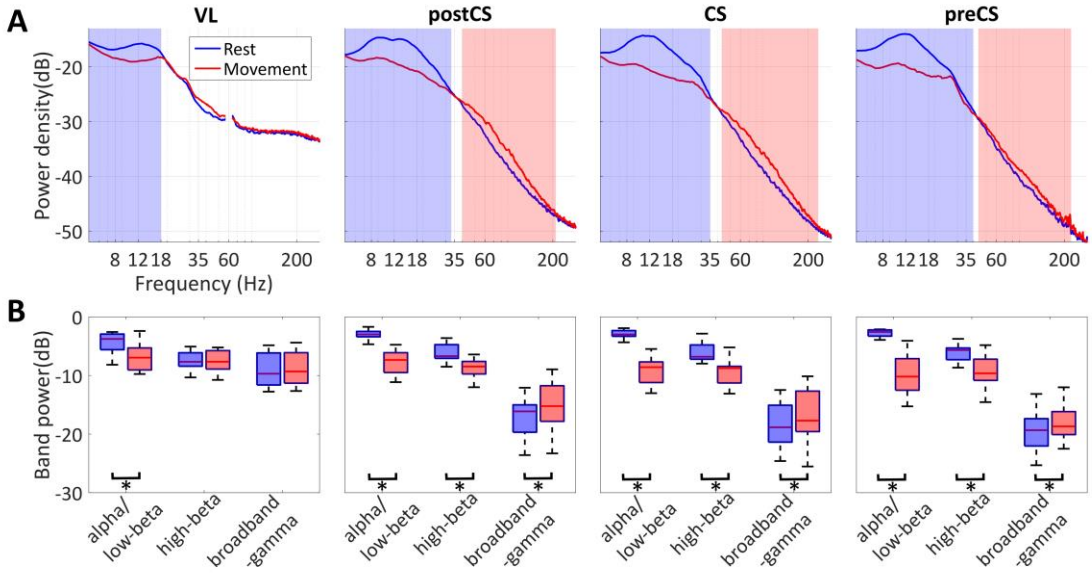


Figure 5-4 Distribution of power in VL and sensorimotor cortex during rest and movement trials. A) Group (11 subjects) average,Power spectral density normalized to the resting state total power of the frequency range of 5-300 Hz. highlighted areas indicate the frequencies with significant spectral power difference between rest (blue) and movement (red). B) Frequency band powers (area under curve) for alpha/low-beta, high-beta, and broadband-gamma during rest and movement. Error boxes represent the first and third quartiles and error bars represent the min and max values. Significant differences are marked by the asterisk (*) indicating significance at $P<0.05$ level.

Because alpha and low-beta oscillations seem to manifest similar movement-related behaviors (as detailed in the paragraph above), an observation that has also been previously reported in ET patients(Air et al., 2012; Kondylis et al., 2016), we treat these oscillations as a single entity for band related analyses. Statistical spectral analysis was performed in three distinct frequency bands of alpha/low-beta (8-18Hz), high-beta (20-35Hz) and broadband-gamma(60-200Hz). As presented in Figure 5-4-B, cortical power significantly decreases in both alpha/low-beta and high-beta ($p=0.001$ for all cortical contacts, Wilcoxon signed rank) and significantly increases in broadband-gamma ($p=0.003$, 0.005, 0.024 for post-CS, CS and pre-CS contacts respectively, Wilcoxon signed rank). In the thalamus, however, power only significantly decreases in alpha/low-beta band

(p=0.005, Wilcoxon signed rank) (Figure 5-4-B). After correcting for multiple comparison, all but movement-related broadband-gamma power increase in pre-CS contact survive the Bonferroni correction test.

5.7.3 Phase coupling between VL and CS is dampened during movement

Movement is associated with a significant decrease in phase based connectivity (dwPLI) between VL and CS measured in the 10-13.5 Hz range, while increases in connectivity were noted between 25.2-30.5 Hz (Figure 5-5-A). For band-based analyses, the only significant movement related change occurs at VL-CS where alpha/low-beta coupling is significantly reduced by movement (p =0.019, Wilcoxon signed rank); movement related increase in high-beta coupling is not significant using this analytic approach (p=0.21, Wilcoxon signed rank) (Figure 5-5-B). Average resting state granger causality in the alpha/low-beta band from VL to cortical contacts is higher than the reverse direction, with significant differences in causality noted between VL and CS (p=0.019, Wilcoxon signed rank, Figure 5-5-C).

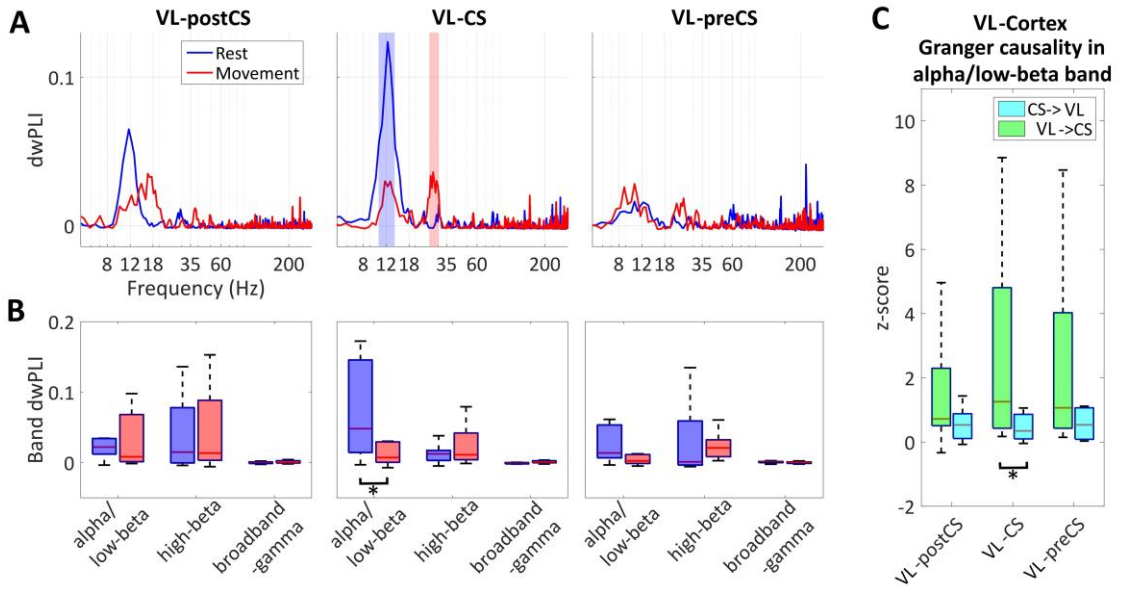


Figure 5-5 Measures of thalamo-cortical connectivity between VL and sensorimotor cortex during rest and movement trials. A) dwPLI calculated in the frequency range of 5-300 Hz. Highlighted regions indicate the frequencies with significant dwPLI difference between rest (blue) and movement (red). B) Frequency band average dwPLI for alpha/low-beta, high-beta, and broadband-gamma during rest and movement. C) Average Resting state granger causality z-scores from VL to cortical contacts and vice versa in alpha/low-beta band. Error boxes represent the first and third quartiles and error bars represent the min and max values.

5.7.4 Alpha/low-beta to broadband-gamma PAC is suppressed during the movement

Group-level analysis of resting state PAC reveals significant coupling between the phase of alpha/low-beta oscillations and amplitude of broadband-gamma activities in cortical contacts (Figure 5-6-A). On an individual basis, of 11 total subjects evaluated, the number of subjects with significant resting PAC were 7 for postCS, 9 for CS and 8 for preCS contact. In contrast, group level analyses during movement demonstrates an absence of PAC (Figure 5-6-A). On an individual basis, the number of subjects with significant PAC during movement was 5 for postCS (4 of which had significant resting state PAC), 3 for CS (2 with resting state PAC) and 5 for preCS (4 with resting state PAC) contact. Indeed, movement is associated with a significant decrease in cortical

PAC for motor contacts of the cortex (p=0.003, 0.005 for CS and preCS contacts respectively, Wilcoxon signed rank, Figure 5-6-B).

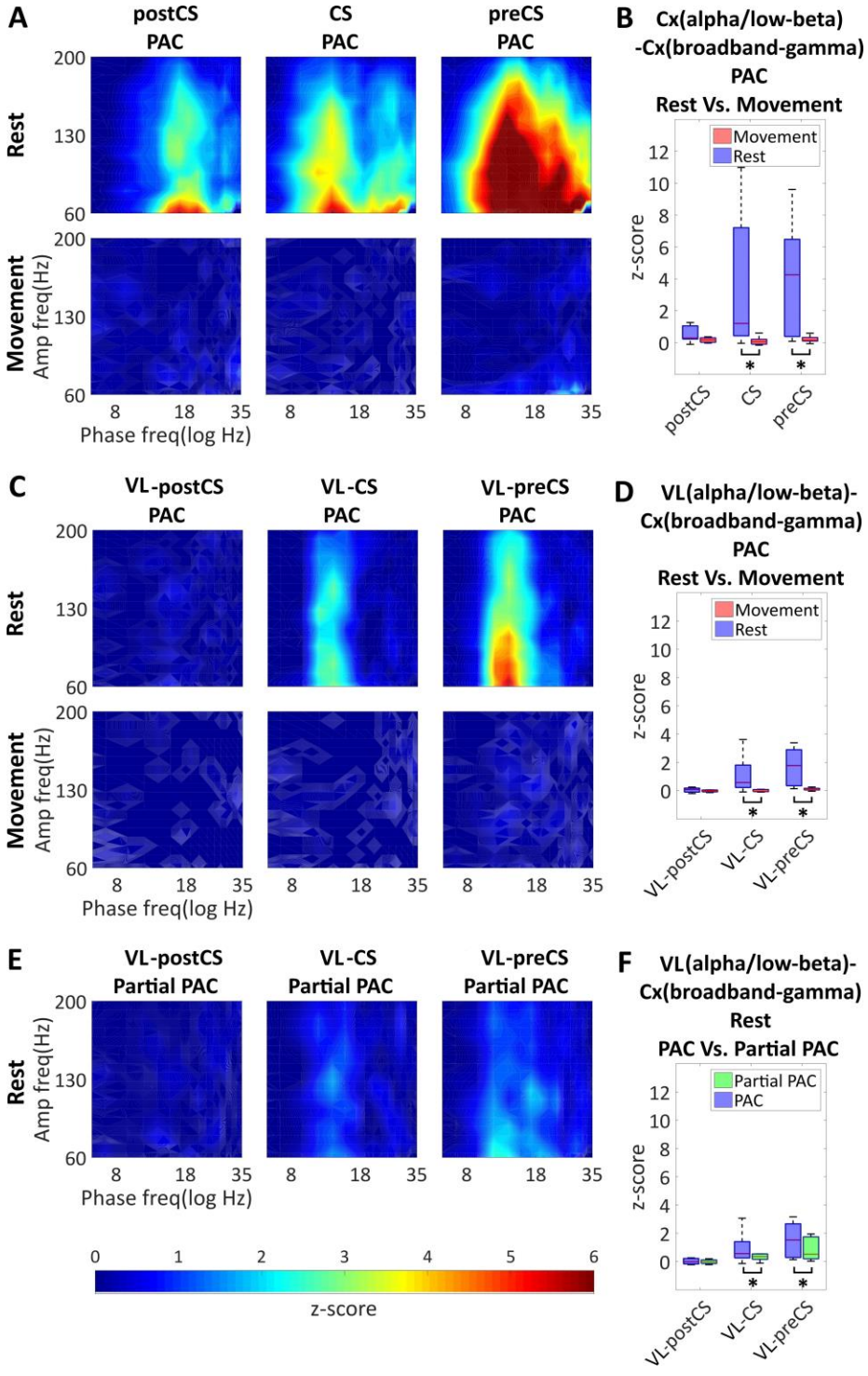


Figure 5-6 A) Cortical PAC between the phase of cortical contacts and the amplitude of the same signal during rest and movement. B) Average cortical PAC between the phase of alpha/low-beta and amplitude of broadband-gamma activities during rest and movement. C) Thalamo-cortical PAC between the phase of VL and the amplitude of the cortical signals during rest and movement. D) Average thalamo-cortical PAC between the phase of alpha/low-beta and amplitude of broadband-gamma activities during rest

and movement. E) Resting state thalamo-cortical partial PAC between the phase of VL and the amplitude of the cortical signals when the confounding bias of cortical phase was removed. F) Average thalamo-cortical PAC and partial PAC between the phase of alpha/low-beta and amplitude of broadband-gamma activities during rest. Error boxes represent the first and third quartiles and error bars represent the min and max values.

Similarly, at rest, thalamo-cortical PAC is observed between the phase of thalamic alpha/low-beta oscillations and the amplitude of cortical broadband-gamma activities (Figure 5-6-C, number of subjects with significant resting PAC were 2 for postCS, 9 for CS and 10 for preCS contact). Like that seen in the cortex, thalamocortical PAC is absent during movement at the group level (Figure 5-6-C, number of subjects with significant movement PAC were 1 for postCS (which did not have a significant resting state PAC) and 2 each for both CS and preCS contacts (which all had significant resting state PAC as well). Like cortical PAC, movement is associated with a significant decrease in thalamocortical PAC between the VL and peri-rolandic cortices ($p=0.001$, for both CS and preCS contacts, Wilcoxon signed rank, Figure 5-6-D).

5.7.5 Validating the partial PAC method using a simulated dataset

To evaluate the partial PAC method we generated two sets of data. Each set of data include a low frequency 13Hz sine wave with its phase randomized every 1 second and band pass filtered between 3 and 23Hz which for the sake of this paper we called thalamic signal. Each set also includes a combination of random phase low frequency sine wave as explained before and a high frequency 150Hz sine wave which we called cortical signal. A random white was also added to both signals. For dataset#1, each signal is partitioned in 3 segments with equal length. In the first and third segment there is not phase coupling or PAC in any of the signals while in the second segment, thalamic phase is coupled to the cortical phase and thalamic and cortical phase are both coupled to the cortical amplitude. Similarly dataset#2 consisted of three equal length segments where in the first segment thalamic phase is coupled to the cortical amplitude but there is no cortical PAC or thalamo-cortical phase coupling. In the second there is no thalamo-cotical or

cortical PAC but there is thalamo-cortival phase coupling and in the third segment there is no thalamo-cortical phase coupling or PAC but there is cortical PAC (Figure 5-7-A).

Figure 5-7-B shows the result of applying thalamo-cortical PAC, cortical PAC and thalamo-cortical partial PAC on the two dataset. As expected for both dataset there is a thalamo-cortical and cortical PAC between phase frequencies around 13Hz and amplitude frequencies around 150Hz. The partial thalamo-cortical PAC cannot be observed for dataset#1 as this coupling is the result of the phase coupling and cortical PAC in the second segment. On the other hand partial thalamo-cortical PAC exists for dataset 2 as the thalamo-cortical PAC (segment 1) is independent of thalamo-cortical phase coupling (segment 2) and cortical PAC (segment 3).

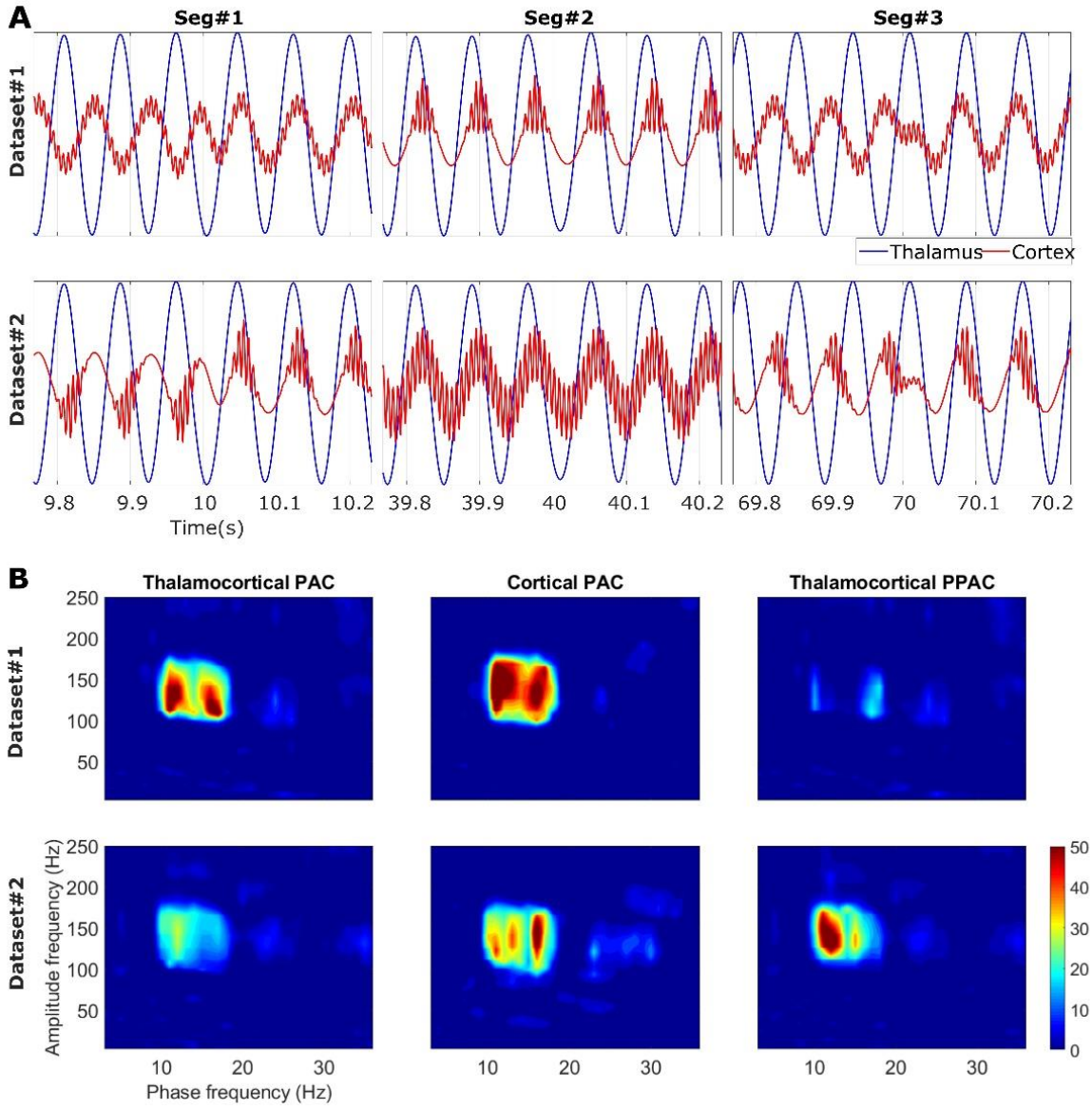


Figure 5-7 A) Zoomed in segments of the simulated datasets. Simulated thalamic signal (blue) is a 13Hz sine wave and simulated cortical signal (red) is the combination of a 13Hz and a 150Hz sine waves. For the illustration purpose the random white noise in both signals is not included in this figure. Seg#2 of dataset#1 contains thalamic and cortical signals with phase synchrony cortical and thalamo-cortical PAC simultaneously. For dataset#2, seg#1 contains thalamo-cortical PAC, seg #2 contains thalamo-cortical phase coupling and seg#3 contains cortical PAC. B) Z-scores for thalamo-cortical and cortical PAC as well as thalamo-cortical partial PAC for the simulated datasets.

5.7.6 Cortical PAC has confounding bias on the observed thalamocortical PAC

To determine the relative contribution of alpha-low beta oscillations in the cortex as opposed to the similar low frequency oscillations in thalamus in driving PAC, we applied the method of "partial PAC," described in the methods. After accounting for the possible contributions of local cortical alpha-low beta phase driving PAC, residual thalamo-cortical PAC between VL and motor cortical contacts is significantly reduced and almost non-apparent ($p=0.002$, 0.001 for CS and preCS contacts respectively, Wilcoxon signed rank, Figure 5-6-E and Figure 5-6-F).

5.8 Discussion

The precise role of the thalamus in voluntary motor control remains unclear. In a prior report, we assessed thalamo-cortical coupling across cortical regions and found a strong correlation between thalamic low frequency oscillatory power, thalamo-cortical coherence, and cortical PAC (Malekmohammadi et al., 2015). Still, questions remain about the specific dynamics in the motor thalamo-cortical network and the precise causal relationships between thalamic low frequency oscillations and cortical high frequency activity. We aimed to use unique intraoperative opportunities to gain insights by analyzing the oscillatory mechanisms by which the thalamo-cortical network transfers and processes information during a voluntary movement task. Our analyses confirm previously reported movement-related suppression of alpha and low-beta oscillations across sensorimotor cortex (N E Crone et al., 1998; Kilavik et al., 2013; Kondylis et al., 2016; Malekmohammadi, AuYong, Ricks-Oddie, et al., 2018) and VL (Brücke et al., 2013) as well as augmentation of broadband-gamma activities in cortex (N E Crone et al., 1998; Nathan E. Crone et al., 2006; Dalal et al., 2008; Ohara, 2000; Pfurtscheller et al., 2003). Moreover, our results are in line with findings of Opri et al. which demonstrates the suppression of thalamo-cortical coherence and PAC, and importantly provide more definitive evidence of the precise contributions

of thalamic oscillatory activity in modulating cortical gamma activity related movement execution via directed thalamo-cortical oscillatory coupling.

Broadband-gamma activity in sensorimotor cortex have been consistently found to be temporally and spatially specific to movement (Brovelli et al., 2005; Brunner et al., 2009; Nathan E. Crone et al., 2011b; Dalal et al., 2008; Leuthardt et al., 2007; K. J. Miller et al., 2007; Pfurtscheller et al., 2003). Hence uncovering the dynamic relationship between thalamo-cortical network oscillations and cortical broadband-gamma activities provides an opportunity to understand the underlying mechanisms of voluntary movement execution and the role of the thalamus in regulating this activity. Importantly, we confirm prior findings that motor cortical PAC between the phase of alpha/low-beta and amplitude of broadband-gamma activities in essential tremor, as reported by Kondylis and colleagues (Kondylis et al., 2016). Still, the precise role of the thalamus in contributing to or regulating cortical PAC has not been extensively investigated.

It is important to consider that significant PAC can be observed in the absence of true physiological coupling (Aru et al., 2015; Ole Jensen et al., 2016). While we have followed Aru et al. suggestions to increase the specificity of our PAC measurement, movement-related reduction in PAC could be due to movement-related reduction of power in alpha/low-beta band. While we cannot rule out this effect, our primary conclusion of the relative contribution of thalamus and cortex to PAC would still hold. In another study Cole et al. convincingly shows that PAC can arise from non-sinusoidal phase-encoding oscillations. Given low freqency alpha/low-beta oscillations generally are thought to occur over large spatial distributions, one would expect that a PAC measurement that reflects non-sinusoidal waveforms would result in lack of spatial specificity. The fact that we observe PAC both within the cortex and across the thalamocortical network in a spatially specific manner suggests the observed PAC represents true cross frequency coupling rather than emerging as a

result of underlying non-sinusoidal low frequency oscillations. While we acknowledge the limitation of our methods, potential solutions such as mesuring the spike activity as a reprentation of broadband gamma, spatial specificity and consistency of our PAC results all point to correct charactarization of PAC as a method of measuring coupling between alpha/low-beta oscillations and broadband gamma activity.

We confirm thalamo-cortical alpha/low beta phase coupling at rest with the first direct evidence of causal flow from thalamus to the motor cortex. Importantly, this coupling is significantly reduced during voluntary movement. We next provide evidence of alpha-low- beta thalamocortical phase coupling (as measured by dwPLI) and thalamocortical PAC (between the phase of VL and the broadband gamma power in motor cortical contact) during rest. These observations leave open two distinct possibilities with respect to the role of thalamus in movement execution: that thalamus directly modulates cortical broadband activity via thalamo-cortical afferents or that thalamus serves to set a system state (via propagation of network-wide low frequency oscillations) which in turn locally modulates cortical broadband activity. In the latter case, observed thalamo-cortical PAC would be an epiphenomenon of underlying thalamocortical coherence. In fact, using the method of partial PAC to account for the local contributions of motor cortical alpha/low beta oscillations significantly reduced the resting thalamo-cortical PAC, suggesting indirect thalamic regulation of cortical activity via induction of cortical alpha/low beta (based on causal flow analyses). This result and interpretation is consistent with prior theories of the function of LFOs as an inhibitory mechanism to facilitate routing of information across large scale brain regions(Hari & Salmelin, 1997; O. Jensen et al., 2005; Ole Jensen & Mazaheri, 2010; K. J. Miller et al., 2010). Importantly, given the results of the directional flow of signals, one can confidently

conclude that thalamus is not simply a barometer of cortical activity, but is in fact propagating low-frequency oscillatory activity that contributes to local intra-cortical modulation.

The current results specifically address the potential role of VL thalamus in motor regulation. Afferents from the cerebellum are concentrated in the posterior region of ventrolateral thalamus (VLp aka. ViM) (Bosch-Bouju et al., 2013; Kuramoto et al., 2011; Nakamura et al., 2014; Sakai et al., 1996) which is preferentially interconnected with primary motor cortex (M1) (Anderson & DeVito, 1987; Haber & Calzavara, 2009; McFarland & Haber, 2002; Rouiller et al., 1998). On the other hand, animal studies show that afferents from the GPi preferentially target the anterior region of Ventrolateral thalamus (VLa)(Bosch-Bouju et al., 2013; Kuramoto et al., 2011; Nakamura et al., 2014; Sakai et al., 1996) which is mainly interconnected to premotor cortex (Anderson & DeVito, 1987; Haber & Calzavara, 2009; McFarland & Haber, 2002; Rouiller et al., 1998). The curent results may therefore not be generalizable to all thalamocortical motor circuits, especially in light of the fact that the exact role of each circuit in movement execution is not fully understood. While one model holds that thalamic nuclei serve as nodes of information integration where preparatory and performance aspects of the movement are "spirally" processed in an open feedback loop (Bosch-Bouju et al., 2013; Haber & Calzavara, 2009; McFarland & Haber, 2002), the current results suggest that at least one role of the VL thalamus is to broadly influence resting cortical tone, perhaps changing motor network state, serving a permissive role in voluntary motor execution. While our block-task experiment including repetive finger tapping movements provided a large enough time window to accurately measure PAC, we were unable to capture more temporally dynamic tasks that could potentially provide more information about distinct aspects of movement and movement regulation and should be the focus of future work. Moreover, we acknowledge that the findings of this study is limited to essential tremor patients however

movement-related decrease in cortical PAC has also been reported in patients with Parkinson disease (De Hemptinne et al., 2015b) and epilepsy patients (Kai J. Miller et al., 2012) with no movement disorder. Therefore we do not expect that the underlying mechanism of information transfer in thalamocortical network of healthy individuals would be significantly different; we suspect that only the magnitude of the movement-related changes and frequency bands of coupling may differ but that the same general principles would hold.

6 Conclusion & future work

We used a neurosurgical approach to refine the functional map of the visual and motor systems. Using unique opportunities to implant neurostimulators in blind subjects and patients with movement disorders we studied the mechanism of light perception and movement execution in human brain. While non-invasive techniques such as fMRI have depicted a broad picture of event-related neural activation maps, our approach was motivated by therapeutic application of these maps. For example the anatomical template map of the primary visual cortex is only beneficial to the extent of general organization of the retinotopic map with respect to cortical surface and does not account for subject-specific variances. Moreover a structural map of the thalamocortical network can only identify the target for DBS lead implant and falls short on explaining the therapeutic mechanism in which electrical stimulation relives symptoms of movement disorders.

We provide the first comprehensive assessment of stability, safety, and stimulation parameters of a chronic visual cortical prosthesis, confirming the long term feasibility and safety of this approach. While, previous studies on chronically implanted neurostimulators attest to the feasibility of cortical visual prostheses, our case study described in chapter 3 was an essential step towards a safe device by modern clinical standards. Furthermore our exploration of stimulation parameters on phosphene thresholds and intensities provided critical insight into the basis of conscious visual perception via cortical stimulation. After implanting four blind subjects with Orion we extended our efforts to provide them with a functional assistive device by developing a map of the visual field.

Given the time consuming process of creating the experimental absolute map, the anatomical template map provided a shortcut to generate an initial phosphene map right after electrode implantation surgery. The differences between experimental absolute map and anatomical

template map motivated us to search for an evaluation technique and design the phosphene connection experiment. Inspired by the consistency of phosphene connection trials we were able to calculate an optimum map with respect to relative location phosphenes which outperformed the other mapping techniques. However we must our evaluation method only measures the subject performance in the simple task of identifying the relative location of two sequential phospehenes. The simulation of direction of motion experiment was our effort towards measuring the functional vision performance in identifying a moving object, however it did not show a significant difference when utilizing different mapping techniques. This can be attributed to a variety of perceptual errors that are not related to the mapping technique. Therefore as the next step, we aim to carefully understand the sources of error in identifying direction of motion and address them separately. For example by selecting only a few phosphenes distributed uniformly in the visual field we could minimize the effects of a non-uniform map with overwhelming number of phosphenes and examine subjects' ability to identify direction of motion based on a short sequence of phosphenes.

When creating a subject-specific map of the primary visual cortex we must also consider that these maps may not be rigid and could be "learned" by subjects. Given that visuo-motor plasticity can improve in sighted subjects(Roller et al., 2001) it is safe to assume blind subjects can also learn to improve their performance using an imperfect phosphene map. To test these hypothesis we aim to design experimental paradigms that provide subjects with an additional corrective nonvisual (ex. audio) feedback to improve their performance in a visuo-motor task. Such experiments can also highlight the extent in which the learning component can change the functional map of the visual cortex and provide another avenue to increase the performance of cortical visual prostheses.

In our approach to to undestand the invasive correlates of thalamocortical network we recorded LFP signals from thalamus and moror cortex of ET patients undergoing DBS implantation surgery.

Using different measures of network connectivity we provided direct evidence of causal flow of low frequency oscillations from VL thalamus to motor cortices and that VL thalamus likely serves an indirect role in regulating movement-related cortical gamma activity via modulation of local low frequency oscillations. This chain of oscillatory couplings could potentially be the underlying mechanism in which brain networks dynamically modulate task specific information processing. This knowledge provides us with a broad picture of the cortical-subcortical connectivity and interactions, providng a framework within which to identify the irregularities through which neural disorders emerge.

DBS has been a conventional therapy for more than three decades however its exact therapetic mechanism is not well understood. Our effort to understand the movement-related thalamocortical oscillations was the first step to build a model of thalamocortical interactions which can be modulated by DBS. Hence our next step is to understand the stimulation-related behavior of this network particularly in the presence of therapeutic effect. Similar to our goal with blind individuals, we aim to enhance the DBS efficacy to improve the quality of life of patients with movement disorders.

Development of neurotherapeutic technologies is closely tied to our understanding of functional brain mapping. While therapeutic brain stimulation has been effectively used to create prosthese or relive some movement disorder symptoms, our functional understanding of these therapies is limited. In this dissertation we aimed to use the unique opprotunities provided by invasive brain stimulation thearpies to depict a functional mapping of the brain particularly visual and motor systems. Our findings on visual cortex mapping and oscillatory dynamic of the motor system not only allows for development of more effective brain stimulation in these systems but also expands

our undersatnding of information perception, processing, and transmission in the whole cortical and subcortical structures.

7 References

Ahuja, A. K., Dorn, J. D., Caspi, A., McMahon, M. J., Dagnelie, G., DaCruz, L., Stanga, P., Humayun, M. S., & Greenberg, R. J. (2011a). Blind subjects implanted with the Argus II retinal prosthesis are able to improve performance in a spatial-motor task. *British Journal of Ophthalmology*. https://doi.org/10.1136/bjo.2010.179622

Ahuja, A. K., Dorn, J. D., Caspi, A., McMahon, M. J., Dagnelie, G., DaCruz, L., Stanga, P., Humayun, M. S., & Greenberg, R. J. (2011b). Blind subjects implanted with the Argus II retinal prosthesis are able to improve performance in a spatial-motor task. *British Journal of Ophthalmology*, *95*(4), 539–543. https://doi.org/10.1136/bjo.2010.179622

Air, E. L., Ryapolova-Webb, E., de Hemptinne, C., Ostrem, J. L., Galifianakis, N. B., Larson, P. S., Chang, E. F., & Starr, P. A. (2012). Acute effects of thalamic deep brain stimulation and thalamotomy on sensorimotor cortex local field potentials in essential tremor. *Clinical Neurophysiology*. https://doi.org/10.1016/j.clinph.2012.04.020

Alexander, G. E., Crutcher, M. D., & Delong, M. R. (1991). Chapter 6 Basal ganglia-thalamocortical circuits: Parallel substrates for motor, oculomotor, "prefrontal" and "limbic" functions. *Progress in Brain Research*, *85*(C), 119–146. https://doi.org/10.1016/S0079-6123(08)62678-3

Aminoff, E. M., Li, Y., Pyles, J. A., Ward, M. J., Richardson, R. M., & Ghuman, A. S. (2016). Associative hallucinations result from stimulating left ventromedial temporal cortex. *Cortex*. https://doi.org/10.1016/j.cortex.2016.07.012

Ammann, F., Klein, D., & Franceschetti, A. (1965). Genetic and epidemiological investigations on pigmentary degeneration of the retina and allied disorders in Switzerland. *Journal of the Neurological Sciences*. https://doi.org/10.1016/0022-510X(65)90079-1

Amunts, K., Malikovic, A., Mohlberg, H., Schormann, T., & Zilles, K. (2000). Brodmann's Areas 17 and 18 Brought into Stereotaxic Space—Where and How Variable? *NeuroImage*, *11*(1), 66–84. https://doi.org/10.1006/nimg.1999.0516

Anderson, M. E., & DeVito, J. L. (1987). An analysis of potentially converging inputs to the rostral ventral thalamic nuclei of the cat. *Experimental Brain Research*.

https://doi.org/10.1007/BF00248792

Andersson, J. L. R., Jenkinson, M., & Smith, S. (2007). Non-linear registration, aka spatial normalisation. FMRIB Technial Report TR07JA2. In *Oxford Centre for Functional Magnetic Resonance Imaging of the Brain, Department of Clinical Neurology, Oxford University, Oxford, UK* (Issue June).

Andrews, T. J., Halpern, S. D., & Purves, D. (1997). Correlated Size Variations in Human Visual Cortex, Lateral Geniculate Nucleus, and Optic Tract. *The Journal of Neuroscience*, *17*(8), 2859–2868. https://doi.org/10.1523/JNEUROSCI.17-08-02859.1997

Arathorn, D. W., Stevenson, S. B., Yang, Q., Tiruveedhula, P., & Roorda, A. (2013). How the unstable eye sees a stable and moving world. *Journal of Vision*. https://doi.org/10.1167/13.10.22

Aru, J., Aru, J., Priesemann, V., Wibral, M., Lana, L., Pipa, G., Singer, W., & Vicente, R. (2015). Untangling cross-frequency coupling in neuroscience. In *Current Opinion in Neurobiology* (Vol. 31, pp. 51–61). https://doi.org/10.1016/j.conb.2014.08.002

Bach-y-Rita, P., & W. Kercel, S. (2003). Sensory substitution and the human-machine interface. In *Trends in Cognitive Sciences* (Vol. 7, Issue 12, pp. 541–546). https://doi.org/10.1016/j.tics.2003.10.013

Bak, M., Girvin, J. P., Hambrecht, F. T., Kufta, C. V., Loeb, G. E., & Schmidt, E. M. (1990). Visual sensations produced by intracortical microstimulation of the human occipital cortex. *Medical & Biological Engineering & Computing*, *28*(3), 257–259. https://doi.org/10.1007/BF02442682

Bartlett, J. R., & Doty, R. W. (1980). An exploration of the ability of macaques to detect microstimulation of striate cortex. *Acta Neurobiologiae Experimentalis*, *40*(4), 713–727.

Beauchamp, M. S., Oswalt, D., Sun, P., Foster, B. L., Magnotti, J. F., Niketeghad, S., Pouratian, N., Bosking, W. H., & Yoshor, D. (2020). Dynamic Stimulation of Visual Cortex Produces Form Vision in Sighted and Blind Humans. *Cell*. https://doi.org/10.1016/j.cell.2020.04.033

Behrens, T. E. J., Berg, H. J., Jbabdi, S., Rushworth, M. F. S., & Woolrich, M. W. (2007). Probabilistic diffusion tractography with multiple fibre orientations: What can we gain?

NeuroImage, *34*(1), 144–155. https://doi.org/10.1016/j.neuroimage.2006.09.018

Benjamini, Y., & Hochberg, Y. (1995). controlling the false discovery rate: a practical and powerful approach to multiple testing. *Journal of Royal Statistical Society*, *57*(1), 289–300.

Benson, N. (2012). *An anatomical template of human striate retinotopy*. https://cfn.upenn.edu/aguirre/wiki/public:retinotopy_template

Benson, N. C., Butt, O. H., Brainard, D. H., & Aguirre, G. K. (2014). Correction of Distortion in Flattened Representations of the Cortical Surface Allows Prediction of V1-V3 Functional Organization from Anatomy. *PLoS Computational Biology*. https://doi.org/10.1371/journal.pcbi.1003538

Benson, N. C., Butt, O. H., Datta, R., Radoeva, P. D., Brainard, D. H., & Aguirre, G. K. (2012). The Retinotopic Organization of Striate Cortex Is Well Predicted by Surface Topology. *Current Biology*, *22*(21), 2081–2085. https://doi.org/10.1016/j.cub.2012.09.014

Biran, R., Martin, D. C., & Tresco, P. A. (2005). Neuronal cell loss accompanies the brain tissue response to chronically implanted silicon microelectrode arrays. *Experimental Neurology*. https://doi.org/10.1016/j.expneurol.2005.04.020

Blanke, O., Landis, T., & Seeck, M. (2000). Electrical cortical stimulation of the human prefrontal cortex evokes complex visual hallucinations. *Epilepsy & Behavior : E&B*. https://doi.org/10.1006/ebeh.2000.0109

Bokil, H., Andrews, P., Kulkarni, J. E., Mehta, S., & Mitra, P. P. (2010). Chronux: A platform for analyzing neural signals. *Journal of Neuroscience Methods*, *192*(1), 146–151. https://doi.org/10.1016/j.jneumeth.2010.06.020

Bokil, H., Purpura, K., Schoffelen, J. M., Thomson, D., & Mitra, P. (2007). Comparing spectra and coherences for groups of unequal size. *Journal of Neuroscience Methods*, *159*(2), 337–345. https://doi.org/10.1016/j.jneumeth.2006.07.011

Bosch-Bouju, C., Hyland, B. I., & Parr-Brownlie, L. C. (2013). Motor thalamus integration of cortical, cerebellar and basal ganglia information: implications for normal and parkinsonian conditions. *Frontiers in Computational Neuroscience*. https://doi.org/10.3389/fncom.2013.00163

Bosking, W., Foster, B., Sun, P., Beauchamp, M., & Yoshor, D. (2018). Rules Governing Perception of Multiple Phosphenes by Human Observers. In *bioRxiv*. https://doi.org/10.1101/302547

Bosking, W. H., Beauchamp, M. S., & Yoshor, D. (2017). Electrical Stimulation of Visual Cortex: Relevance for the Development of Visual Cortical Prosthetics. *Annual Review of Vision Science*. https://doi.org/10.1146/annurev-vision-111815-114525

Bosking, W. H., Sun, P., Ozker, M., Pei, X., Foster, B. L., Beauchamp, M. S., & Yoshor, D. (2017). Saturation in Phosphene Size with Increasing Current Levels Delivered to Human Visual Cortex. *The Journal of Neuroscience*. https://doi.org/10.1523/JNEUROSCI.2896-16.2017

Brindley, G. S., & Lewin, W. S. (1968). The sensations produced by electrical stimulation of the visual cortex. *The Journal of Physiology*, *196*(2), 479–493. https://doi.org/10.1113/jphysiol.1968.sp008519

Brittain, J. S., & Brown, P. (2014). Oscillations and the basal ganglia: Motor control and beyond. In *NeuroImage*. https://doi.org/10.1016/j.neuroimage.2013.05.084

Brovelli, A., Lachaux, J., Kahane, P., & Boussaoud, D. (2005). High gamma frequency oscillatory activity dissociates attention from intention in the human premotor cortex. *NeuroImage*. https://doi.org/S1053-8119(05)00404-0 [pii]\r10.1016/j.neuroimage.2005.05.045

Brücke, C., Bock, A., Huebl, J., Krauss, J. K., Schönecker, T., Schneider, G. H., Brown, P., & Kühn, A. A. (2013). Thalamic gamma oscillations correlate with reaction time in a Go/noGo task in patients with essential tremor. *NeuroImage*. https://doi.org/10.1016/j.neuroimage.2013.02.038

Brunner, P., Ritaccio, A. L., Lynch, T. M., Emrich, J. F., Wilson, J. A., Williams, J. C., Aarnoutse, E. J., Ramsey, N. F., Leuthardt, E. C., Bischof, H., & Schalk, G. (2009). A practical procedure for real-time functional mapping of eloquent cortex using electrocorticographic signals in humans. *Epilepsy and Behavior*. https://doi.org/10.1016/j.yebeh.2009.04.001

Bundey, S., & Crews, S. J. (1984). A study of retinitis pigmentosa in the City of Birmingham. II Clinical and genetic heterogeneity. *Journal of Medical Genetics*. https://doi.org/10.1136/jmg.21.6.417

Bunker, C. H., Berson, E. L., Bromley, W. C., Hayes, R. P., & Roderick, T. H. (1984). Prevalence of retinitis pigmentosa in maine. *American Journal of Ophthalmology*. https://doi.org/10.1016/0002-9394(84)90636-6

Canolty, R. T., & Knight, R. T. (2010). The functional role of cross-frequency coupling. In *Trends in Cognitive Sciences*. https://doi.org/10.1016/j.tics.2010.09.001

Capelle, C., Trullemans, C., Arno, P., & Veraart, C. (1998). A real-time experimental prototype for enhancement of vision rehabilitation using auditory substitution. *IEEE Transactions on Biomedical Engineering*, *45*(10), 1279–1293. https://doi.org/10.1109/10.720206

Caspi, A., Roy, A., Wuyyuru, V., Rosendall, P. E., Harper, J. W., Katyal, K. D., Barry, M. P., Dagnelie, G., & Greenberg, R. J. (2018). Eye Movement Control in the Argus II Retinal-Prosthesis Enables Reduced Head Movement and Better Localization Precision. *Investigative Opthalmology & Visual Science*, *59*(2), 792. https://doi.org/10.1167/iovs.17-22377

Cassidy, M., Mazzone, P., Oliviero, A., Insola, A., Tonali, P., Lazzaro, V. Di, & Brown, P. (2002). Movement-related changes in synchronization in the human basal ganglia. *Brain*, *125*(6), 1235–1246. https://doi.org/10.1093/brain/awf135

Congdon, N. G., Friedman, D. S., & Lietman, T. (2003). Important Causes of Visual Impairment in the World Today. In *Journal of the American Medical Association* (Vol. 290, Issue 15, pp. 2057–2060). https://doi.org/10.1001/jama.290.15.2057

Crews, J. E., & Campbell, V. A. (2004). Vision Impairment and Hearing Loss among Community-Dwelling Older Americans: Implications for Health and Functioning. *American Journal of Public Health*, *94*(5), 823–829. https://doi.org/10.2105/AJPH.94.5.823

Crone, N E, Miglioretti, D. L., Gordon, B., & Lesser, R. P. (1998). Functional mapping of human sensorimotor cortex with electrocorticographic spectral analysis. II. Event-related synchronization in the gamma band. *Brain : A Journal of Neurology*, *121 (Pt 1*, 2301–

2315. https://doi.org/10.1093/brain/121.12.2301

Crone, Nathan E., Korzeniewska, A., & Franaszczuk, P. J. (2011a). Cortical gamma responses: Searching high and low. In *International Journal of Psychophysiology*. https://doi.org/10.1016/j.ijpsycho.2010.10.013

Crone, Nathan E., Korzeniewska, A., & Franaszczuk, P. J. (2011b). Cortical gamma responses: Searching high and low. In *International Journal of Psychophysiology*. https://doi.org/10.1016/j.ijpsycho.2010.10.013

Crone, Nathan E., Sinai, A., & Korzeniewska, A. (2006). Chapter 19 High-frequency gamma oscillations and human brain mapping with electrocorticography. In *Progress in Brain Research*. https://doi.org/10.1016/S0079-6123(06)59019-3

Da Cruz, L., Coley, B. F., Dorn, J., Merlini, F., Filley, E., Christopher, P., Chen, F. K., Wuyyuru, V., Sahel, J., Stanga, P., Humayun, M., Greenberg, R. J., & Dagnelie, G. (2013). The Argus II epiretinal prosthesis system allows letter and word reading and long-term function in patients with profound vision loss. *British Journal of Ophthalmology*. https://doi.org/10.1136/bjophthalmol-2012-301525

da Cruz, L., Dorn, J. D., Humayun, M. S., Dagnelie, G., Handa, J., Barale, P. O., Sahel, J. A., Stanga, P. E., Hafezi, F., Safran, A. B., Salzmann, J., Santos, A., Birch, D., Spencer, R., Cideciyan, A. V., de Juan, E., Duncan, J. L., Eliott, D., Fawzi, A., … Greenberg, R. J. (2016). Five-Year Safety and Performance Results from the Argus II Retinal Prosthesis System Clinical Trial. *Ophthalmology*. https://doi.org/10.1016/j.ophtha.2016.06.049

Dagnelie, G. (2008). Psychophysical Evaluation for Visual Prosthesis. *Annual Review of Biomedical Engineering*. https://doi.org/10.1146/annurev.bioeng.10.061807.160529

Dalal, S. S., Guggisberg, A. G., Edwards, E., Sekihara, K., Findlay, A. M., Canolty, R. T., Berger, M. S., Knight, R. T., Barbaro, N. M., Kirsch, H. E., & Nagarajan, S. S. (2008). Five-dimensional neuroimaging: Localization of the time-frequency dynamics of cortical activity. *NeuroImage*. https://doi.org/10.1016/j.neuroimage.2008.01.023

Dale, A. M., Fischl, B., & Sereno, M. I. (1999a). Cortical surface-based analysis: I. Segmentation and surface reconstruction. *NeuroImage*, *9*(2), 179–194.

https://doi.org/10.1006/nimg.1998.0395

Dale, A. M., Fischl, B., & Sereno, M. I. (1999b). Cortical Surface-Based Analysis. *NeuroImage*, *9*(2), 179–194. https://doi.org/10.1006/nimg.1998.0395

De Hemptinne, C., Ryapolova-Webb, E. S., Air, E. L., Garcia, P. A., Miller, K. J., Ojemann, J. G., Ostrem, J. L., Galifianakis, N. B., & Starr, P. A. (2013). Exaggerated phase-amplitude coupling in the primary motor cortex in Parkinson disease. *Proceedings of the National Academy of Sciences of the United States of America*, *110*(12), 4780–4785. https://doi.org/10.1073/pnas.1214546110

De Hemptinne, C., Swann, N. C., Ostrem, J. L., Ryapolova-Webb, E. S., San Luciano, M., Galifianakis, N. B., & Starr, P. A. (2015a). Therapeutic deep brain stimulation reduces cortical phase-amplitude coupling in Parkinson's disease. *Nature Neuroscience*. https://doi.org/10.1038/nn.3997

De Hemptinne, C., Swann, N. C., Ostrem, J. L., Ryapolova-Webb, E. S., San Luciano, M., Galifianakis, N. B., & Starr, P. A. (2015b). Therapeutic deep brain stimulation reduces cortical phase-amplitude coupling in Parkinson's disease. *Nature Neuroscience*. https://doi.org/10.1038/nn.3997

Delorme, A., & Makeig, S. (2004). EEGLAB: An open source toolbox for analysis of single-trial EEG dynamics including independent component analysis. *Journal of Neuroscience Methods*, *134*(1), 9–21. https://doi.org/10.1016/j.jneumeth.2003.10.009

Deroy, O., & Auvray, M. (2012). Reading the world through the skin and ears: A new perspective on sensory substitution. *Frontiers in Psychology*, *3*(NOV). https://doi.org/10.3389/fpsyg.2012.00457

Dobelle, W. H., & Mladejovsky, M. G. (1974a). Phosphenes produced by electrical stimulation of human occipital cortex, and their application to the development of a prosthesis for the blind. *The Journal of Physiology*. https://doi.org/10.1113/jphysiol.1974.sp010766

Dobelle, W. H., & Mladejovsky, M. G. (1974b). Phosphenes produced by electrical stimulation of human occipital cortex, and their application to the development of a prosthesis for the blind. *The Journal of Physiology*, *243*(2), 553–576.

https://doi.org/10.1113/jphysiol.1974.sp010766

Dobelle, W. H., Mladejovsky, M. G., & Girvin, J. P. (1974). Artificial Vision for the Blind: Electrical Stimulation of Visual Cortex Offers Hope for a Functional Prosthesis. *Science*, *183*(4123), 440–444. https://doi.org/10.1126/science.183.4123.440

Dobelle, W. H., Quest, D. O., Antunes, J. L., Roberts, T. S., & Girvin, J. P. (1979). Artificial vision for the blind by electrical stimulation of the visual cortex. *Neurosurgery*, *5*(4), 521–527. https://doi.org/10.1227/00006123-197910000-00022

Dobelle, Wm H. (2000). Artificial vision for the blind by connecting a television camera to the visual cortex. *ASAIO Journal*, *46*(1), 3–9. https://doi.org/10.1097/00002480-200001000-00002

Dobelle, Wm H., Mladejovsky, M. G., Evans, J. R., Roberts, T. S., & Girvin, J. P. (1976). Braille reading by a blind volunteer by visual cortex stimulation. *Nature*, *259*(5539), 111–112. https://doi.org/10.1038/259111a0

Dorn, J. D., Ahuja, A. K., Caspi, A., da Cruz, L., Dagnelie, G., Sahel, J.-A., Greenberg, R. J., McMahon, M. J., & Argus II Study Group, for the. (2013). The Detection of Motion by Blind Subjects With the Epiretinal 60-Electrode (Argus II) Retinal Prosthesis. *JAMA Ophthalmology*, *131*(2), 183. https://doi.org/10.1001/2013.jamaophthalmol.221

Dykstra, A. R., Chan, A. M., Quinn, B. T., Zepeda, R., Keller, C. J., Cormier, J., Madsen, J. R., Eskandar, E. N., & Cash, S. S. (2012). Individualized localization and cortical surface-based registration of intracranial electrodes. *NeuroImage*, *59*(4), 3563–3570. https://doi.org/10.1016/j.neuroimage.2011.11.046

Edwards, T. L., Cottriall, C. L., Xue, K., Simunovic, M. P., Ramsden, J. D., Zrenner, E., & MacLaren, R. E. (2018). Assessment of the Electronic Retinal Implant Alpha AMS in Restoring Vision to Blind Patients with End-Stage Retinitis Pigmentosa. *Ophthalmology*. https://doi.org/10.1016/j.ophtha.2017.09.019

Fernandez, E., Alfaro, A., Toledano, R., Albisua, J., & García, A. (2015). Perceptions elicited by electrical stimulation of human visual cortex. *Investigative Ophthalmology & Visual Science*, *56*(7), 777.

Fernández, E., & Normann, R. A. (2017). CORTIVIS Approach for an Intracortical Visual Prostheses. In *Artificial Vision* (pp. 191–201). Springer.

Foerster, O. (1929). Beitrage zur Pathophysiologie der Sehbahn und der Sehsphare. *J. Psychol. Neurol., Lpz.*, *39*, 463.

Foffani, G., Bianchi, A. M., Baselli, G., & Priori, A. (2005). Movement-related frequency modulation of beta oscillatory activity in the human subthalamic nucleus. *Journal of Physiology*, *568*(2), 699–711. https://doi.org/10.1113/jphysiol.2005.089722

Freeman, E. E., Egleston, B. L., West, S. K., Bandeen-Roche, K., & Rubin, G. (2005). Visual acuity change and mortality in older adults. *Investigative Ophthalmology & Visual Science*, *46*, 4040–4045. https://doi.org/10.1167/iovs.05-0687

Frick, K. D., Gower, E. W., Kempen, J. H., & Wolff, J. L. (2007). Economic impact of visual impairment and blindness in the United States. *Archives of Ophthalmology*, *125*(4), 544–550. https://doi.org/10.1001/archopht.125.4.544

Gallay, M. N., Jeanmonod, D., Liu, J., & Morel, A. (2008). Human pallidothalamic and cerebellothalamic tracts: anatomical basis for functional stereotactic neurosurgery. *Brain Structure and Function*, *212*(6), 443–463. https://doi.org/10.1007/s00429-007-0170-0

Geddes, L. A., & Bourland, J. D. (1985). The Strength-Duration Curve. *IEEE Transactions on Biomedical Engineering*, *BME-32*(6), 458–459. https://doi.org/10.1109/TBME.1985.325456

Gescheider, G. (1997). Chapter 1: Psychophysical measurement of thresholds. *Psychophysics: Method, Theory, and Application*, 1–36.

Ghuman, A. S., Brunet, N. M., Li, Y., Konecky, R. O., Pyles, J. A., Walls, S. A., Destefino, V., Wang, W., & Richardson, R. M. (2014). Dynamic encoding of face information in the human fusiform gyrus. *Nature Communications*. https://doi.org/10.1038/ncomms6672

Goss-Varley, M., Dona, K. R., McMahon, J. A., Shoffstall, A. J., Ereifej, E. S., Lindner, S. C., & Capadona, J. R. (2017). Microelectrode implantation in motor cortex causes fine motor deficit: Implications on potential considerations to Brain Computer Interfacing and Human Augmentation. *Scientific Reports*. https://doi.org/10.1038/s41598-017-15623-y

Gröndahl, J. (1986). Tapeto-retinal degeneration in four Norwegian counties II: Diagnostic evaluation of 407 relatives and genetic evaluation of 87 families. *Clinical Genetics*. https://doi.org/10.1111/j.1399-0004.1986.tb00768.x

Haber, S. N., & Calzavara, R. (2009). The cortico-basal ganglia integrative network: The role of the thalamus. In *Brain Research Bulletin*. https://doi.org/10.1016/j.brainresbull.2008.09.013

Haim, M. (2002). Epidemiology of retinitis pigmentosa in Denmark. *Acta Ophthalmologica*. https://doi.org/10.1017/CBO9781107415324.004

Hanneton, S., Auvray, M., & Durette, B. (2010). The Vibe: A versatile vision-to-audition sensory substitution device. *Applied Bionics and Biomechanics*, *7*(4), 269–276. https://doi.org/10.1080/11762322.2010.512734

Hari, R., & Salmelin, R. (1997). Human cortical oscillations: A neuromagnetic view through the skull. In *Trends in Neurosciences*. https://doi.org/10.1016/S0166-2236(96)10065-5

He, B., Dai, Y., Astolfi, L., Babiloni, F., Yuan, H., & Yang, L. (2011). EConnectome: A MATLAB toolbox for mapping and imaging of brain functional connectivity. *Journal of Neuroscience Methods*. https://doi.org/10.1016/j.jneumeth.2010.11.015

Hinds, O. P., Rajendran, N., Polimeni, J. R., Augustinack, J. C., Wiggins, G., Wald, L. L., Diana Rosas, H., Potthast, A., Schwartz, E. L., & Fischl, B. (2008). Accurate prediction of V1 location from cortical folds in a surface coordinate system. *NeuroImage*, *39*(4), 1585–1599. https://doi.org/10.1016/j.neuroimage.2007.10.033

Hirshorn, E. A., Li, Y., Ward, M. J., Richardson, R. M., Fiez, J. A., & Ghuman, A. S. (2016). Decoding and disrupting left midfusiform gyrus activity during word reading. *Proceedings of the National Academy of Sciences*. https://doi.org/10.1073/pnas.1604126113

Holmes, G. (1918). DISTURBANCES OF VISION BY CEREBRAL LESIONS. *British Journal of Ophthalmology*, *2*(7), 353–384. https://doi.org/10.1136/bjo.2.7.353

Hu, D. N. (1987). Prevalence and mode of inheritance of major genetic eye diseases in China. *J Med Genet*. https://doi.org/10.1136/jmg.24.10.584

Ivers, R. Q., Norton, R., Cumming, R. G., Butler, M., & Campbell, a J. (2000). Visual

impairment and risk of hip fracture. *American Journal of Epidemiology*, *152*(7), 633–639. https://doi.org/10.1093/aje/152.7.633

Javitt, J. C., Wang, F., & West, S. K. (1996). Blindness Due to Cataract: Epidemiology and Prevention. *Annual Review of Public Health*, *17*(1), 159–177. https://doi.org/10.1146/annurev.pu.17.050196.001111

Jenkinson, M. (2002). Improved Optimization for the Robust and Accurate Linear Registration and Motion Correction of Brain Images. *NeuroImage*, *17*(2), 825–841. https://doi.org/10.1016/S1053-8119(02)91132-8

Jenkinson, M., Bannister, P., Brady, M., & Smith, S. (2002). Improved optimization for the robust and accurate linear registration and motion correction of brain images. *NeuroImage*, *17*(2), 825–841. https://doi.org/10.1016/S1053-8119(02)91132-8

Jensen, O., Goel, P., Kopell, N., Pohja, M., Hari, R., & Ermentrout, B. (2005). On the human sensorimotor-cortex beta rhythm: Sources and modeling. *NeuroImage*. https://doi.org/10.1016/j.neuroimage.2005.02.008

Jensen, Ole, & Mazaheri, A. (2010). Shaping Functional Architecture by Oscillatory Alpha Activity: Gating by Inhibition. *Frontiers in Human Neuroscience*. https://doi.org/10.3389/fnhum.2010.00186

Jensen, Ole, Spaak, E., & Park, H. (2016). Discriminating valid from spurious indices of phase-amplitude coupling. *ENeuro*. https://doi.org/10.1523/ENEURO.0334-16.2016

Jones, G. C., Rovner, B. W., Crews, J. E., & Danielson, M. L. (2009). Effects of Depressive Symptoms on Health Behavior Practices Among Older Adults With Vision Loss. *Rehabilitation Psychology*, *54*(2), 164–172. https://doi.org/10.1037/a0015910

Jorfi, M., Skousen, J. L., Weder, C., & Capadona, J. R. (2015). Progress towards biocompatible intracortical microelectrodes for neural interfacing applications. In *Journal of Neural Engineering*. https://doi.org/10.1088/1741-2560/12/1/011001

Kaminski, M. J., & Blinowska, K. J. (1991). A new method of the description of the information flow in the brain structures. *Biological Cybernetics*. https://doi.org/10.1007/BF00198091

Kapeller, C., Ogawa, H., Schalk, G., Kunii, N., Coon, W. G., Scharinger, J., Guger, C., & Kamada, K. (2018). Real-time detection and discrimination of visual perception using electrocorticographic signals. *Journal of Neural Engineering*. https://doi.org/10.1088/1741-2552/aaa9f6

Kilavik, B. E., Zaepffel, M., Brovelli, A., MacKay, W. A., & Riehle, A. (2013). The ups and downs of beta oscillations in sensorimotor cortex. In *Experimental Neurology* (Vol. 245, pp. 15–26). https://doi.org/10.1016/j.expneurol.2012.09.014

Kim, T., Troyk, P. R., & Bak, M. (2006). Active Floating Micro Electrode Arrays (AFMA). *Annual International Conference of the IEEE Engineering in Medicine and Biology - Proceedings*. https://doi.org/10.1109/IEMBS.2006.259981

Kipke, D. R., Shain, W., Buzsaki, G., Fetz, E., Henderson, J. M., Hetke, J. F., & Schalk, G. (2008). Advanced Neurotechnologies for Chronic Neural Interfaces: New Horizons and Clinical Opportunities. *Journal of Neuroscience*. https://doi.org/10.1523/JNEUROSCI.3879-08.2008

Kondylis, E. D., Randazzo, M. J., Alhourani, A., Lipski, W. J., Wozny, T. A., Pandya, Y., Ghuman, A. S., Turner, R. S., Crammond, D. J., & Richardson, R. M. (2016). Movement-related dynamics of cortical oscillations in Parkinson's disease and essential tremor. *Brain*, *139*(8), 2211–2223. https://doi.org/10.1093/brain/aww144

Krause, F. (1924). Die Sehbahn in Chirurgischer Beziehung und die Faradische Reizung des Sehzentrums. *Klinische Wochenschrift*, *3*(28), 1260–1265. https://doi.org/10.1007/BF01735820

Kravitz, D. J., Saleem, K. S., Baker, C. I., & Mishkin, M. (2011). A new neural framework for visuospatial processing. In *Nature Reviews Neuroscience*. https://doi.org/10.1038/nrn3008

Kravitz, D. J., Saleem, K. S., Baker, C. I., Ungerleider, L. G., & Mishkin, M. (2013). The ventral visual pathway: An expanded neural framework for the processing of object quality. In *Trends in Cognitive Sciences*. https://doi.org/10.1016/j.tics.2012.10.011

Kuramoto, E., Fujiyama, F., Nakamura, K. C., Tanaka, Y., Hioki, H., & Kaneko, T. (2011). Complementary distribution of glutamatergic cerebellar and GABAergic basal ganglia

afferents to the rat motor thalamic nuclei. *European Journal of Neuroscience*. https://doi.org/10.1111/j.1460-9568.2010.07481.x

Lee, H. W., Hong, S. B., Seo, D. W., Tae, W. S., & Hong, S. C. (2000). Mapping of functional organization in human visual cortex Electrical cortical stimulation. *Neurology*, *54*(4), 849–854.

Lenay, C., Gapenne, O., Hanneton, S., Marque, C., & Genouëlle, C. (2003). Sensory Substitution : Limits and Perspectives. *Touching for Knowing Cognitive Psychology of Haptic Manual Perception*, *19*, 275–292. https://doi.org/10.1016/S0733-8619(03)00096-3

Leuthardt, E. C., Miller, K., Anderson, N. R., Schalk, G., Dowling, J., Miller, J., Moran, D. W., & Ojemann, J. G. (2007). Electrocorticographic frequency alteration mapping: A clinical technique for mapping the motor cortex. *Neurosurgery*. https://doi.org/10.1227/01.NEU.0000255413.70807.6E

Leuthardt, E. C., Schalk, G., Wolpaw, J. R., Ojemann, J. G., & Moran, D. W. (2004). A brain-computer interface using electrocorticographic signals in humans. *Journal of Neural Engineering*. https://doi.org/10.1088/1741-2560/1/2/001

Li, W. H., Tang, T. J. J., & Lui, W. L. D. (2013). Going beyond vision to improve bionic vision. *2013 IEEE International Conference on Image Processing, ICIP 2013 - Proceedings*. https://doi.org/10.1109/ICIP.2013.6738320

Liu, H., Agam, Y., Madsen, J. R., & Kreiman, G. (2009). Timing, Timing, Timing: Fast Decoding of Object Information from Intracranial Field Potentials in Human Visual Cortex. *Neuron*. https://doi.org/10.1016/j.neuron.2009.02.025

Liu, X., McCreery, D. B., Bullara, L. A., & Agnew, W. F. (2006). Evaluation of the stability of intracortical microelectrode arrays. *IEEE Transactions on Neural Systems and Rehabilitation Engineering*. https://doi.org/10.1109/TNSRE.2006.870495

López-Azcárate, J., Tainta, M., Rodríguez-Oroz, M. C., Valencia, M., González, R., Guridi, J., Iriarte, J., Obeso, J. A., Artieda, J., & Alegre, M. (2010). Coupling between beta and high-frequency activity in the human subthalamic nucleus may be a pathophysiological mechanism in Parkinson's disease. *Journal of Neuroscience*, *30*(19), 6667–6677.

https://doi.org/10.1523/JNEUROSCI.5459-09.2010

Löwenstein, K., & Borchardt, M. (1918). Symptomatologie und elektrische Reizung bei einer Schußverletzung des Hinterhauptlappens. *Deutsche Zeitschrift Für Nervenheilkunde*, *58*(3–6), 264–292. https://doi.org/10.1007/BF01629694

Lowery, Arthur J., Rosenfeld, J. V., Lewis, P. M., Browne, D., Mohan, A., Brunton, E., Yan, E., Maller, J., Mann, C., Rajan, R., Rosa, M., & Pritchard, J. (2015). Restoration of vision using wireless cortical implants: The Monash Vision Group project. *Proceedings of the Annual International Conference of the IEEE Engineering in Medicine and Biology Society, EMBS*. https://doi.org/10.1109/EMBC.2015.7318543

Lowery, Arthur James, Rosenfeld, J. V, Rosa, M. G. P., Brunton, E., Rajan, R., Mann, C., Armstrong, M., Mohan, A., Josh, H., & Kleeman, L. (2017). Monash Vision Group's Gennaris Cortical Implant for Vision Restoration. In *Artificial Vision* (pp. 215–225). Springer.

Lozano, A. M. (2000). Vim thalamic stimulation for tremor. *Archives of Medical Research*. https://doi.org/10.1016/S0188-4409(00)00081-3

Luo, Y. H. L., & da Cruz, L. (2016). The Argus® II Retinal Prosthesis System. In *Progress in Retinal and Eye Research*. https://doi.org/10.1016/j.preteyeres.2015.09.003

Luo, Y. H. L., Zhong, J. J., & da Cruz, L. (2015). The use of Argus® II retinal prosthesis by blind subjects to achieve localisation and prehension of objects in 3-dimensional space. *Graefe's Archive for Clinical and Experimental Ophthalmology*. https://doi.org/10.1007/s00417-014-2912-z

Malekmohammadi, M., AuYong, N., Price, C. M., Tsolaki, E., Hudson, A. E., & Pouratian, N. (2018). Propofol-induced changes in α-β sensorimotor cortical connectivity. *Anesthesiology: The Journal of the American Society of Anesthesiologists*, *128*(2), 305–316.

Malekmohammadi, M., AuYong, N., Ricks-Oddie, J., Bordelon, Y., & Pouratian, N. (2018). Pallidal deep brain stimulation modulates excessive cortical high β phase amplitude coupling in Parkinson disease. *Brain Stimulation*, *11*(3), 607–617. https://doi.org/10.1016/j.brs.2018.01.028

Malekmohammadi, M., Elias, W. J., & Pouratian, N. (2015). Human Thalamus Regulates Cortical Activity via Spatially Specific and Structurally Constrained Phase-Amplitude Coupling. *Cerebral Cortex*, *25*(6), 1618–1628. https://doi.org/10.1093/cercor/bht358

Mani, J., Diehl, B., Piao, Z., Schuele, S. S., Lapresto, E., Liu, P., Nair, D. R., Dinner, D. S., & Lüders, H. O. (2008). Evidence for a basal temporal visual language center: Cortical stimulation producing pure alexia. *Neurology*. https://doi.org/10.1212/01.wnl.0000334755.32850.f0

Marg, E., & Dierssen, G. (1965). Reported visual percepts from stimulation of the human brain with microelectrodes during therapeutic surgery. In *Confinia neurologica*.

Margalit, E., Weiland, J. D., Clatterbuck, R. E., Fujii, G. Y., Maia, M., Tameesh, M., Torres, G., D'Anna, S. A., Desai, S., Piyathaisere, D. V., Olivi, A., De Juan, E., & Humayun, M. S. (2003). Visual and electrical evoked response recorded from subdural electrodes implanted above the visual cortex in normal dogs under two methods of anesthesia. *Journal of Neuroscience Methods*. https://doi.org/10.1016/S0165-0270(02)00345-X

Margalit, Eyal, Maia, M., Weiland, J. D., Greenberg, R. J., Fujii, G. Y., Torres, G., Piyathaisere, D. V., O'Hearn, T. M., Liu, W., Lazzi, G., Dagnelie, G., Scribner, D. A., De Juan, E., & Humayun, M. S. (2002). Retinal prosthesis for the blind. In *Survey of Ophthalmology*. https://doi.org/10.1016/S0039-6257(02)00311-9

Maynard, E. M., Nordhausen, C. T., & Normann, R. A. (1997). The Utah Intracortical Electrode Array: A recording structure for potential brain-computer interfaces. *Electroencephalography and Clinical Neurophysiology*. https://doi.org/10.1016/S0013-4694(96)95176-0

McFarland, N. R., & Haber, S. N. (2002). Thalamic relay nuclei of the basal ganglia form both reciprocal and nonreciprocal cortical connections, linking multiple frontal cortical areas. *The Journal of Neuroscience : The Official Journal of the Society for Neuroscience*.

Merabet, L. B., Rizzo, J. F., Pascual-Leone, A., & Fernandez, E. (2007). "Who is the ideal candidate?" Decisions and issues relating to visual neuroprosthesis development, patient testing and neuroplasticity. *Journal of Neural Engineering*. https://doi.org/10.1088/1741-

2560/4/1/S15

Merrill, D. R., Bikson, M., & Jefferys, J. G. R. (2005a). Electrical stimulation of excitable tissue: Design of efficacious and safe protocols. In *Journal of Neuroscience Methods* (Vol. 141, Issue 2, pp. 171–198). https://doi.org/10.1016/j.jneumeth.2004.10.020

Merrill, D. R., Bikson, M., & Jefferys, J. G. R. (2005b). Electrical stimulation of excitable tissue: design of efficacious and safe protocols. *Journal of Neuroscience Methods*, *141*(2), 171–198. https://doi.org/10.1016/j.jneumeth.2004.10.020

Mewett, D. T., Nazeran, H., & Reynolds, K. J. (2001). Removing power line noise from recorded EMG. *Annual Reports of the Research Reactor Institute, Kyoto University*, *3*, 2190–2193. https://doi.org/10.1109/IEMBS.2001.1017205

Miller, K. J., Leuthardt, E. C., Schalk, G., Rao, R. P. N., Anderson, N. R., Moran, D. W., Miller, J. W., & Ojemann, J. G. (2007). Spectral Changes in Cortical Surface Potentials during Motor Movement. *Journal of Neuroscience*. https://doi.org/10.1523/JNEUROSCI.3886-06.2007

Miller, K. J., Schalk, G., Fetz, E. E., den Nijs, M., Ojemann, J. G., & Rao, R. P. N. (2010). Cortical activity during motor execution, motor imagery, and imagery-based online feedback. *Proceedings of the National Academy of Sciences*. https://doi.org/10.1073/pnas.0913697107

Miller, Kai J., Hermes, D., Honey, C. J., Hebb, A. O., Ramsey, N. F., Knight, R. T., Ojemann, J. G., & Fetz, E. E. (2012). Human Motor Cortical Activity Is Selectively Phase-Entrained on Underlying Rhythms. *PLoS Computational Biology*. https://doi.org/10.1371/journal.pcbi.1002655

Nair, D. R., Burgess, R., McIntyre, C. C., & Lüders, H. (2008). Chronic subdural electrodes in the management of epilepsy. In *Clinical Neurophysiology*. https://doi.org/10.1016/j.clinph.2007.09.117

Nakamura, K. C., Sharott, A., & Magill, P. J. (2014). Temporal coupling with cortex distinguishes spontaneous neuronal activities in identified basal ganglia-recipient and cerebellar-recipient zones of the motor thalamus. *Cerebral Cortex*.

https://doi.org/10.1093/cercor/bhs287

Narabayashi, H. (1989). Stereotaxic vim thalamotomy for treatment of tremor. *European Neurology*. https://doi.org/10.1159/000116450

Naumann, J. (2012). *Search for Paradise: A Patient's Account of the Artificial Vision Experiment*. Xlibris.

Ohara, S. (2000). Movement-related change of electrocorticographic activity in human supplementary motor area proper. *Brain*. https://doi.org/10.1093/brain/123.6.1203

Ohye, C., Hirai, T., Miyazaki, M., Shibazaki, T., & Nakajima, H. (1982). Vim thalamotomy for the treatment of various kinds of tremor. *Stereotactic and Functional Neurosurgery*. https://doi.org/10.1159/000101611

Oliver, J. E., Hattenhauer, M. G., Herman, D., Hodge, D. O., Kennedy, R., Fang-Yen, M., & Johnson, D. H. (2002). Blindness and glaucoma: a comparison of patients progressing to blindness from glaucoma with patients maintaining vision. *American Journal of Ophthalmology*, *133*(6), 764–772. https://doi.org/10.1016/S0002-9394(02)01403-4

Oostenveld, R., Fries, P., Maris, E., & Schoffelen, J.-M. (2011). FieldTrip: Open Source Software for Advanced Analysis of MEG, EEG, and Invasive Electrophysiological Data. *Computational Intelligence and Neuroscience*, *2011*, 1–9. https://doi.org/10.1155/2011/156869

Opri, E., Cernera, S., Okun, M. S., Foote, K. D., & Gunduz, A. (2019). The Functional Role of Thalamocortical Coupling in the Human Motor Network. *The Journal of Neuroscience : The Official Journal of the Society for Neuroscience*, *39*(41), 8124–8134. https://doi.org/10.1523/JNEUROSCI.1153-19.2019

Panetsos, F., Sanchez-Jimenez, A., Cerio, E. D. De, Diaz-Guemes, I., & Sanchez, F. M. (2011). Consistent phosphenes generated by electrical microstimulation of the visual thalamus. An experimental approach for thalamic visual neuroprostheses. *Frontiers in Neuroscience*. https://doi.org/10.3389/fnins.2011.00084

Parvizi, J., Jacques, C., Foster, B. L., Withoft, N., Rangarajan, V., Weiner, K. S., & Grill-Spector, K. (2012). Electrical Stimulation of Human Fusiform Face-Selective Regions

Distorts Face Perception. *Journal of Neuroscience*. https://doi.org/10.1523/JNEUROSCI.2609-12.2012

Penfield, W., & Rasmussen, T. (1950). The Cerebral Cortex of Man. A Clinical Study of Localization of Function.pdf. In *Academic Medicine*. https://doi.org/10.1097/00001888-195009000-00037

Petroff, O. A., Spencer, D. D., Goncharova, I. I., & Zaveri, H. P. (2016). A comparison of the power spectral density of scalp EEG and subjacent electrocorticograms. *Clinical Neurophysiology*, *127*(2), 1108–1112. https://doi.org/10.1016/j.clinph.2015.08.004

Pezaris, J. S., & Reid, R. C. (2007). Demonstration of artificial visual percepts generated through thalamic microstimulation. *Proceedings of the National Academy of Sciences*. https://doi.org/10.1073/pnas.0608563104

Pfurtscheller, G., Graimann, B., Huggins, J. E., Levine, S. P., & Schuh, L. A. (2003). Spatiotemporal patterns of beta desynchronization and gamma synchronization in corticographic data during self-paced movement. *Clinical Neurophysiology*. https://doi.org/10.1016/S1388-2457(03)00067-1

Potter, K. A., Buck, A. C., Self, W. K., & Capadona, J. R. (2012). Stab injury and device implantation within the brain results in inversely multiphasic neuroinflammatory and neurodegenerative responses. *Journal of Neural Engineering*. https://doi.org/10.1088/1741-2560/9/4/046020

Randazzo, M. J., Kondylis, E. D., Alhourani, A., Wozny, T. A., Lipski, W. J., Crammond, D. J., & Richardson, R. M. (2016). Three-dimensional localization of cortical electrodes in deep brain stimulation surgery from intraoperative fluoroscopy. *NeuroImage*, *125*, 515–521. https://doi.org/10.1016/j.neuroimage.2015.10.076

Rangarajan, V., Hermes, D., Foster, B. L., Weiner, K. S., Jacques, C., Grill-Spector, K., & Parvizi, J. (2014). Electrical Stimulation of the Left and Right Human Fusiform Gyrus Causes Different Effects in Conscious Face Perception. *Journal of Neuroscience*. https://doi.org/10.1523/JNEUROSCI.0527-14.2014

Resnikoff, S., & Pararajasegaram, R. (2001). Blindness prevention programmes: past, present,

and future. *Bulletin of the World Health Organization*, *79*(3), 222–226.

Richard, P., & Bosking, W. H. (2012). Mapping of the Human Visual System. *Clinical Brain Mapping*, 219.

Roller, C. A., Cohen, H. S., Kimball, K. T., & Bloomberg, J. J. (2001). Variable practice with lenses improves visuo-motor plasticity. *Cognitive Brain Research*, *12*(2), 341–352. https://doi.org/10.1016/S0926-6410(01)00077-5

Romero, S., Pelayo, F. J., Morillas, C. A., Martínez, A., & Fernández, E. (2006). Reconfigurable Retina-Like Preprocessing Platform for Cortical Visual Neuroprostheses. In *Handbook of Neural Engineering*. https://doi.org/10.1002/9780470068298.ch16

Rouiller, E. M., Tanné, J., Moret, V., Kermadi, I., Boussaoud, D., & Welker, E. (1998). Dual morphology and topography of the corticothalamic terminals originating from the primary, supplementary motor, and dorsal premotor cortical areas in Macaque monkeys. *Journal of Comparative Neurology*. https://doi.org/10.1002/(SICI)1096-9861(19980629)396:2<169::AID-CNE3>3.0.CO;2-Z

Rush, A. D., & Troyk, P. R. (2012). A power and data link for a wireless-implanted neural recording system. *IEEE Transactions on Biomedical Engineering*, *59*(12 PART2), 3255–3262. https://doi.org/10.1109/TBME.2012.2214385

Saalmann, Y. B., Pinsk, M. A., Wang, L., Li, X., & Kastner, S. (2012). The pulvinar regulates information transmission between cortical areas based on attention demands. *Science*. https://doi.org/10.1126/science.1223082

Sabuncu, M. R., Yeo, B. T. T., Van Leemput, K., Fischl, B., & Golland, P. (2010). A Generative Model for Image Segmentation Based on Label Fusion. *IEEE Transactions on Medical Imaging*, *29*(10), 1714–1729. https://doi.org/10.1109/TMI.2010.2050897

Sahel, J. A., da Cruz, L., Hafezi, F., Stanga, P. E., Merlini, F., Coley, B., Greenberg, R. J., & Group, A. I. S. (2011). Subjects Blind From Outer Retinal Dystrophies Are Able To Consistently Read Short Sentences Using The ArgusTM Ii Retinal Prosthesis System. *ARVO Meeting Abstracts*.

Sakai, S. T., Inase, M., & Tanji, J. (1996). Comparison of cerebellothalamic and pallidothalamic

projections in the monkey (Macaco, fuscata): A double anterograde labeling study. In *Journal of Comparative Neurology*. https://doi.org/10.1002/(SICI)1096-9861(19960429)368:2<215::AID-CNE4>3.0.CO;2-6

Schaeffner, L. F., & Welchman, A. E. (2017). Mapping the visual brain areas susceptible to phosphene induction through brain stimulation. *Experimental Brain Research*. https://doi.org/10.1007/s00221-016-4784-4

Schira, M. M., Tyler, C. W., Spehar, B., & Breakspear, M. (2010). Modeling Magnification and Anisotropy in the Primate Foveal Confluence. *PLoS Computational Biology*, *6*(1), e1000651. https://doi.org/10.1371/journal.pcbi.1000651

Schmidt, E. M., Bak, M. J., Hambrecht, F. T., Kufta, C. V., O'Rourke, D. K., & Vallabhanath, P. (1996a). Feasibility of a visual prosthesis for the blind based on intracortical micro stimulation of the visual cortex. *Brain*, *119*(2), 507–522. https://doi.org/10.1093/brain/119.2.507

Schmidt, E. M., Bak, M. J., Hambrecht, F. T., Kufta, C. V., O'Rourke, D. K., & Vallabhanath, P. (1996b). Feasibility of a visual prosthesis for the blind based on intracortical microstimulation of the visual cortex. *Brain*, *119*(2), 507–522. https://doi.org/10.1093/brain/119.2.507

Schneider, T., & Neumaier, A. (2001). Algorithm 808: ARfit---a matlab package for the estimation of parameters and eigenmodes of multivariate autoregressive models. *ACM Transactions on Mathematical Software*. https://doi.org/10.1145/382043.382316

Schnitzler, A., Münks, C., Butz, M., Timmermann, L., & Gross, J. (2009). Synchronized brain network associated with essential tremor as revealed by magnetoencephalography. *Movement Disorders*. https://doi.org/10.1002/mds.22633

Schwartz, A. B., Cui, X. T., Weber, D. J. J., & Moran, D. W. (2006). Brain-Controlled Interfaces: Movement Restoration with Neural Prosthetics. In *Neuron*. https://doi.org/10.1016/j.neuron.2006.09.019

Shannon, R. V. (1992). A Model of Safe Levels for Electrical Stimulation. *IEEE Transactions on Biomedical Engineering*, *39*(4), 424–426. https://doi.org/10.1109/10.126616

Sillay, K. A., Rutecki, P., Cicora, K., Worrell, G., Drazkowski, J., Shih, J. J., Sharan, A. D., Morrell, M. J., Williams, J., & Wingeier, B. (2013). Long-term measurement of impedance in chronically implanted depth and subdural electrodes during responsive neurostimulation in humans. *Brain Stimulation*. https://doi.org/10.1016/j.brs.2013.02.001

Singh, A., & Bötzel, K. (2013). Globus pallidus internus oscillatory activity is related to movement speed. *European Journal of Neuroscience*, *38*(11), 3644–3649. https://doi.org/10.1111/ejn.12369

Stanga, P., Sahel, J., Mohand-Said, S., DaCruz, L., Caspi, A., Merlini, F., & Greenberg, R. (2013). Face Detection using the Argus® II Retinal Prosthesis System. *Investigative Ophthalmology & Visual Science*.

Stevens, G. A., White, R. A., Flaxman, S. R., Price, H., Jonas, J. B., Keeffe, J., Leasher, J., Naidoo, K., Pesudovs, K., Resnikoff, S., Taylor, H., & Bourne, R. R. A. (2013). Global prevalence of vision impairment and blindness: Magnitude and temporal trends, 1990-2010. *Ophthalmology*, *120*(12), 2377–2384. https://doi.org/10.1016/j.ophtha.2013.05.025

Stingl, K, Bartz-Schmidt, K. U., Besch, D., Gekeler, F., Greppmaier, U., Hörtdörfer, G., Koitschev, A., Peters, T., Sachs, H., Wilhelm, B., & Zrenner, E. (2012). What can blind patients see in daily life with the subretinal Alpha IMS implant? Current overview from the clinical trial in Tübingen. *Der Ophthalmologe : Zeitschrift Der Deutschen Ophthalmologischen Gesellschaft*. https://doi.org/10.1007/s00347-011-2479-6

Stingl, Katarina, Bartz-Schmidt, K. U., Besch, D., Braun, A., Bruckmann, A., Gekeler, F., Greppmaier, U., Hipp, S., Hortdorfer, G., Kernstock, C., Koitschev, A., Kusnyerik, A., Sachs, H., Schatz, A., Stingl, K. T., Peters, T., Wilhelm, B., & Zrenner, E. (2013). Artificial vision with wirelessly powered subretinal electronic implant alpha-IMS. *Proceedings of the Royal Society B: Biological Sciences*. https://doi.org/10.1098/rspb.2013.0077

Stingl, Katarina, Bartz-Schmidt, K. U., Besch, D., Chee, C. K., Cottriall, C. L., Gekeler, F., Groppe, M., Jackson, T. L., MacLaren, R. E., Koitschev, A., Kusnyerik, A., Neffendorf, J., Nemeth, J., Naeem, M. A. N., Peters, T., Ramsden, J. D., Sachs, H., Simpson, A., Singh, M. S., … Zrenner, E. (2015). Subretinal Visual Implant Alpha IMS - Clinical trial interim report. *Vision Research*. https://doi.org/10.1016/j.visres.2015.03.001

Thompson, M. C., Herron, J. A., Brown, T., Ojemann, J. G., Ko, A. L., & Chizeck, H. J. (2017). Demonstration of a stable chronic electrocorticography-based brain-computer interface using a deep brain stimulator. *2016 IEEE International Conference on Systems, Man, and Cybernetics, SMC 2016 - Conference Proceedings*. https://doi.org/10.1109/SMC.2016.7844686

Tort, A. B. L., Komorowski, R., Eichenbaum, H., & Kopell, N. (2010). Measuring phase-amplitude coupling between neuronal oscillations of different frequencies. *Journal of Neurophysiology*, *104*(2), 1195–1210.

Troyk, P. R. (2017). The Intracortical Visual Prosthesis Project. In *Artificial Vision* (pp. 203–214). Springer.

Tsang, E. W., Hamani, C., Moro, E., Mazzella, F., Lozano, A. M., Hodaie, M., Yeh, I. J., & Chen, R. (2012). Movement related potentials and oscillatory activities in the human internal globus pallidus during voluntary movements. *Journal of Neurology, Neurosurgery and Psychiatry*, *83*(1), 91–97. https://doi.org/10.1136/jnnp.2011.243857

Tsiokos, C., Hu, X., & Pouratian, N. (2013). 200-300Hz movement modulated oscillations in the internal globus pallidus of patients with Parkinson's Disease. *Neurobiology of Disease*. https://doi.org/10.1016/j.nbd.2013.01.020

Tsiokos, C., Malekmohammadi, M., AuYong, N., & Pouratian, N. (2017). Pallidal low β-low γ phase-amplitude coupling inversely correlates with Parkinson disease symptoms. *Clinical Neurophysiology*. https://doi.org/10.1016/j.clinph.2017.08.001

Tsolaki, E., Downes, A., Speier, W., Elias, W. J., & Pouratian, N. (2018). The potential value of probabilistic tractography-based for MR-guided focused ultrasound thalamotomy for essential tremor. *NeuroImage: Clinical*. https://doi.org/10.1016/j.nicl.2017.12.018

Vaillancourt, D. E., Sturman, M. M., Metman, L. V., Bakay, R. A. E., & Corcos, D. M. (2003). Deep brain stimulation of the VIM thalamic nucleus modifies several features of essential tremor. *Neurology*. https://doi.org/10.1212/01.WNL.0000086371.78447.D2

Varma, R., Vajaranant, T. S., Burkemper, B., Wu, S., Torres, M., Hsu, C., Choudhury, F., & McKean-Cowdin, R. (2016). Visual impairment and blindness in adults in the United States.

JAMA Ophthalmology, *134*(7), 802–809. https://doi.org/10.1001/jamaophthalmol.2016.1284

Veraart, C., Raftopoulos, C., Mortimer, J. T., Delbeke, J., Pins, D., Michaux, G., Vanlierde, A., Parrini, S., & Wanet-Defalque, M. C. (1998). Visual sensations produced by optic nerve stimulation using an implanted self-sizing spiral cuff electrode. *Brain Research*. https://doi.org/10.1016/S0006-8993(98)00977-9

Veraart, C., Wanet-Defalque, M. C., Gérard, B., Vanlierde, A., & Delbeke, J. (2003). Pattern Recognition with the Optic Nerve Visual Prosthesis. *Artificial Organs*. https://doi.org/10.1046/j.1525-1594.2003.07305.x

Vinck, M., Oostenveld, R., van Wingerden, M., Battaglia, F., & Pennartz, C. M. (2011). An improved index of phase-synchronization for electrophysiological data in the presence of volume-conduction, noise and sample-size bias. *Neuroimage*, *55*(4), 1548–1565. https://doi.org/10.1016/j.neuroimage.2011.01.055

Wandell, B. A., Dumoulin, S. O., & Brewer, A. A. (2007). Visual field maps in human cortex. In *Neuron*. https://doi.org/10.1016/j.neuron.2007.10.012

Wang, C., Brunton, E., Haghgooie, S., Cassells, K., Lowery, A., & Rajan, R. (2013). Characteristics of electrode impedance and stimulation efficacy of a chronic cortical implant using novel annulus electrodes in rat motor cortex. *Journal of Neural Engineering*. https://doi.org/10.1088/1741-2560/10/4/046010

Wang, D. D., de Hemptinne, C., Miocinovic, S., Ostrem, J. L., Galifianakis, N. B., San Luciano, M., & Starr, P. A. (2018). Pallidal deep-brain stimulation disrupts pallidal beta oscillations and coherence with primary motor cortex in Parkinson's disease. *Journal of Neuroscience*, *38*(19), 4556–4568.

Weiland, J. D., Liu, W., & Humayun, M. S. (2005). Retinal Prosthesis. *Annual Review of Biomedical Engineering*. https://doi.org/10.1146/annurev.bioeng.7.060804.100435

West, S., & Sommer, A. (2001). Prevention of blindness and priorities for the future. *Bulletin of the World Health Organization*, *79*(3), 244–248. https://doi.org/S0042-96862001000300014 [pii]

Winawer, J., & Parvizi, J. (2016). Linking Electrical Stimulation of Human Primary Visual Cortex, Size of Affected Cortical Area, Neuronal Responses, and Subjective Experience. *Neuron*, *92*(6), 1213–1219. https://doi.org/10.1016/j.neuron.2016.11.008

Wyler, A. R., Ojemann, G. A., Lettich, E., & Ward, A. A. (1984). Subdural strip electrodes for localizing epileptogenic foci. *Journal of Neurosurgery*. https://doi.org/10.3171/jns.1984.60.6.1195

Yoshor, D., Bosking, W. H., Ghose, G. M., & Maunsell, J. H. R. (2007a). Receptive fields in human visual cortex mapped with surface electrodes. *Cerebral Cortex*, *17*(10), 2293–2302. https://doi.org/10.1093/cercor/bhl138

Yoshor, D., Bosking, W. H., Ghose, G. M., & Maunsell, J. H. R. (2007b). Receptive Fields in Human Visual Cortex Mapped with Surface Electrodes. *Cerebral Cortex*, *17*(10), 2293–2302. https://doi.org/10.1093/cercor/bhl138

Yoshor, D., Bosking, W. H., Lega, B. C., Sun, P., & Maunsell, J. H. R. (2008). Local cortical function after uncomplicated subdural electrode implantation. *Journal of Neurosurgery*. https://doi.org/10.3171/JNS/2008/108/01/0139

Yu, H., Bronte-Stewart, H., Hill, B., de Solages, C., Whitmer, D., & Henderson, J. M. (2012). High frequency deep brain stimulation attenuates subthalamic and cortical rhythms in Parkinson's disease. *Frontiers in Human Neuroscience*. https://doi.org/10.3389/fnhum.2012.00155

Zhang, X., Bullard, K. M. K., Cotch, M. F., Wilson, M. R., Rovner, B. W., McGwin, G., Owsley, C., Barker, L., Crews, J. E., & Saaddine, J. B. (2013). Association between depression and functional vision loss in persons 20 years of age or older in the United States, NHANES 2005-2008. *JAMA Ophthalmology*, *131*(5), 573–581. https://doi.org/10.1001/jamaophthalmol.2013.2597

Zheng, D. D., Christ, S. L., Lam, B. L., Tannenbaum, S. L., Bokman, C. L., Arheart, K. L., McClure, L. A., Fernandez, C. A., & Lee, D. J. (2014). Visual acuity and increased mortality: The role of allostatic load and functional status. *Investigative Ophthalmology and Visual Science*, *55*(8), 5144–5150. https://doi.org/10.1167/iovs.14-14202

Zrenner, E., Bruckmann, A., Greppmaier, U., Hoertdoerfer, G., Kernstock, C., Sliesoraityte, I., Stingl, K., & Wilhelm, B. (2011). Improvement of Visual Orientation and Daily Skills Mediated by Subretinal Electronic Implant Alpha IMS in Previously Blind RP Patients. *ARVO Meeting Abstracts*.